Analysis of Fast Acting Active Disturbance Rejection Control Based Load Frequency Control

By

Md. Mijanur Rahman

A Thesis Submitting to the Department of Electrical and Electronic Engineering of Bangladesh University of Engineering and Technology in Partial Fulfilment of the Requirement for the Degree of

Master of Science in Electrical and Electronic Engineering

Department of Electrical and Electronic Engineering

BANGLADESH UNIVERSITY OF ENGINEERING AND TECHNOLOGY

Dhaka-1000, Bangladesh

September 2015

This thesis titled **"Analysis of Fast Acting Active Disturbance Rejection Control Based Load Frequency Control"** submitted by Md. Mijanur Rahman, Roll No. 0412062104F, Session: April 2012, has been accepted as satisfactory in partial fulfillment of the requirement for the degree of Master of Science in Electrical and Electronic Engineering on September 09, 2015.

BOARD OF EXAMINERS

1. 9/9/2015

Dr. Abdul Hasib Chowdhury
Associate Professor
Department of Electrical and Electronic Engineering
BUET, Dhaka-1000, Bangladesh

Chairman
(Supervisor)

2.

Dr. Taifur Ahmed Chowdhury
Professor and Head
Department of Electrical and Electronic Engineering
BUET, Dhaka-1000, Bangladesh

Member
(Ex-officio)

3.

Dr. Md. Quamrul Ahsan
Professor
Department of Electrical and Electronic Engineering
BUET, Dhaka-1000, Bangladesh

Member

4.

Dr. Md. Fayyaz Khan
Professor
Department of Electrical and Electronic Engineering
United International University
House # 80, Road # 8A (Old 15),
Satmasjid Road, Dhanmondi, Dhaka-1209

Member
(External)

Declaration

It is hereby declared that this thesis titled "**Analysis of Fast Acting Active Disturbance Rejection Control Based Load Frequency Control**" or any part of it has not been submitted elsewhere for the award of any degree or diploma.

Signature of the candidate

9.9.2015

Md. Mijanur Rahman

Acknowledgements

The author would like to thank Dr. Abdul Hasib Chowdhury for his guidance, patience and advice throughout the research. This thesis would not have been completed without his support and guidance. I would like to express my gratitude and gratefulness for his instructions, continuous encouragement, valuable discussions, and careful review during the period of this research. His perpetual motivation gave the confidence to carry out this work. I am thankful to him for providing all the necessary information and proper guidance.

I would also like to thank the authority of this university (BUET) for providing with the necessary assistance and allowing to use the university's computers and library resources.

I would also like to pay my solemn regards to my family, friends and colleagues who supported me generously and encourage me enormously to complete this work.

Last but not the least I am really grateful to almighty Allah, without His mercy and help, it would not have been possible to complete the work properly and in time.

Abstract

A large-scale power system is composed of multiple control areas that are connected to each other through tie lines. As active power changes, the frequencies of the areas and tie-line power exchange deviate from their scheduled values which may greatly degrade the performance of the power system.

Load frequency control (LFC) has two major assignments, which are to maintain the standard value of frequency and to keep the tie-line power exchange under schedule in the presence of any load change. An area control error (ACE), defined as a linear combination of tie-line power and frequency deviations, is regarded as the controlled output of LFC. LFC regulates ACE to zero. When dealing with the LFC problem of power systems, unexpected external disturbances, parameter uncertainties and model uncertainties of the power system pose big challenges for controller design.

Active disturbance rejection control (ADRC) generalizes the discrepancy between the mathematical model and the real system as a disturbance, and rejects the disturbance actively, hence the name active disturbance rejection control. As a result controller does not require accurate model information and is inherently robust against structural uncertainties.

In a power system, synchronous machine electrically closer to the point of impact picks up the greater share of the load regardless of their size. Moreover, generators nearer to the disturbance show largest response and rest of the generators show smaller response. The inertia constant (H) of generators affects the system frequency response. It has been observed that the minimum frequency deviations belong to the generators that have larger inertia constant and response of generators with lower inertia constant responses faster during the disturbance of an interconnected system. Tie-line power exchanges between two areas depend on the tie-line synchronizing co-efficient and the frequency of two areas.

An LFC controller that incorporates these factors in its design is expect to show faster and better response characteristics.

Table of Contents

List of Figures

List of Tables

List of Abbreviations

AC	Alternating current
ACE	Area control error
ADRC	Active disturbance rejection control
BPS	Bangladesh power system
ESO	Extended state observer
GA	Genetic algorithm
GALMI	Genetic algorithm and linear matrix inequalities
LFC	Load frequency control
MEMS	Micro electromechanical system
PI	Proportional-integral
PID	Proportional-integral- derivative
TF	Transfer function

Chapter I

Introduction

1.0 Introduction

Power system frequency control or regulation, very well known as load frequency control has been part of the functions of automatic generation control (AGC) and also has been one of the important control problems for research. The reliability and stability of the power system mainly depend upon frequency deviation from its nominal value. The problem is worse in the case of the integrated power system. Both the active power balance and the reactive power balance must be maintained between generating and utilizing the a/c power. These two balances correspond to two equilibrium points: frequency and voltage. Changes in real power affect mainly the system frequency, while the reactive power is less sensitive to changes in frequency and is mainly dependent on changes in voltage magnitude. Thus, real and reactive powers are controlled separately. When either of the two balances is broken and reset a new level, the equilibrium points will float. Thus, the control issue in power systems can be decomposed into two independent problems. One is of the active power and frequency control while the other is about the reactive power and voltage control. The active power and frequency control are referred to as load frequency control (LFC) [1]. The users of electric power changes load randomly and momentarily. It will be no way to maintain the balances of both the active and reactive powers without control. As a result of the imbalance, the frequency and voltage levels will be varying with the change of the loads. Thus, a control system is critical to cancel the effects of the random load changes and to keep the frequency and voltage at the standard values.

The foremost task of LFC is to keep the frequency constant against the randomly varying active power loads, which are also referred to as unidentified external disturbance. Another task of the LFC is to regulate the tie-line power exchange error. A typical large-scale power system is comprised of several areas of generating units. In order to increase the fault tolerance of the entire power system, these generating units are connected via tie-lines. The use of tie-line power imports a new error into the control problem, i.e., tie-line power exchange error. When a sudden active power load change occurs in an area, the area will obtain energy via tie-lines from other areas. But eventually, the area that is subjected to the load change should balance it without external support. Otherwise there would be economic conflicts between the areas. Hence each area requires a separate load frequency controller to regulate the tie-line power exchange error so that all the areas in an interconnected power system can set their set points differently. Another problem is that the interconnection of power systems results in huge increases in the order of the system and the number of the tuning controller parameters. So, the requirement of the LFC is intended to be robust against the uncertainties of the system model and the variations of system parameters in reality.

1.1 Background and Present State of the Problem

The LFC issues have been tackled with by the various researchers in different time through AGC regulator, excitation controller design and control performance with respect to parameter variation or uncertainties and different load characteristics. A blackout in an electric system means that the complete system collapses. Such a blackout affects all electricity consumers in the area. It can originate from several causes. One example is the loss of generation, e.g. the trip of a power plant that causes a mismatch between production and load. This puts a strain on other generators, resulting in under-frequency in the system while it "catches up", and may result in the further loss of other generators. Increasing number of major power grid blackouts that have been experienced around the world in recent years [2 - 4], for example, United States and Canada (November 2003) Russia (2005), Bangladesh (2007 and 2014) shows that today's power system operation requires more careful consideration of all forms of system instability and control problems and to introduce more effective and robust control strategies.

The LFC has two major assignments, which are to maintain the standard value of frequency and to keep the tie-line power exchange under schedule in the presence of any load change [1]. An area control error (ACE), defined as a linear combination of tie line power and frequency deviations, is taken as the controlled output of LFC. LFC regulates ACE to zero such that frequency and tie-line power errors are forced to zeros as well.

A lot of control techniques has been proposed by the researches in there pioneer work to design LFC controllers [5]-[6]. The controllers are based on:

A. Classical control techniques

1) LQR based controlling techniques

2) Proportional, derivative, integral controlling techniques

B. Soft computing/Artificial intelligence techniques

1) Fuzzy logic based techniques

2) Neural network based techniques

3) Genetic algorithm based techniques

4) Particle swarm based techniques

5) Hybrid and other techniques

The load frequency control techniques are described by different researchers.

The pioneering work by a number of control engineers, namely Bode, Nyquist, and Black, has established links between the frequency response of a control system and its closed-loop transient performance in the time domain. The investigations carried out using classical control approaches reveal that it will result in relatively large overshoots and transient frequency deviation [7]. Moreover, the settling time of the system frequency deviation is comparatively long and is of the order of 10–20s [8].

Among various types of load frequency controller, the PI controller is most widely applied to speed-governing system for LFC scheme [9, 10]. Most of proposed techniques were based on the classical proportional and integral (PI) or proportional, integral and derivative (PID) controllers. Its use is not only for their simplicities, but also due to its success in a large number of industrial applications [11]. A PI controller design on a three-area interconnected power plant is presented in [12], where the controller parameters of the PI controller are tuned using trial-and-error approach. The PI controller tuned through genetic algorithm linear matrix inequalities (GALMI) [13] has become increasingly popular in recent years.

For PID controller design, overshoot/undershoot and settling time are used as objective function for multi-objective optimization in LFC problem [14]. The development of design techniques for load frequency control of a power system in the last few years is very significant. Automatic generation control (AGC) regulator designs are based on adaptive control schemes [15]. The main contribution of the proposed controller is to enhance the controlled performance of the conventional PID controller by adding a self-tuning on the existing conventional PID controller. The conventional PID controller with online self-tuning pre compensation has a superior performance than the conventional PID controller. J. Han identifies four fundamental technical limitations in the existing PID framework in [16], and proposed the corresponding technical and conceptual solutions, including the following: 1) the error computation; 2) noise degradation in the derivative control; 3) over simplification and the loss of performance in the control law in the form of a linear weighted sum; and 4) complications brought by the integral control.

In [17] a fuzzy logic based intelligent controller is designed to facilitate the smooth operation and less oscillatory when system is subjected to a sudden load change. Fuzzy controller is based on a logical system called fuzzy logic which is much closer in spirit to human thinking and natural language than classical logical systems [18, 19]. The complexity and multi-variable conditions of the power system, conventional control methods may not give satisfactory solutions [20]. On the other hand, their robustness and reliability make fuzzy controllers useful in solving a wide range of control problems [21]. Load frequency control in two area system using fuzzy logic algorithm is found to be suitable [22].

Plain fuzzy rule based expert systems have some drawbacks as [23]. It is difficult to acquire knowledge and there is no adaptability and hence for dynamic time varying system, it is unable to perform well due to change in system. To overcome these drawbacks, [24], a new intelligent control technique is proposed based on polar fuzzy sets. The polar fuzzy sets were first introduced in 1990 [25]. Polar fuzzy logic controller performs to improve the stability and dynamic performance of the power system.

In the last few years, considerable progress has been made in application of Artificial Neural Networks *(*ANN). Load frequency control using artificial neural network is described in [26].

After the evolution of soft computing tools, researchers are trying to find better output using newer techniques that are based on Genetic Algorithms and Particle Swarm. These are also called optimization techniques. Genetic algorithms (GA) are global search techniques, based on the operations observed in natural selection and genetics. Panda *et al.* proposed GA along with decomposition technique as developed has been used to obtain the optimum megawatt frequency control of multi-area electric energy systems [27]. No doubt that GA gives better results to previous techniques but it has some problems.

Finding the optimal solution for complex high dimensional, multimodal problems often requires very expensive fitness function evaluations. Also, genetic algorithm does not handle well with complexity. That is, where the number of elements which are exposed to mutation is large there is often an exponential increase in search space size [28].

Some researchers proposed different methodologies of PSO to solve the problem of LFC. Omari et al. are tuned the gain of PID gains using Particle Swarm Optimization (PSO) technique [29]. Boroujeni *et al.* proposed a PSO tuned IP controller to control frequency deviation and compared the result with conventional IP controller [30].

To improve the performance of power system, researchers introduced hybridized techniques. A newly intelligent control technique is the design of a fuzzy system by evolutionary algorithms has been proposed, of which the best known are genetic fuzzy systems [31]. In this work, they apply the idea of evolutionary fuzzy systems to the LFC problem. During control a fuzzy system issued to decide adaptively the proper proportional and integral gains of a PI controller according the area-control error and its change [32].

During the early stage of research, the LFC was based on centralized control strategy [33], which is mainly for "the need to exchange information from control areas spread over distantly connected geographical territories along with their increased computational and storage complexities" [3]. In order to overcome the limitation, decentralized LFC has recently been developed, by which each area executes its control based on locally available state variables [34]. The solutions to the four fundamental technical limitations in the existing PID framework, 1) a simple differential equation to be used as a transient profile generator; 2) a noise-tolerant tracking differentiator; 3) the power of nonlinear control feedback; and 4) the total disturbance estimation and rejection has been implemented by introducing a new controller named Active disturbance rejection control (ADRC).

ADRC an increasingly popular practical control technique, was first proposed by J. Han in [35] and has been modified by Z. Gao in [36, 37]. The design of ADRC only relies on the most direct characteristics of a physical plant, which are input and output. Specifically, the information required for the control purpose is analyzed and extracted from the input and output of the system. ADRC generalizes the discrepancy between the mathematical model and the real system as a disturbance, and rejects the disturbance actively, hence the name active disturbance rejection control. Since ADRC is independent of the precise model information of the physical system, it is very robust against parameter uncertainties and external disturbances [38].

As discussed in [30], ADRC can be understood as a combination of an extended state observer (ESO) and a state feedback controller, where the ESO is utilized to observe the generalized disturbance, which is also taken as an extended state, and the state feedback controller is used to regulate the tracking error between the real output and a reference signal for the physical plant. In addition, a concept of bandwidth parameterization is proposed in [36] to minimize the number of tuning parameters of ADRC. Using this concept, ADRC only has two tuning parameters, of which one is for the controller, and the other is for the observer. The two tuning parameters directly reflect the response speeds of the ESO and the closed-loop control system respectively. The few tuning parameters also make the implementation of ADRC feasible in practice. The detailed explanations about how to select the tuning parameters for ADRC are provided in [37]. At the beginning of the research of ADRC, time-domain analyses of the controller dominated the publications. Recently, a transfer function representation of ADRC has been presented in [38], where frequency-domain analyses have been successfully conducted on a second-order linear plant.

In the performance analyses in [27], the Bode diagram and the stability margins of the closed-loop system have been obtained. The unchanged values of the margins against the variations of system parameters demonstrate the notable robustness of ADRC against parameter uncertainties in the plant. Besides [38], a high order ADRC design was developed on a general transfer function form with zeros [39]. The design method was verified on a 3rd order plant with one zero and a known time delay. However, this design approach did not consider the positive zeros for the transfer function form of an inherently unstable system. The physical system with positive zeros is still an unsolved problem for ADRC.

ADRC has been broadly employed in industry. The implementation of ADRC in motion control has been reported in [37] in the past few years. ADRC is also employed in DC converters, chemical processes and web tension control as presented in [40–42]. An application of ADRC solution to the control problem of a micro electromechanical system (MEMS) gyroscope is presented in [43]. The hardware implementations of ADRC for the MEMS gyroscope were introduced in [44, 45]. ADRC has also been implemented in electrostatic micro-mechanical actuator, fiber optic gyro servo stabilized system, and electric power assist steering system and shunt hybrid active power filter in [46-49].

In practical applications, there are multiple parameters that require tuning in an ADRC controller. A concept of bandwidth parameterization is proposed in [37]. Using this concept, ADRC has only two tuning parameters, the observer bandwidth (ω_0) and feedback controller bandwidth (ω_c). Researchers have considered different values for ω_0 and ω_c. A range of ω_0 is presented in [37] but no procedure for selecting the observer bandwidth is offered. A thumb rule has been illustrated between the relationship of ω_0 and ω_c in [37, 50]. For LFC of a multi-area power system ω_0 is considered as four times to ω_c [30]. In other works on LFC [51, 52] ω_0 is considered as five times of ω_c. In [53] a third controlling parameter, the sampling frequency (T), has been considered, improves the response time. There is hardly any works in ADRC based LFC by considering these three parameters.

A novel design of a robust decentralized LFC has been proposed for an interconnected power system in [51]. Moreover, the effect of variation of system parameters on ACE, frequency error and tie-line power error also reported. It is seen that the system responses remain almost same due to the variation of system parameters in ADRC based LFC. An ADRC based decentralized LFC for interconnected three-area power systems is presented in [52] where the development of ADRC based LFC solution has been shown for systems with non-reheat, reheat and hydraulic turbine. The ADRC is modified using Repetitive Controller (RC) and applied to the power system with two different turbine units in [54] and enhanced the performance of ADRC as a controller. The RC is implemented between the ADRC and the plant of power system dynamic model. The basic principle of RC states that the controlled output tracks a set of reference inputs without steady state error if the model which generates these references is included in the stable closed loop system.

ADRC has been studied for LFC of Bangladesh Power System (BPS) [58]. The work proposes feedback connections by considering the minimum ACE as well as frequency deviation and tie-line error where load change has been considered in a single area only, not simultaneously in all areas.

In a power system consisting of interconnected areas, each area agrees to export or import a scheduled amount of power through transmission-line interconnections, or tie-lines, to its neighboring areas. Tie-line power exchange of a power system is inversely proportional with the reactance of transmission line [55]. Besides, the reactance of the transmission lines is dependent with the length of line. So the distance between two areas has a great impact on power flow through tie. In [56], it has been described that immediately after disturbance in a power system, generators share the impact according to their electrical proximity to the point of impact. That means the machine electrically closer to the point of impact will pick up the greater share of the load regardless of their size. It is observed that minimum frequency deviations belong to the generators that have larger inertia constant (H) in [57]. An ADRC based LFC controller considering all these factors has not been reported yet.

The successful examples reported in [35–58] have legitimated the effectiveness of ADRC in LFC and its great advantages over conventional control techniques such as PID control.

1.2 Thesis Objective

The objectives of this works are to investigate the effects of the following on the performance of the ADRC based LFC controller:

i. Effect of tie-line impedance,
ii. Effect of generator inertia constant (*H*),
iii. Effect of generator electrical proximity to the point of impact in a power system,
iv. Effect of different feedback connection from load rich area to generation rich area.

The possible outcome would be a faster acting ADRC based LFC controller for interconnected power system that considers tie-line impedance, generator inertia constant (*H*), generator electrical proximity to the point of impact and optimal feedback connection in its design. Moreover, this would provides a comprehensive study on the effects of change in three parameters (ω_c , ω_0 and T) on the performance of an ADRC based LFC in single- and multi-area power systems. This would give good insight in choosing the controller parameter for an ADRC based LFC.

1.3 Organization of the Thesis

The thesis is organized as follows. Chapter I is the introductory chapter that represents a brief literature survey on the LFC problem. Chapter II presents the model of the power plant. The major components of the power plant are discussed in this chapter. A Laplace transform representation of the decentralized area of the power plant is also developed in Chapter II.

Chapter III introduces the design of an interconnected power system for ADRC based LFC. First the application of ADRC to a second-order motion system is developed. Then ADRC is generalized to an n^{th} order plant with zeros in the transfer function representation of the plant. Finally the development of ADRC based LFC on the interconnected power system is presented in the chapter. Chapter IV presents the simulation results for the effectiveness of ADRC in LFC by comparing with the performance of PID controller. Parameterization of ADRC for LFC of single-area and multi-area power system has also been presented in the chapter IV. Chapter V presents the simulation results of an interconnected power system. It presents the effect of tie-line impedance, generator inertia constant, and generator electrical proximity to the point of impact on ADRC based LFC of an interconnected power system. This section also proposed the feedback connections from various load rich areas to generation rich areas of an interconnected power system. Chapter VI is the concluding chapter.

Chapter II

Dynamics of the Power Generating System

2.0 Introduction

A comprehensive introduction to the dynamic models of general power systems can be found in [1]. In this chapter, the modeling of a typical power generating system, including the modeling of two types of generating units, the tie-line modeling and the modeling of parallel operation of interconnected areas are presented in [1, 58, and 59].

2.1 Power generating Units

2.1.1 Turbines

A turbine unit in power systems is used to transform the natural energy, such as energy from steam or water, into mechanical power (ΔP_m) that is supplied to the generator. In LFC model, there are three kinds of commonly used turbines: non-reheat, reheat and hydraulic turbines, all of which can be modeled by transfer function [1].

No-reheat turbines are first-order units. A time delay (denoted by T_{ch}) occurs between switching the valve and producing the turbine torque. The transfer function of the non-reheat turbine can be represented as

$$G_{NR}(s) = \frac{\Delta P_m(s)}{\Delta P_v(s)} = \frac{1}{T_{ch}s+1} \tag{1}$$

where ΔP_v is the valve/gate position change and the load reference set point can be used to adjust the valve/gate positions.

Reheat turbines are modeled as second-order units, since they have different stage due to high and low steam pressure. The transfer function can be represented as

$$G_R(s) = \frac{\Delta P_m(s)}{\Delta P_v(s)} = \frac{F_{hp}T_{rh}\,s+1}{(T_{ch}s+1)(T_{rh}s+1)} \tag{2}$$

where T_{rh} stands for the low pressure reheat time and F_{hp} represents the high pressure stage rating.

Hydrolic turbines are non-minimum phase units due to the water inertia. In the hydrolic turbain the water pressure response in opposite to the gate position change at first and recovers after the transient response. Thus the transfer function of the hydrolic turbine is in the form of Eq.(3).

$$G_H(s) = \frac{\Delta P_m(s)}{\Delta P_v(s)} = \frac{-T_w s+1}{(T_w/2)s+1} \tag{3}$$

2.1.2 Generators

A generator unit in power systems converts the mechanical power received from the turbine into electrical power. But for LFC, we focus on the rotor speed output (frequency of the power systems) of the generators instead of the energy transformation. Since the electrical power is hard to store in large amounts, the balance has to be maintained between the generated power and the load demand.

Once a load change occurs, the mechanical power sent from the turbine will no longer match the electrical power generated by the generator. This error between the mechanical (ΔP_m) and the electrical power (ΔP_{el}) is integrated into the rotor speed deviation ($\Delta\omega_r$), which can be turned into the frequency bias (Δf) by multiplying 2π. The relationship between ΔP_m and Δf is shown in figure 2.1, where M is the inertia constant of the generator.

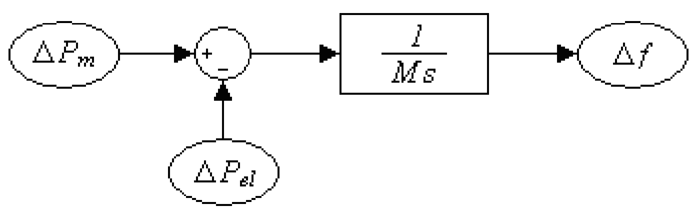

Fig. 2.1: Block diagram of a power generating unit

The power loads can be decomposed into resistive loads (ΔP_L), which remain constant when the rotor speed is changing, and motor loads that change with load speed. If the mechanical power remain unchanged, the motor load will compensate the load change at a rotor speed that is different from a scheduled value, which is shown in Figure 2.2, where D is the load damping constant.

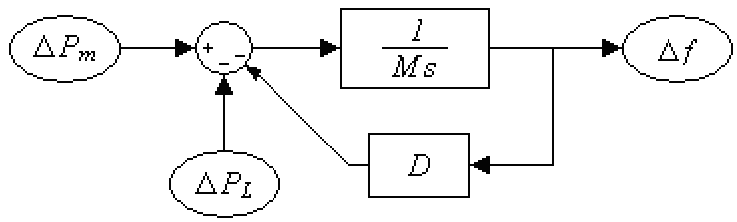

Fig. 2.2: Block diagram of the generator with load damping effect included

The reduced form of Figure 2.2 is shown in Figure 2.3, which is the generator model that we plan to use for the LFC design. The Laplace-transform representation of the block diagram in Figure 2.3 is given by Eq. (4).

$$\Delta P_m(s) - \Delta P_L(s) = (Ms + D)\Delta f(s) \tag{4}$$

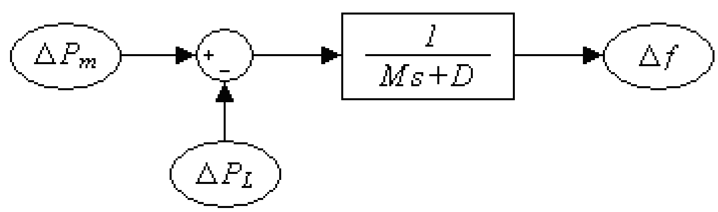

Fig. 2.3: Reduced block diagram of the generator with the load damping effect included

2.1.3 Governors

Governors are the units that are used in power systems to sense the frequency bias caused by the load change and cancel it by varying the turbine inputs. The schematic diagram of a speed governing unit is shown in Figure 2.4, where *R* is the speed regulation characteristic and T_g is the time constant of the governor. Without load reference, when the load change occurs, part of the change will compensate by the valve/gate adjustment while the rest of the change is represented in the form of frequency deviation. The goal of the LFC is to regulate frequency deviation in the presence of varying active power load. Thus the load reference set point can be used to adjust the valve/gate positions so that all the load change is cancelled by the power generation rather than resulting in a frequency deviation.

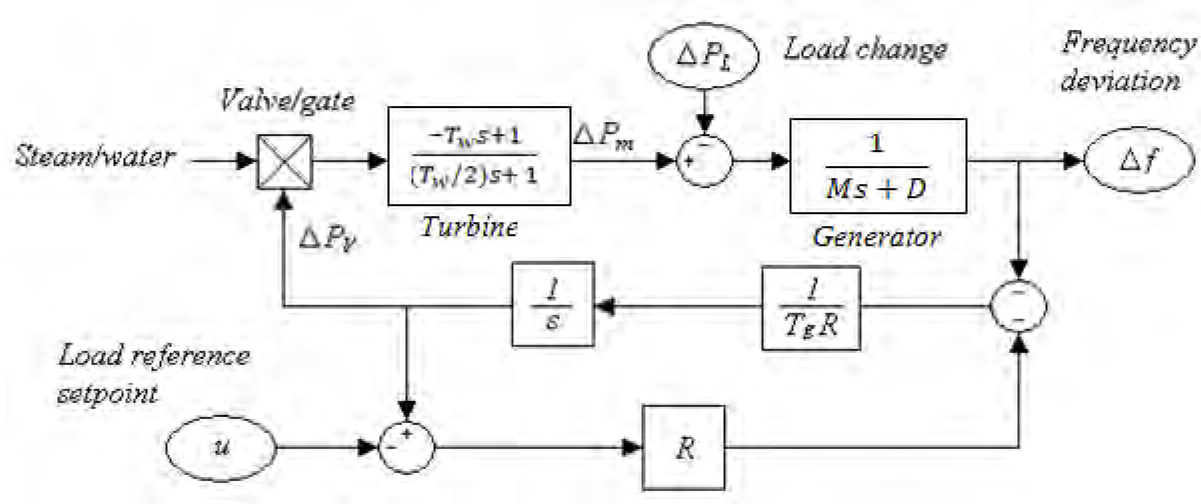

Fig. 2.4: Schematic diagram of a speed governing unit

The reduced form of Figure 2.4 is shown in Figure 2.5. The Laplace transform representation of the block diagram in Figure 2.5 is given by equation (5).

$$U(s) - \frac{\Delta F(s)}{R} = (T_g s + 1)\, \Delta P_v(s) \qquad (5)$$

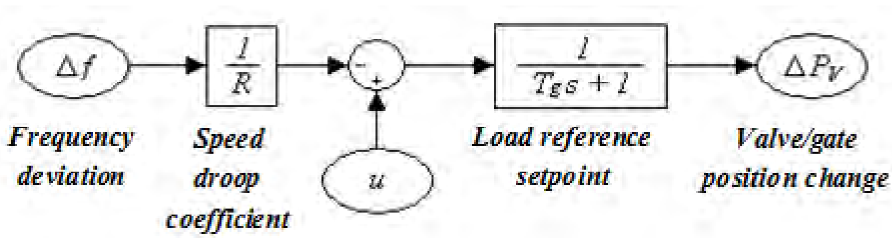

Fig. 2.5: Reduced block diagram of the speed governing unit

2.2 Interconnected power Systems

2.2.1 Tie-Lines

In an interconnected power system, different areas are connected with each other via tie-lines. When the frequencies in two areas are different, a power exchange occurs through the tie-line that connected the two areas. The tie-line connections can be modeled as shown in Figure 2.6. The Laplace transform representation of the block diagram in Figure 2.6 is given by Eq. (6).

$$\Delta P_{tie}(s) = \frac{1}{s} T_{ij} (\Delta F_i(s) - \Delta F_j(s)) \qquad (6)$$

where ΔP_{tie} is tie-line exchange power between areas i and j, and T_{ij} is the tie-line synchronizing torque coefficient between area i and j [1]. From Figure 2.6, we can see that the tie-line power error is the integral of the frequency difference between the two areas.

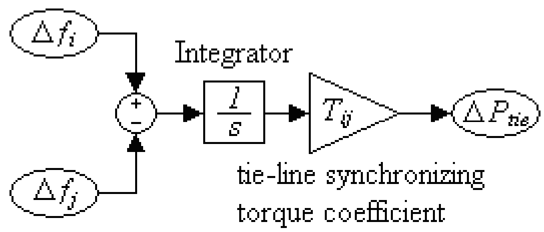

Fig. 2.6: Block diagram of the tie-lines

2.2.2 Area Control Error

As discussed in Chapter I, the goals of LFC are not only to cancel frequency error in each area, but also to drive the tie-line power exchange according to schedule. Since the tie-line power error is the integral of the frequency difference between each pair of areas, if we control frequency error back to zero, any steady state errors in the frequency of the system would result in tie-line power errors. Therefore we need to include the information of the tie-line power deviation into our control input. As a result, an area control error (ACE) is defined as

$$ACE=\sum_{j=1,\ldots,n,j\neq i} \Delta P_{tie\ ij} + B_i \Delta f_i \tag{7}$$

where B_i is the frequency response characteristic for area i and

$$B_i = D_i + \frac{1}{R_i} \tag{8}$$

This ACE signal is used as the plant output of each power generating area. Driving ACEs in all areas to zeros will result in zeros for all frequency and tie-line power errors in the system.

2.2.3 Parallel Operation

If there is several power generating units operating in parallel in the same area, an equivalent generator will be developed for simplicity. The equivalent generator inertia constant (M_{eq}), load damping constant (D_{eq}) and frequency response characteristic (B_{eq}) can be represented as follows.

$$M_{eq} = \sum_{i=1,\ldots,n} M_i \quad (9)$$

$$D_{eq} = \sum_{i=1,\ldots,n} D_i \quad (10)$$

$$B_{eq} = \sum_{i=1,\ldots,n} \frac{1}{R_i} + \sum_{i=1,\ldots,n} D_i \quad (11)$$

2.3 Dynamic Model of Single- Area Power Generating Plant

With the power generating plants and the tie-line connections of interconnected areas introduced in Sections 2.1 and 2.2, a complete form of one-area power generating unit can be constructed as Figure 2.7.

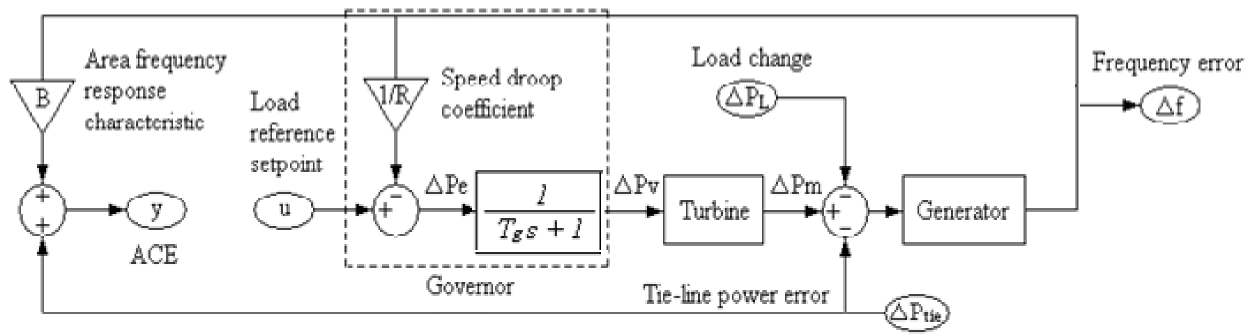

Figure 2.7: Schematic of single-area power generating plant

In Figure 2.7, there are three inputs, which are the controller input *U(s)*, load disturbance $\Delta P_L(s)$, and tie-line power error $\Delta P_{tie}(s)$, one ACE output *Y(s)* and one generator output Δf. The term ΔP_e is not in Figure 2.4 because it does not have a physical meaning. The frequency deviation (Δf) is integrates and then multiplying by tie-line synchronizing co-efficient and it is termed as ΔP_{tie} is for single-area power system. We note the input of the equivalent unit in the governor as ΔP_e for simplicity when developing the Laplace transform of the one-area power generating plant.

2.4 Laplace Transform Model of Single-area Power Generating Plant

We consider the plant shown in Figure 2.7. The relationships between the inputs and output in Figure 2.7 can be described as

$$U(s) - \frac{1}{R}\Delta F(s) = \Delta P_e(s) \quad (12)$$

$$G_{EU}(s)\Delta P_e(s) = \Delta P_v(s) \quad (13)$$

$$G_{Tur}(s)\Delta P_v(s) = \Delta P_m(s) \tag{14}$$

$$\left(\Delta P_m(s) - \Delta P_L(s) - \Delta P_{tie\ ij}(s)\right) G_{gen}(s) = \Delta F(s) \tag{15}$$

$$Y(s) = B\Delta F(s) + \Delta P_{tie}(s) \tag{16}$$

where, $G_{EU}(s)$, $G_{Tur}(s)$ and $G_{Gen}(s)$ are the transfer functions for the equivalent unit, the turbine and the generator respectively.

For the ease of transfer function development, let the transfer function from $\Delta P_e(s)$ that we defined in Figure 2.7 to the mechanical power deviation $\Delta P_m(s)$ be $G_{ET}(s) = Num_{ET}(s) / Den_{ET}(s)$, where $Num_{ET}(s)$ and $Den_{ET}(s)$ are the numerator and denominator of $G_{ET}(s)$ respectively. The representation of $Num_{ET}(s)$ and $Den_{ET}(s)$ may vary from different generating units. For the non-reheat unit, the combined transfer function of the equivalent unit in governor $G_{ET}(s)$ can be expressed as

$$G_{ET}(s) = \frac{Num_{ET}(s)}{Den_{ET}(s)} = \frac{1}{(T_g s + 1)(T_{ch} s + 1)} \tag{17}$$

For the reheat unit, we have

$$G_{ET}(s) = \frac{Num_{ET}(s)}{Den_{ET}(s)} = \frac{F_{hp} T_{rh} s + 1}{(T_g s + 1)(T_{ch} s + 1)(T_{rh} + 1)} \tag{18}$$

Define the transfer function of the generator as

$$G_{Gen}(s) = \frac{1}{Den_m(s)} = \frac{1}{Ms + D} \tag{19}$$

where, $Den_M(s)$ represents the denominator of $G_{Gen}(s)$. The Laplace transform of the one-area power generating plant can be simplified as

$$Y(s) = G_p(s)U(s) + G_D(s)\Delta P_L(s) + G_{tie}(s)\Delta P_{tie}(s) \tag{20}$$

where

$$G_p(s) = \frac{RBNum_{ET}(s)}{Num_{ET}(s) + RDen_{ET}(s)Den_M(s)} \tag{21}$$

$$G_D(s) = \frac{-RBden_{ET}(s)}{Num_{ET}(s) + RDen_{ET}(s)Den_M(s)} \tag{22}$$

$$G_{tie}(s) = \frac{Num_{ET}(s) + RDen_{ET}(s)Den_M(s) - RBden_{ET}(s)}{Num_{ET}(s) + RDen_{ET}(s)Den_M(s)} \tag{23}$$

The modeling of each part in the power generating unit is discussed in this chapter, followed by the Laplace transform development of the decentralized power generating area. The control objective of the LFC problem has been specified as to drive the ACE in each area back to zero. This chapter has laid the groundwork for both the controller design and the constructions of the power test systems.

Chapter III

Design of Active Disturbance Rejection Controller

3.0 Introduction

In the model of the power system developed in last chapter, the parameter values in the model fluctuate depending on system and power flow conditions which change almost every minute. Therefore, dealing with the parameter uncertainties will be an essential factor to choose a control solution to the load frequency control (LFC) problem. In this chapter, the design strategies of ADRC controller are developed on a general transfer function model of a physical system. Both time-domain and frequency-domain representations of ADRC are derived in this chapter.

3.1 Active Disturbance Rejection control

Although we aim to develop ADRC for interconnected power plant, we will introduce the design idea of ADRC on a second order plant for the convenience of explanation. The design of ADRC has been considered from [58].
Let us consider a motion system that can be describe as

$$\ddot{y}(t) + a_1 \dot{y}(t) + a_2 y(t) = bu(t) + w(t) \tag{24}$$

where u(t) is the input force of the system, y(t) is the position output, w(t) represents the external disturbance of the system, a_1, a_2 and b are the coefficient of the differential equation. ADRC design approach can be summarized as four steps.

Step 1: Reformation of the plant

Equation (1) can be rewritten as

$$\ddot{y}(t) = bu(t) + w(t) - a_1 \dot{y}(t) - a_2 y(t) \tag{25}$$

The partial information of the plant - $a_1 \dot{y}(t) - a_2 y(t)$ can be referred to as internal dynamics. The internal dynamics of the system combined with the external disturbance *w (t)* can form a generalized disturbance, denoted as d (t).So equation (2) can be rewritten as

$$\ddot{y}(t)= bu(t) + d(t) \tag{26}$$

The generalized disturbance contains both the unknown external disturbance and the uncertainties in internal dynamics. So, as the generalized disturbance is observed and cancelled by ADRC, the uncertainties included in the disturbance will be cancelled as well.

Step 2: Estimation of the generalized disturbance

As discussed in step 1, the generalized disturbance needs to be cancelled after reforming the plant. One way is to obtain the dynamic model of the disturbance and cancel it theoretically. But this idea does not match with the original intention to set up a controller with little information required from the plant. Moreover the external disturbances cannot be modeled and could be random. Thus another way has to be used to cancel the generalized disturbance rather than to cancel it theoretically. A practical method is to treat the generalized disturbance as an extra state of the system and use an observer to estimate its value. This observer is known as an extended state observer (ESO).

The state space model of equation (3) is

$$\dot{x} = Ax + Bu + E\,\dot{d}$$
$$y = Cx \tag{27}$$

where $x = \begin{bmatrix} x_1 \\ x_2 \\ x_3 \end{bmatrix}$,

Let, $x_1 = y$, $x_2 = \dot{y}$, $x_3 = d$, $A = \begin{bmatrix} 0 & 1 & 0 \\ 0 & 0 & 1 \\ 0 & 0 & 0 \end{bmatrix}$, $B = \begin{bmatrix} 0 \\ b \\ 0 \end{bmatrix}$, $E = \begin{bmatrix} 0 \\ 0 \\ 1 \end{bmatrix}$ and $C = [1 \quad 0 \quad 0]$

It is assumed that d has local Lipchitz continuity and $\dot{d}$ is bounded within domain of interests. The ESO is driven as

$$\dot{z} = Az + Bu + L(y - \hat{y})$$
$$\hat{y} = Cz \tag{28}$$

where $z = [z_1 \quad z_2 \quad z_3]^T$ is the estimated state vector of x and $\hat{y}$ is the estimated system output of y. L is the ESO gain vector and $L = [\beta_1 \quad \beta_2 \quad \beta_3]^T$. To locate all the Eigen values of the ESO at $-\omega_0$, the value of the elements of the vector L are chosen as

$$\beta_i = \binom{3}{1} . \omega_0^i \,, \; i=1, 2,3 \tag{29}$$

with a well tuned ESO , z_i will track x_i closely, Then we will have

$$z_3 \approx x_3 \approx d \tag{30}$$

Step3: Simplification of the plant

With the control law

$$u = \frac{u_0 - z_3}{b} \tag{31}$$

The system describe in equation (26) becomes

$$\ddot{y} = b\,\frac{u_0 - z_3}{b} + d$$

$$\approx (u_0 - d) + d$$

$$\ddot{y} \approx u_0 \tag{32}$$

From (32), we can see that with the accurate estimation of ESO, the second order LTI system could be simplified into a pure integral plant approximately. Then a classic state feedback control law could be used to drive the plant output y to a desired reference signal.

Step 4: Control Law for the Simplified Plant

The state feedback control law for the simplified plant $\ddot{y} = u_0$ as chosen as

$$u_o = k_1(r - z_1) - k_2 z_2 \tag{33}$$

From (28), z_1 will track y and x_2 will track $\dot{y}$. Then substituting u_0 in $\ddot{y} = u_0$ yields

$$\ddot{y} = k_1 r - k_1 y - k_2 \dot{y} \tag{34}$$

The Laplace transform of (34) is

$$S^2 Y(s) + k_2 s Y(s) + k_1 Y(s) = k_1 R(s) \tag{35}$$

The closed loop transfer function from the reference signal to the position output is

$$G_{cl}(s) = \frac{Y(s)}{R(s)} = \frac{k1}{s^2 + k_2 s + k_1} \tag{36}$$

Let, $k_1 = \omega^2_c$ and $k_2 = 2\omega_c$. We will have

$$G_{cl}(s) = \frac{\omega_c^2}{s^2+2\omega_c+\omega_c^2} \\ = \omega_c^2/(s+\ \omega_c)2 \tag{37}$$

where, ω_c represent the bandwidth of the controller. With the increase of the ω_c, the tracking speed of the output of ADRC controlled system will increase as well as the tracking error and over shoot percentage of the output will be decreased.

3.2 Generalized ADRC Design of a Plant

In the Laplace domain, a plant with disturbance can be represented as

$$Y(s) = G_p(s).U(s) + W(s) \tag{38}$$

where $U(s)$ and $Y(s\ )$ are the input and output respectively, $W(s)$ is the generalized disturbance. In (38), the general transfer function of a physical plant $G_p(s)$ can be represented as

$$\frac{Y(s)}{R(s)} = G_p(s) = \frac{b_m s^m + b_{m-1}\ \ s^{m-1} + \cdots + b_1\ \ s + b_0}{a_n\ \ s^n + a_{n-1}\ \ s^{n-1} + \cdots + a_1\ s + a_0} \tag{39}$$

where a_i and b_j $(i=1,\dots, n, j=1,\dots, m)$ are the coefficient of the transfer function.

From (39), we can infer that the basic idea of ADRC design is based on the transfer function of the plant without zeros. Thus in order to implement ADRC for the system represented by (38), we need to develop an equivalent model of (39) so that the transfer function only has poles. The error between two models can be included into the generalized disturbance term.

In order to develop the non-zero equivalent model of (39), the following polynomial long division is conducted on $1/G_p(s)$.

$$\frac{1}{G_p\ (s)} = \frac{a_n\ \ s^n + a_{n-1}\ \ s^{n-1} + \ldots\ldots + a_1\ s + a_0}{b_m s^m + b_{m-1}\ \ s^{m-1} + \cdots + b_1\ \ s + b_0}$$

$$= c_{n-m}\ \ s^{n-m} + bc_{n-m-1}\ \ s^{n-m\ -1}\ + \ldots + c_1 s + c_0 + G_{left}(s) \tag{40}$$

In (40), c_i $(i=0,\dots n\text{-}m)$ are coefficients of polynomial division result, and the $G_{left}(s)$ is a reminder, which can be represented by

$$G_{left}(s) = \frac{d_{m-1}\ s^{m-1} + d_{m-2}\ s^{m-2} + \ldots\ldots + d_1\ s + d_0}{b_m s^m + b_{m-1}\ s^{m-1} + \cdots\cdots + b_1\ s + b_0} \qquad (41)$$

In (41), d_j ($j=0,\ldots, m-1$) are coefficient of the numerator of the remainder. Substituting (40) into (38) we have,

$$[c_{n-m}\ s^{n-m} + bc_{n-m-1}\ s^{n-m-1} + \ldots + c_1 s + c_0 + G_{left}(s)].Y(s) = U(s) + W'(s) \qquad (42)$$

where $W'(s) = W(s)/G_p$

Eq. (42) can be rewritten as

$$[c_{n-m}\ s^{n-m} Y(s) = U(s) - [c_{n-m-1}\ s^{n-m-1} + \ldots + c_1 s + c_0 + G_{left}(s)].Y(s) + W'(s) \qquad (43)$$

Finally, we have

$$s^{n-m}\ Y(s) = \frac{1}{c_{n-m}} U(s) + D(s) \qquad (44)$$

where

$$D(s) = -\frac{1}{c_{n-m}} [c_{n-m-1}\ s^{n-m-1} + \ldots + c_1 s + c_0 + G_{left}(s)].Y(s) + \frac{1}{c_{n-m}} W'(s) \qquad (45)$$

From (40), it can be seen that

$$c_{n-m} = \frac{a_n}{b_m} \qquad (46)$$

However, it is difficult to get the expression of the other coefficients in (40) and (41). Fortunately for the development process of ADRC, $D(s)$ is treated as the generalized disturbance and will be estimated in time domain so that we do not actually need the exact expression for the c_i and d_j $(i=0,\ldots, n\text{-}m, j=0,\ldots,m\text{-}1)$ in (40) and (41).

From (44), it is seen that the two characteristics (relative order between input and output and controller gain) have been extracted from the plant by modifying the Laplace transform. Instead of using the order of plant n, the relative order n-m may be utilizing as the order of the controller system. The high frequency gain (b), is the ratio between the coefficient of the highest order terms of the numerator and the denominator. So (44) can be written as

$$s^{n-m}\ Y(s) = bU(s) + D(s) \qquad (47)$$

where $b = \frac{1}{c_{n-m}}$

Now the state space model of (38) is

$$SX(s) = AX(s) + BU(s) + Es\ D(s) \qquad (48)$$

$$Y(s) = C\,X(s)$$

where

$$X(s) = \begin{bmatrix} X_1(s) \\ X_2(s) \\ \vdots \\ X_{n-m}(s) \end{bmatrix}$$

$$A = \begin{bmatrix} 0 & 1 & 0 & \dots & 0 \\ 0 & \ddots & 1 & \ddots & \vdots \\ \vdots & \ddots & 0 & \ddots & 0 \\ \vdots & \ddots & \ddots & \ddots & 1 \\ 0 & 0 & \cdots & \dots & 0 \end{bmatrix}, \quad B = \begin{bmatrix} 0 \\ \vdots \\ 0 \\ b \\ 0 \end{bmatrix}, E = \begin{bmatrix} 0 \\ \vdots \\ 0 \\ 1 \end{bmatrix}, \quad C = [1 \quad 0 \quad \dots \quad 0]$$

In (47), $D(s)$ is still required to have local Lipchitz continuity and $sD(s)$ is bounded with domain of interest. The ESO of the plant is

$$sZ(s) = AZ(s) + BU(s) + L\,(Y(s) -)\hat{Y}(s)$$

$$\hat{Y}(s) = CZ(s) \tag{49}$$

where $Z(s) = [z_1(s) \quad z_2(s) \dots \quad z_{n-m}(s)]^{T}$ and $L = [\beta_1 \quad \beta_2 \dots \quad \beta_{n-m}]^{T}$

In order to locate all the Eigen values of the ESO to $-\omega_0$, the observer gain are chosen as

$$\beta_i = \binom{n-m}{i}.\,\omega_0^{i}, \qquad i = 1, \dots, n-m \tag{50}$$

With a well tuned ESO, $Z_i(s)$ will be able to estimate the value of $X_i(s)$ closely $(i = 1, \dots, n-m)$. Then we have

$$Z_{n-m}(s) = \hat{D}(s) \approx D(s) \tag{51}$$

The control law

$$U(s) = (U_0(s) - Z_{n-m}(s))/b \tag{52}$$

will reduce (24) to a pure integral part, i.e.,

$$s^{n-m} \quad Y(s) = \text{b}.\frac{\text{U}_0(\text{s}) - Z_{n-m}(s)}{b} + D(s)$$

$$= U_0(s) - \widehat{D}(s) + D(s)$$

$$\approx U_0(s) \tag{53}$$

The control law for the pure integral plant is

$$U_0(s) = k_1\,(R(s) - Z_1(s)) - k_2\,Z_2(s) - \ldots - K_{n-m-1}\,Z_{n-m-1}(s) \tag{54}$$

To further simplify the process, all the closed loop poles of the PD controller are set to $-\omega_{c.}$

Then the controller gain in (54) has to be selected as

$$K_i = \binom{n-m-1}{n-m-i}.\, \omega_c^{\text{n-m-1}} \quad , i = 1, \ldots, n\text{-}m\text{-}1 \tag{55}$$

3.3 Summary of the chapter

In this chapter, the design process of ADRC has been divided into four steps. In first step, plant reformation has been shown. In second step, the generalized disturbances have been estimated by extended state observer (ESO). Simplification of the plant has been presents in third step. In last step, the control law has been applied to simplified plant. ADRC has been implemented on a second-order system. Then it has been extended to a system with a general-form transfer function of any order. Both time-domain and frequency-domain representation of ADRC has been developed.

Chapter IV

Performance Analysis and Parameterization of ADRC

4.0 Introduction

In this chapter, the effectiveness of ADRC in LFC is verified by applying it in a single area power system where the system consists of a generating unit with non-reheat turbine, generator and governor. This test has been used to compare the control performances between the PID controller and the ADRC. In another part, the parameters of ADRC based LFC has been proposed for single- and multi- area power system. Here multi area system consists of three single area power systems. Each area consists of a generating unit with non-reheat turbine, generator and governor. All simulations in this thesis have been completed using MATLAB Simulink.

4.1 Comparison of the performance of PID based LFC and ADRC based LFC

PID controller based LFC

The primary task of LFC is to keep the frequency constant against the randomly varying active power loads, which are also referred to as unknown external disturbance. Another task of the LFC is to regulate the tie-line power exchange error. These two tasks can be achieved by using a controller PID controller. The implementation of PID based LFC of a single area power system has been presented in Figs. 4.1. It is assumed that all generators are coherent in an area, and as such generators are represented by a single equivalent generator. A non-reheat turbine system is considered.

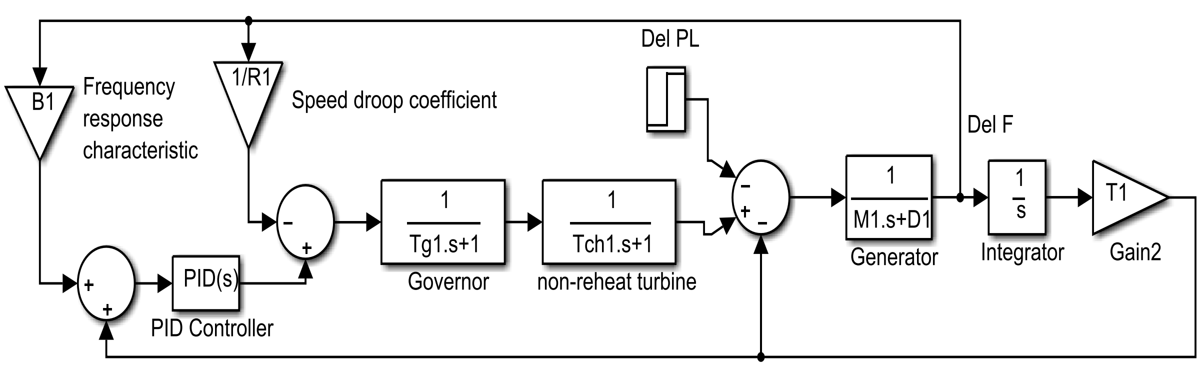

Fig. 4.1 Single area power system with non-reheat turbine with PID based LFC

ADRC controller based LFC

The main goal of LFC can also be achieved by using ADRC controller. The same single area power system has been considered for ADRC based LFC in Fig. 4.2.

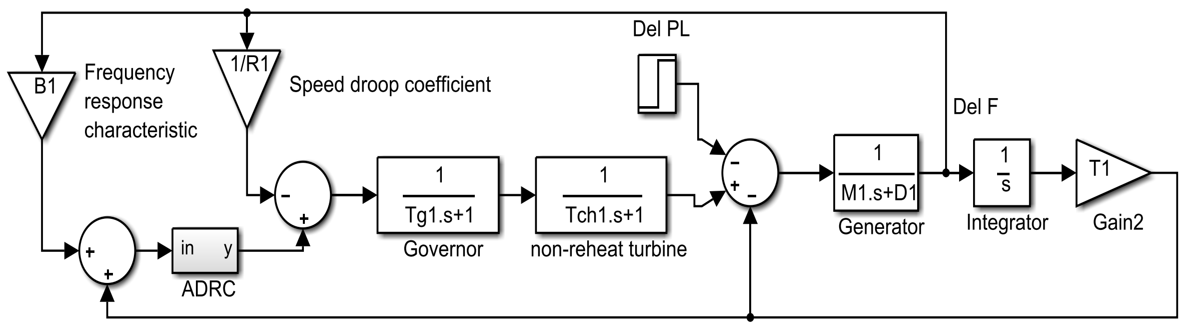

Fig. 4.2 Single area power system with non-reheat turbine with ADRC based LFC

The performance of ADRC has been compared with PID controller. The test has been done on a non-reheat turbine system considering a load change of 1.0 p.u. at 2 seconds for both PID and ADRC. The parameter of the power system has been obtained from [58] and listed in Table A-1 [Annexure A]. The ADRC and PID parameters have been listed in Table A-2[Annexure A]. The definitions of the parameters have already been given in Chapter II. The comparative performance of PID based LFC and ADRC based LFC can be seen from the Figs. 4.3 to 4.5.

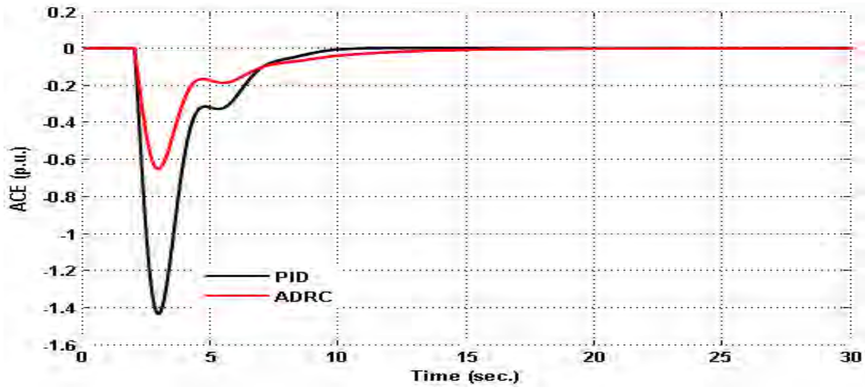

Fig. 4.3 Comparison of ACE for ADRC and PID

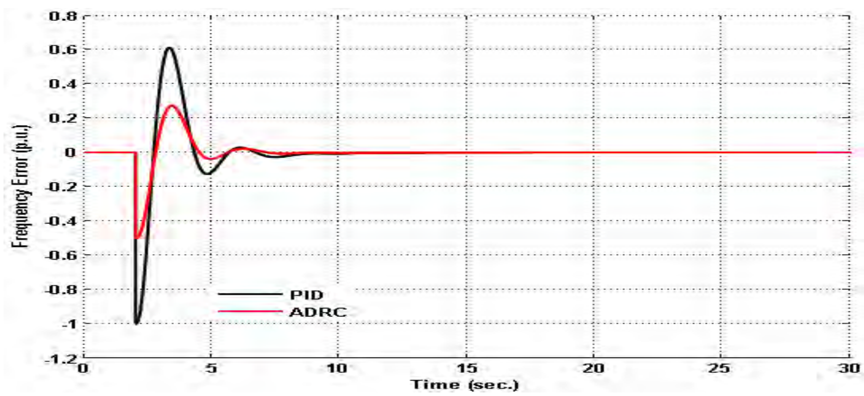

Fig. 4.4 Comparison of frequency deviation for ADRC and PID

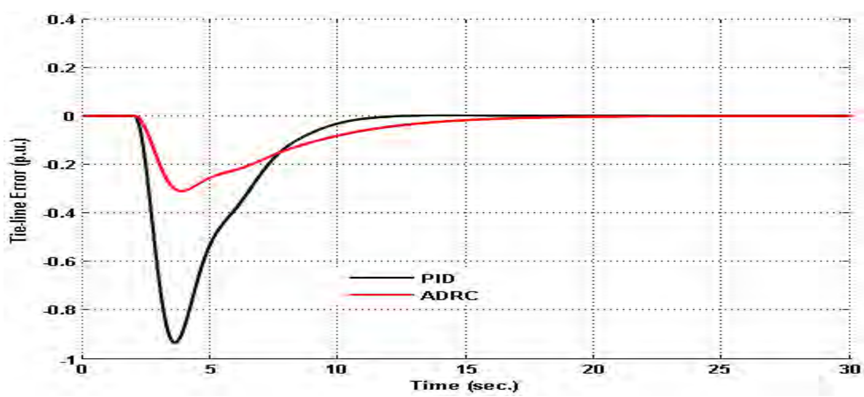

Fig. 4.5 Comparison of tie-line error for ADRC and PID

In Fig. 4.3, the peak magnitude (M_p) of ACE has been observed 1.42 p.u. and 0.63 p.u. for PID based LFC and ADRC based LFC respectively but the time required to settle down the ACE of PID based LFC has been obtained 3 sec. lower than ADRC based LFC. The error magnitude of frequency deviation in ADRC based LFC has been observer haft of the frequency deviation of PID based LFC due to applying same amount of load change as disturbance shown in Fig. 4.4. Similarly, tie-line error magnitudes become 0.63 p.u. lower in ADRC based LFC whereas the settling time for both the controllers are same shown in Fig. 4.5.

From all these figures (Figs. 4.3 to 4.5), it can be seen that remarkble lower error magnitude has been obtained from the ADRC based LFC than PID based LFC due to applying the same amount of load change as disturbance. However, the time required for the responses to settle down has been observed lower in case of PID based LFC. The summary of the performance measures for the single-area power system has been presented in Table 4.1.

Table 4.1 Performance comparison of ADRC based LFC and PID based LFC in single area power system

Error type	**Peak amplitude (M_p in p.u.)**		**Settling time (T_S in sec.)**	
	PID	**ADRC**	**PID**	**ADRC**
ACE	1.42	0.63	10	13
Frequency error	1.0	0.5	8	8
Tie-line error	0.92	0.3	11	16

4.2 Parameterization of ADRC for LFC

The efficacy of the ADRC based LFC with change in observer bandwidth (ω_0), controller bandwidth (ω_c) and controller sampling time (T) has been studied for single area and multi-area power system using MATLAB Simulink. Controller bandwidth has been selected based on the time required to settle down the response. Feedback controller will reject the internal dynamics and external disturbance which will be estimated by the ESO. So the observer bandwidth must be higher than the feedback controller bandwidth [31]. Effectiveness of observer's disturbance estimation depends on the observer gain vector and the gain vectors are represented as the function of observer bandwidth (ω_0).The parameters of the single- and multi- area power systems have been taken from [58] and [52] respectively.

4.2.1 Parameterization of ADRC for Single Area Power System

The block diagram model of a single area power system with ADRC based LFC has been shown in Fig. 4.2. Assuming coherency generators are represented by a single equivalent generator. A non-reheat turbine system has been considered. Effects of parameters variation and for a step load change on frequency and tie flow deviations and, ACE has been presented in Figs. 4.6 and 4.7 and in Table 4.2. It can be seen that the peak amplitudes do not change much. This is because for all the cases the disturbance considered has been the same.

The controller bandwidth(ω_c) has been tuned according to the requirement of how fast and steady the output is wanted to track the set point. Higher bandwidth corresponds to better command following, disturbance rejection and sensitivity to parameter variations. However, bandwidth is limited by the presence of sensor noise and due to the higher value of controller bandwidth (ω_c= 5 rad /sec), it may push the system to its limit, leading to oscillations or even instability as shown in Figs. 4.6 (a) and (c).

As ω_c and ω_0 are increased, the noise in control signal u also increases. Any notable change does not found in magnitude of ACE due to change in observer bandwidth in Fig. 4.7 (a) but for higher bandwidth, the response take longer time to settle down in case of tie-line error in Fig.4.7 (c).The effect of change of controller bandwidth and observer bandwidth are shown in Figs. 4.6 and 4.7 are summarized in Table 4.2.

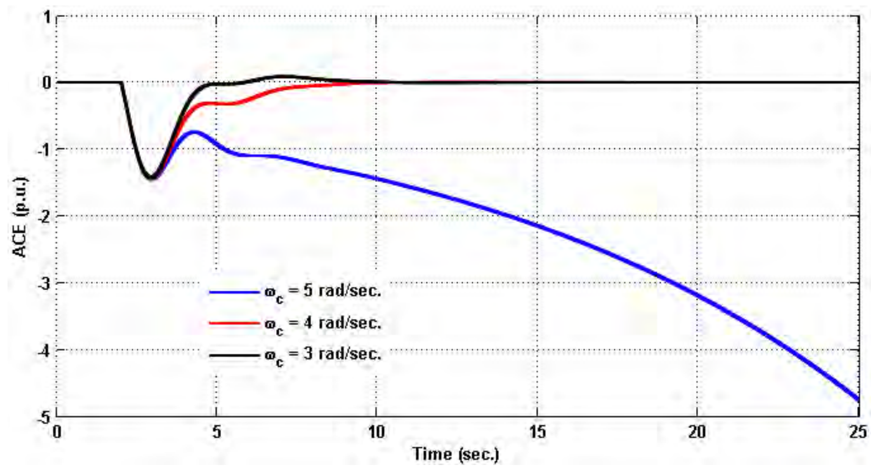

(a)

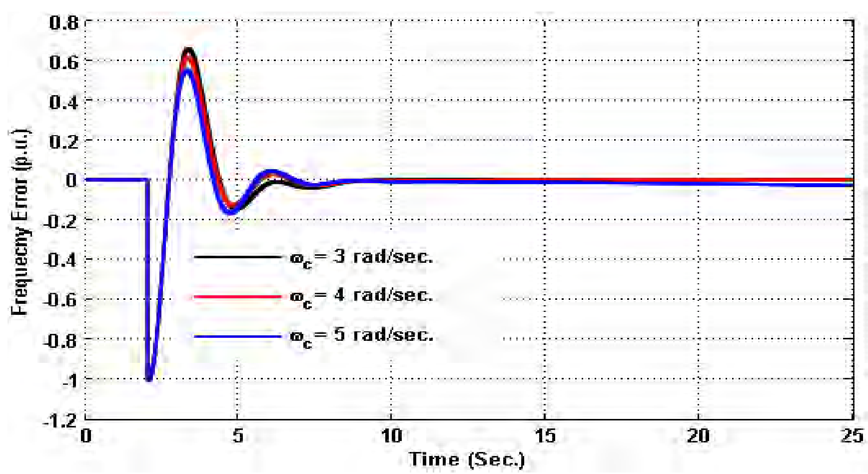

(b)

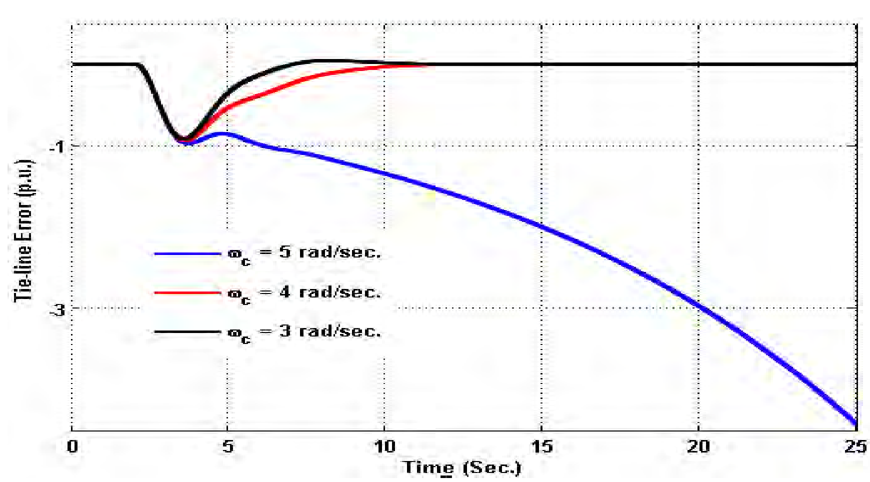

(c)

Fig. 4.6 Effect of change of controller bandwidth on ACE, (a), frequency error, (b) and tie-line error, (c)

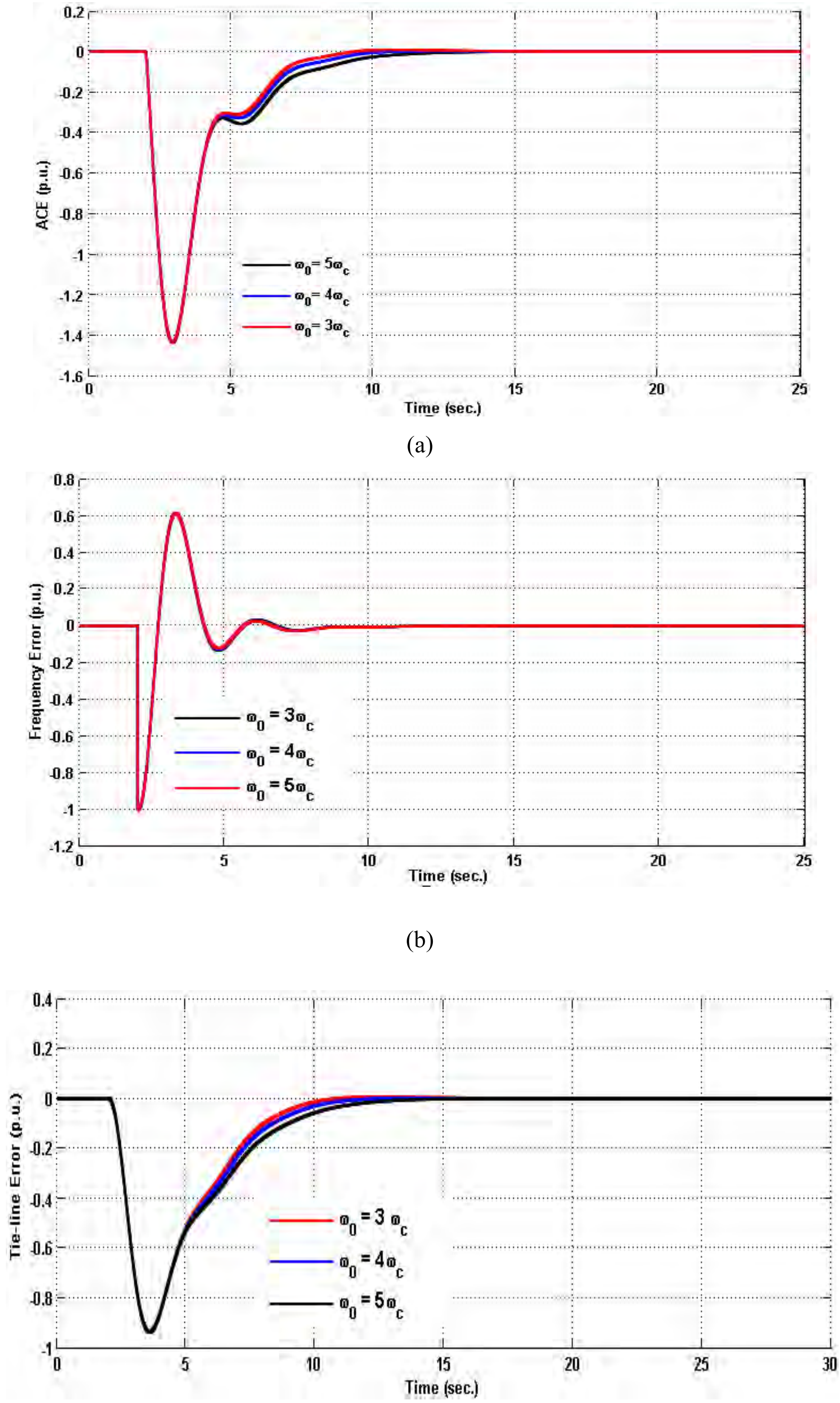

(a)

(b)

(c)

Fig.4.7 Effect of change of observer bandwidth on ACE, (a), frequency error, (b) and tie-line error, (c)

Table 4.2 Performance of single area power system with ADRC parameters variation

Error Type	Parameters Variation	Peak Amplitude (m_p)	T_p (sec.)	T_s (sec.)
ACE	ω_c=3	-1.7	3.0	10.0
	ω_c=4	-1.7	3.0	10.0
	ω_c=5	-1.7	3.0	-
Frequency error	ω_c=3	-0.65	2.0	9.0
	ω_c=4	-0.6	2.0	8.0
	ω_c=5	-0.55	2.0	7.5
Tie-line error	ω_c=3	-0.9	3.5	10.0
	ω_c=4	-0.9	3.5	12.0
	ω_c=5	-0.9	3.5	-
Effects of controller bandwidth variation				
ACE	$\omega_0 = 3\omega_c$	-1.4	3.0	11.0
	$\omega_0 = 4\omega_c$	-1.4	3.0	9.0
	$\omega_0 = 5\omega_c$	-1.4	3.0	10.0
Frequency error	$\omega_0 = 3\omega_c$	-0.6	2.5	8.0
	$\omega_0 = 4\omega_c$	-0.6	2.5	8.0
	$\omega_0 = 5\omega_c$	-0.6	2.5	8.0
Tie-line error	$\omega_0 = 3\omega_c$	-0.9	4.0	11.0
	$\omega_0 = 4\omega_c$	-0.9	4.0	12.0
	$\omega_0 = 5\omega_c$	-0.9	4.0	12.0
Effects of observer bandwidth variation				
ACE	T= 1 sec	-1.4	2.0	10.0
	T= 2sec	-1.45	3.0	9.0
	T=3 sec	-1.70	4.0	11.0
Frequency error	T= 1 sec	-0.6	1.0	8.0
	T= 2sec	-0.6	2.0	8.0
	T=3 sec	-0.7	3.0	10.0
Tie-line error	T= 1 sec	-0.9	2.5	12.5
	T= 2sec	-0.95	3.5	12.0
	T=3 sec	-0.1.2	5.0	14.0

It is very difficult to establish any relationship between observer bandwidth and controller bandwidth but simulation results indicates that observer bandwidth should be chosen four times of controller bandwidth to get the shortest settling time as can be seen from Figs. 4.6 and 4.7 and Table 4.2. In general, the shorter the sampling period the higher the control degree of accuracy for the same plant with increasing observer bandwidth [47]. However, for load frequency control, larger observer bandwidth increases the settling time as can be seen in Figs. 4.7 (a) and (b) and Table 4.2. However, it increases the noise sensitivity of the system.

4.2.2 Parameterization of ADRC for Multi Area Power System

An ADRC based LFC for a three area interconnected power system has been modelled and simulated. The model consists of three generation units, each of which is composed of three major parts: governor, turbine and generator. All generators in one area respond coherently, so they are represented by an equivalent generator. All turbine units are to be considered non-reheat type. Fig. 4.8 presents the dynamic model of one-area in the multi-area power system.

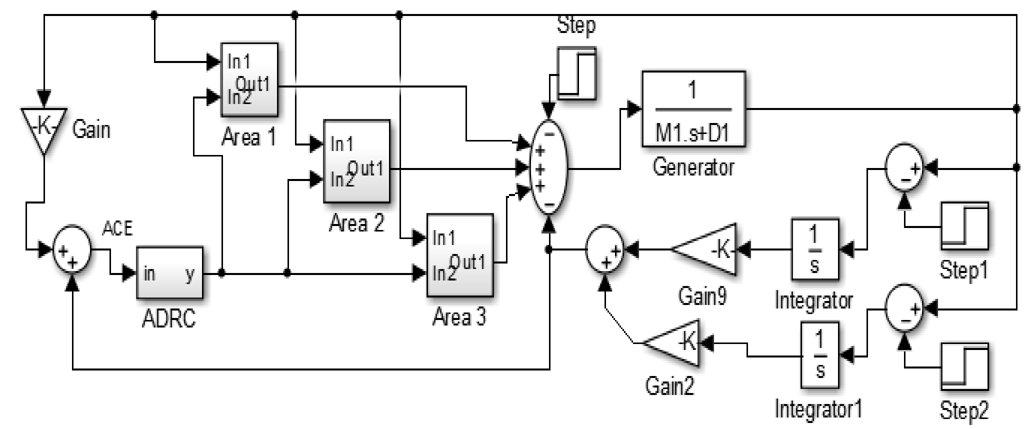

Fig.4.8 One area of multi-area power system

A 0.01 p.u. load change has been added to each area simultaneously. The simulation results have been presented in Table 4.3 for area-1 by varying the three controlling parameters. Peak amplitude is still same for most of the cases due to same load change consideration. The settling time has been calculated by considering the tolerance limit of the response 0.01 p.u. It has been seen that the time required to reaching the peak overshoot and settling time increases with increasing controller bandwidth (m_c) and controller sampling period, respectively. However, a small change in settling time has been noted when the multiplying factor between m_0 and m_c has been increased. This is because a large observer bandwidth increases noise sensitivity.

Table 4.3 Performance of multi-area power system with ADRC parameters variation

Error Type	Parameters Variation	Peak Amplitude (m_p)	T_p (sec.)	T_s (sec.)
ACE	ω_c=3	-0.02	2.0	25
	ω_c=4	-0.02	2.5	25
	ω_c=5	-0.02	3.5	27
Frequency error	ω_c=3	-0.0075	1.5	26
	ω_c=4	-0.005	2.0	27
	ω_c=5	-0.008	3.5	27
Tie-line error	ω_c=3	-0.002	3.5	23
	ω_c=4	-0.008	3.0	26
	ω_c=5	-0.023	3.0	22
Effects of controller bandwidth variation				
ACE	$\omega_0 = 3\omega_c$	-0.02	2.5	22
	$\omega_0 = 4\omega_c$	-0.02	2.5	24
	$\omega_0 = 5\omega_c$	-0.02	2.5	24
Frequency error	$\omega_0 = 3\omega_c$	-0.008	2.0	22
	$\omega_0 = 4\omega_c$	-.0008	2.0	23
	$\omega_0 = 5\omega_c$	-0.008	2.0	22
Tie-line error	$\omega_0 = 3\omega_c$	-0.002	2.5	22
	$\omega_0 = 4\omega_c$	-0.008	2.0	21
	$\omega_0 = 5\omega_c$	-0.022	2.5	20
Effects of observer bandwidth variation				
ACE	T= 1 sec	-0.02	2.0	22
	T= 2sec	-0.02	2.5	26
	T=3 sec	-0.02	3.5	25
Frequency error	T= 1 sec	-0.008	1.5	27
	T= 2sec	-0.007	2.0	27
	T=3 sec	-0.008	3.0	27
Tie-line error	T= 1 sec	-0.002	3.5	24
	T= 2sec	-0.008	3.0	27
	T=3 sec	-0.022	3.5	23

4.3 Modeling of Interconnected Power System for ADRC based LFC

An ADRC based LFC of interconnected power system consisting of three generation rich areas and three load rich areas (3G3L) has been considered in Fig.4.9. Assuming all generators in one area respond coherently, they are represented by an equivalent generator. All load rich areas have been considered as connected to all generation rich areas. Each power plant block has three load disturbance signals as input. The load change signal may be calculated at the load buses by measuring the line power flow at those buses and transmitted to the power plants over optical communication network. The tie-line synchronizing coefficient (*T)* between load rich areas to generation rich areas is dependent on the distance between them and the reactance of the corresponding transmission line. The design parameters of the system and ADRC parameters are listed in Annexure A, Table A-3.

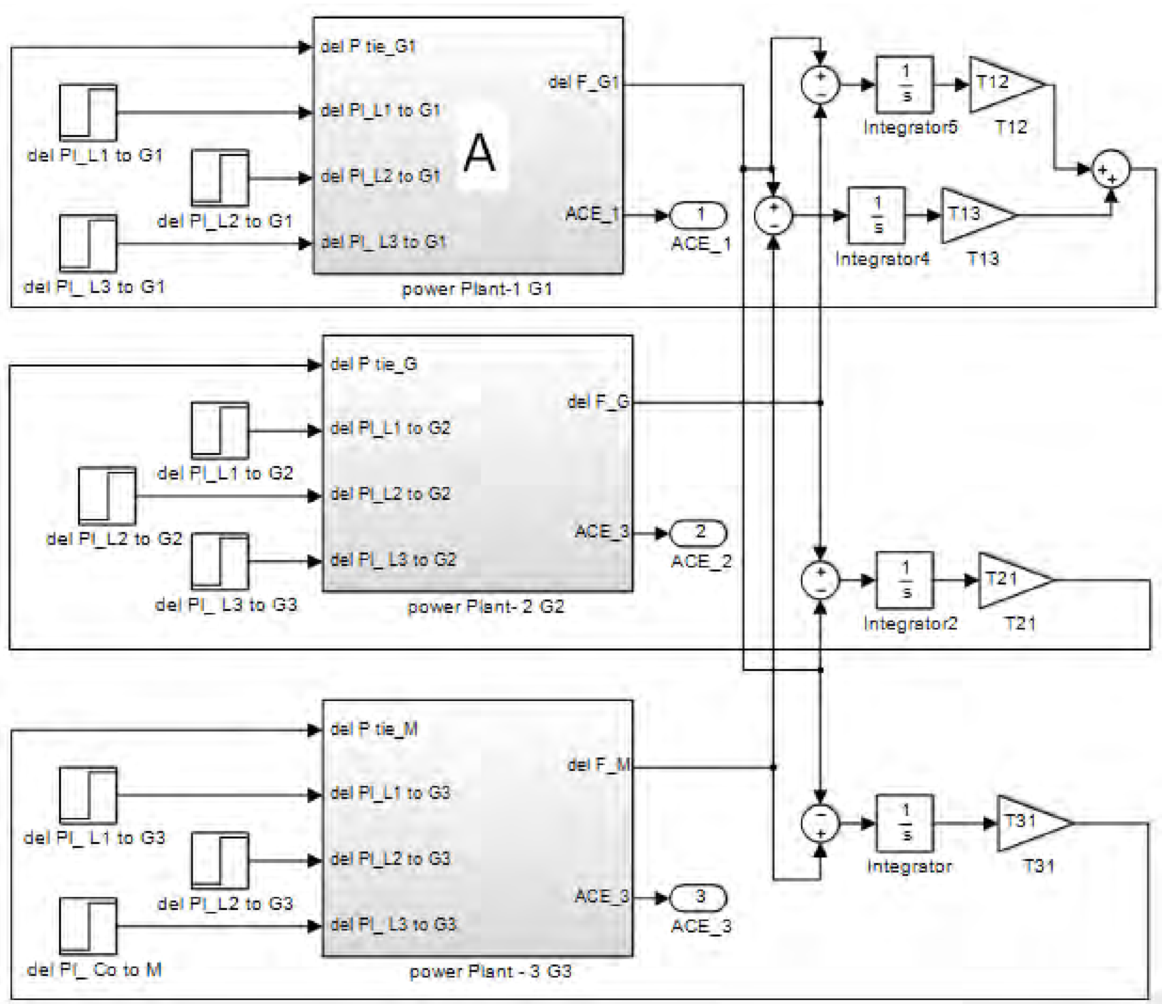

Fig. 4.9 Dynamic model of interconnected power system for ADRC based LFC

All the power plants (G_1, G_2 and G_3) of Fig. 4.9 have been considered similar. The sub-system of power plant 1 has been shown in Fig. 4.10. In generation rich areas, re-heat turbine has been used with governor and generator. The output of the generator of this block is frequency deviation which is first integrated then multiplied by tie-line synchronizing coefficient between load (L_1) to generation (G_1) to get the tie-line deviation (del P tie).

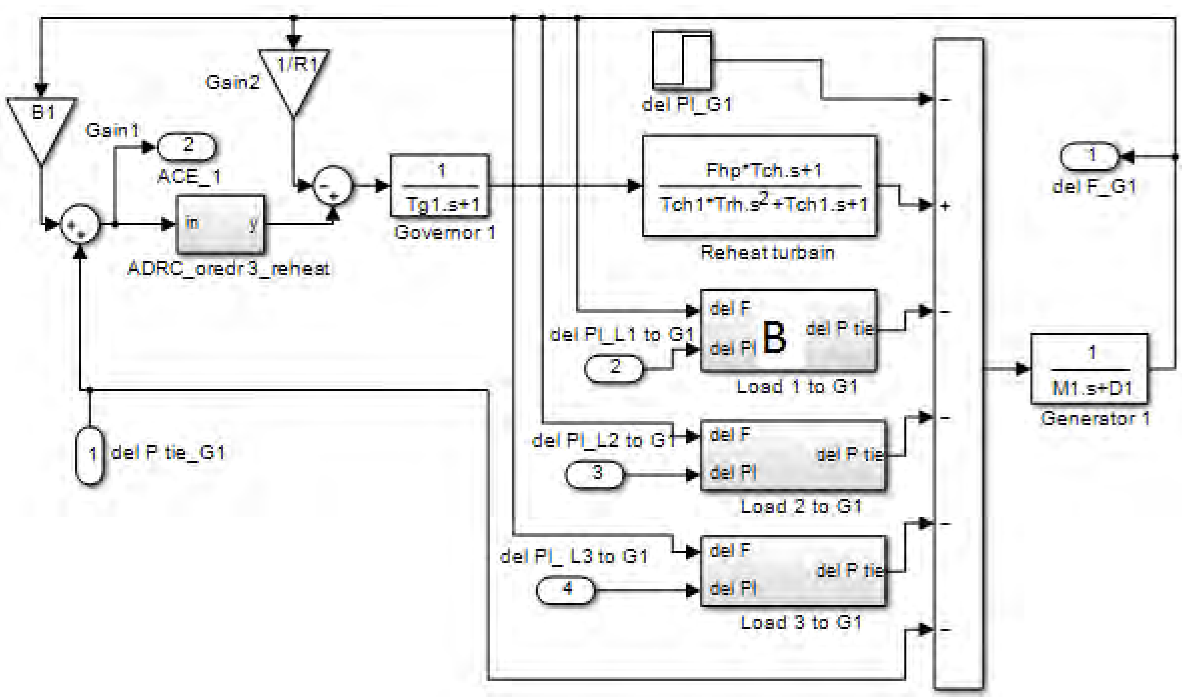

Fig. 4.10 Dynamic model of power plant 1 (block A in Fig.4.9)

The details a load rich area has been shown in Fig. 4.11, where non re-heat turbine has been used with governor and generator. The design of interconnected power system for ADRC based LFC in Figs. (4.9 – 4.11) has been considered from [58].

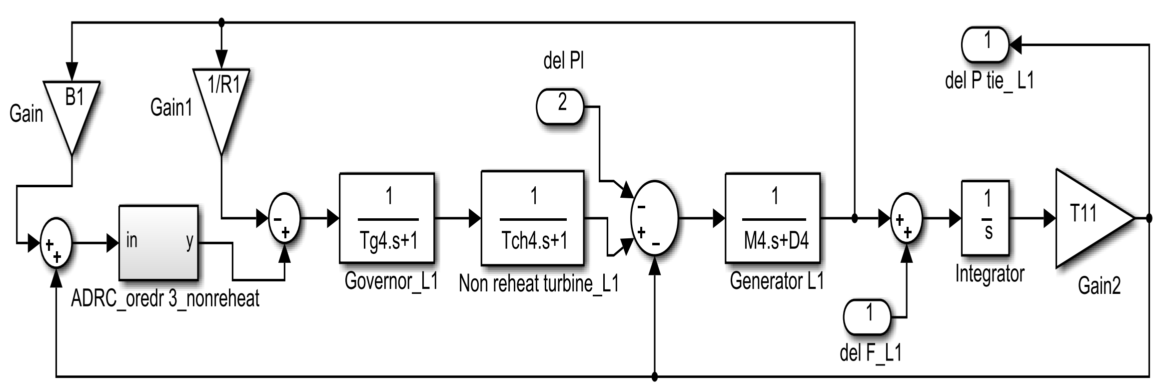

Fig. 4.11 Dynamic model of load change from L_1 to G_1 (block B in Fig. 4.10)

Finally, considering all these Figs. (4.9 – 4.11), the complete model of interconnected power system for ADRC based LFC is ready to calculate the effect of ACE, frequency deviation and tie-line flow deviation if there is any load change from any load rich area to any generation rich area.

4.5 Summary of the chapter

This chapter presents the effectiveness of ADRC as compared with PID controller and a comprehensive study on the effects of change in the ADRC parameters in load frequency controller to regulate the area control error, frequency deviations and tie-line error in single- and multi- area power systems. It will help to enhance the range of applications of ADRC to the power system. Finally the modeling of interconnected power system has been shown.

Chapter V

Fast Acting ADRC based LFC

5.0 Introduction

The generation capacity and the consumption of load for all the regions over the country's interconnected power system are not same. A generation rich area is the one whose available generation is greater than the load and load rich area has available generation less than its load. Power from generation rich areas flow to load rich areas through the tie-line bus.

5.1 Network Elements

5.1.1 Tie-line Synchronizing Coefficient

The total real power that goes out of a particular control area i, $\Delta P_{tie,i}$,equals to the sum of all out f1owing line powers, $P_{tie,ij}$ in the lines connecting area i with neighboring areas, *i.e.,*

$$P_{tie,\,i} = \sum_j P_{tie,ij} \tag{56}$$

where, the simulations are applied to all lines j that terminate in area i. If the line losses are neglected, the individual line power are written in the form

$$P_{tie,ij} = \frac{|V_i||V_j|}{X_{ij} P_{ri}} \sin(\delta_i - \delta_j) \tag{57}$$

where x_{ij} is the reactance of tie-line connecting areas i and j, V_i and V_j are the bus voltages of the line.

If the phase angles deviate from their normal values δ_i^0 *and* δ_j^0 *by the amounts* $\Delta\delta_i$ *and* $\Delta\delta_j$, respectively, one gets the incremental power $\Delta P_{tie,ij}$ over the line as given by

$$\Delta P_{tie,ij} = 2\pi \frac{|V_i||V_j|}{X_{ij} P_{ri}} \cos(\delta_i^0 - \delta_j^0) \left[\int \Delta f_i \, dt - \int \Delta f_j \, dt\right]$$

$$\text{Or, } \Delta P_{tie,ij} = T_{ij} \left[\int \Delta f_i \, dt - \int \Delta f_j \, dt\right] \tag{58}$$

where

$$T_{ij} = 2\pi \frac{|V_i||V_j|}{X_{ij} P_{ij}} \cos(\delta_i^0 - \delta_j^0) \tag{59}$$

is called the tie-line power coefficient or synchronizing coefficient (T).

5.1.2 Generator Electrical Proximity to the Point of Impact

Under normal operating conditions a power system is subjected to numerous random power impacts from sudden application of loads. Each impact will be followed by power swings among groups of machines that respond to the impact differently at different times. The amount of impacts of machines during the fault depends on the distance between the location of disturbance and the generator and it is termed as generator electrical proximity to the point of impact. In large interconnected power systems, it is very important to investigate, how much load impact is being shared by which machine according to their position from the disturbance centre.

For analysing the effect of sudden application of a small load $P_{L\Delta}$ at some point in to the power system, it is assumed that the load has a negligible reactive component. Since the sudden change in load $P_{L\Delta}$ creates an imbalance between generation and load, an oscillatory transient result before the system settles to a new steady state condition.

The phenomenon may be mathematically formulated using the network configuration of Fig. 5.1 considering from [56].

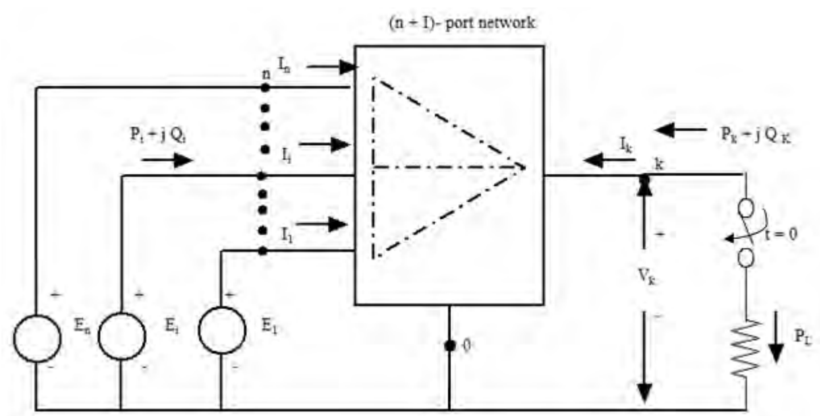

Fig. 5.1 Circuit for measuring the effect of sudden application of small load $P_{\Delta L}$ at some point k in the network

From the circuit in Fig. 5.1, the power into the node *i* can be obtained by adding node *k*, where the load impact $P_{\Delta L}$ is applied.

$$P_i = E_i G_{ii} + \sum_{\substack{j=1 \\ j \neq ik}}^{n} E_i E_j \left(B_{ij} \sin \delta_{ij} + G_{ij} \cos \delta_{ij}\right) + E_i V_k (B_{ik} \sin \delta_{ik} + G_{ik} \cos \delta_{ik})$$

For the case of nearly zero conductance (as network has a very large *X/R* ratio)

$$P_i \cong \sum E_i\, E_j\, B_{ij}\ \sin \delta_{ij} + E_i\, V_k\, B_{ik}\ \sin \delta_{ik} \tag{60}$$

The power into the node *k*

$$P_k = \sum_{\substack{j=1 \\ j \neq k}}^{n} V_k E_j B_{kj}\ \sin \delta_{kj} \tag{61}$$

Assuming the network response to be fast the immediate effect of the application of $P_{\Delta L}$ is that the angle of bus *k* is changed while the magnitude of its voltage V_k is unchanged. So $P_{k\Delta}$ can be written as

$$P_{k\Delta} = \sum_{j=1}^{n} P_{skj}\, \delta_{kj\,\Delta} \tag{62}$$

The equation (62) is valid for any time *t* following the application of the impact.

Let us now consider the case at $t = 0^+$ where it can be determined exactly how much of the impact, $P_{\Delta L}$ is supplied by each generator $P_{i\Delta}$. $i = 1, 2, \ldots, n$

At the instant $t = 0^+$ we know that $\delta_{i\delta} = 0$ for all generators because of rotor inertias. So at node *k*

$$P_{k\Delta}(0^+) = -\sum_{i=1}^{n} P_{i\Delta}(0^+) \tag{63}$$

As $P_{k\Delta} = -P_{L\Delta}$, the equations can be written in terms of the load impact as

$$P_{i\Delta}(0^+) = -\sum_{i=1}^{n} P_{ski}\, \delta_{k\Delta}(0^+) = \sum_{i=1}^{n} P_{i\Delta}(0^+) \tag{64}$$

So from equations (63) and (64) we can write that

$$P_{i\Delta}(0^+) = \left[\frac{P_{sik}}{\sum_{j=1}^{n} P_{sjk}}\right] P_{L\Delta}(0^+) \tag{65}$$

$P_{k\Delta}$ and $P_{i\Delta}$ are the change in power of node *i* and *k* at $t=0^+$ respectively. P_{sik} and P_{sjk} is the change in electrical power of machines *i* and *j* respectively due to the change in loads of node *k*. The equations (63) and (65) indicate that the load impact $P_{L\Delta}$ at a network bus *k* is immediately shared by the synchronous generators according to their synchronizing power coefficients with respect to the bus *k*. Thus the machine electrically close to the point of impact will pick up the greater share of the load regardless of their size.

5.1.3 Inertia Constant of Generator

The inertia constant (H) of generator is the ratio of stored kinetic energy in mega joules at synchronous speed with the machine rating in MVA. Study the effects of H-parameter of generator is very important in LFC of an interconnected system because, higher the inertia constant of a generator, demonstrates the higher capacity of generator to stored the kinetic energy. The mathematical representation of the effect of generator H-parameters in power system has been presented below in [56]. The linearized swing equation for machine i (ignoring damping):

$$\frac{2H_i}{\omega_{Re}}\frac{d^2\Delta\delta_i}{dt^2} = -\Delta P_{ei} \tag{68}$$

The incremental differential equation governing the motion of machine i is given by

$$\frac{2H_i}{\omega_r}\frac{d\omega_{i\nabla}}{dt} + P_{i\Delta}(t) = 0 \tag{67}$$

If $P_{L\Delta}$ is constant for all t, the acceleration in p.u. can be computed by using (62)

$$\frac{1}{\omega_R}\frac{d\omega_{i\Delta}}{dt} = -\frac{P_{sik}}{2H_i}\left(\frac{P_{L\Delta}(0^+)}{\sum_{j=1}^{n} P_{sjk}}\right) \tag{68}$$

The p.u. deceleration of machine i given by (68), is dependent on the synchronizing power coefficient P_{sik} and inertia $H_{i.}$ The mean acceleration of all the machines in the system can be calculated as

$$\frac{d}{dt}\frac{\overline{\omega_\Delta}}{\omega_R} = -\frac{P_{L\Delta}(0^+)}{\sum_{i=1}^{n} 2H_i} \tag{69}$$

While the system as a whole is retarding at a rate given by (66), the individual machines are retarding at different rates. Each machine follows an oscillatory motion governed by its swing equation. When the transient decays, $\frac{d\omega_{i\Delta}}{dt}$ will be the same as $\frac{d\overline{\omega_\Delta}}{dt}$ as given by (69). Substituting this value of $\frac{d\omega_{i\Delta}}{dt}$ in (64) at $t = t_1 > t_o$,

$$\Delta P_{i\Delta}(t_1) = \left[\frac{H_i}{\sum_{j=1}^{n} H_j}\right] P_{L\Delta}(0^+) \tag{70}$$

Thus, after a brief transient period the machines will share in increase in load as a function only of their inertia constants.

5.2 Analysis of ADRC based LFC of Interconnected Power System

For analyzing the faster acting ADRC based LFC of interconnected power system, the variation and effect of network parameters, such as generator inertia constant, generator electrical proximity to the point of impact and tie-line synchronizing co-efficient on the LFC should be considered. The effect of simultaneous load change and individual load change should be studied to proper feedback connection between load rich areas and generation rich areas. All these factors related to the LFC have been illustrated in below.

5.2.1 Effect of Generator Electrical Proximity to the Point of Impact

The effect of generator electrical proximity to the point of impact has been observed by applying a load change as disturbance (0.4 p.u.) to the generation rich area (G_1) from all load rich areas (L_1, L_2 and L_3) in Fig. 5.2. Distance between two areas (G_1 to L_1) has been represented by the corresponding tie-line synchronizing coefficient (T). Higher the value of T lower the distance between two areas. The values of T have been listed in Table A-4[Annexure A].The peak amplitude of ACE, frequency error and tie-line power flow error has been considered as the output response in case of LFC. Since the load impact has been feedback to G_1, the output of LFC has been taken from G_1. L_1G_1 means the load change has been applied from L_1 to G_1. It has been observed that the influence of load change shared immediately by the generators according to their synchronizing power coefficients with respect to the bus at which the load change occurs.

For the application of the same amount of disturbance from various distances to G_1, the response of G_1 has been shown in Fig. 5.2. It has been observed that the magnitude of response has been varied according to the distance between G and L. The magnitude of frequency error due to load change from all load centers has been noticed as same in Fig. 5.2 (b) and it is because of applying the same amount of load change. However, the tie-line power flows of all cases in Fig.

5.2 (c) is not same because the location of the disturbance from G is not same. So the generators of the system have been responded according to the electrical proximity to the point of impact as indicated in Eqs. (63) and (65).

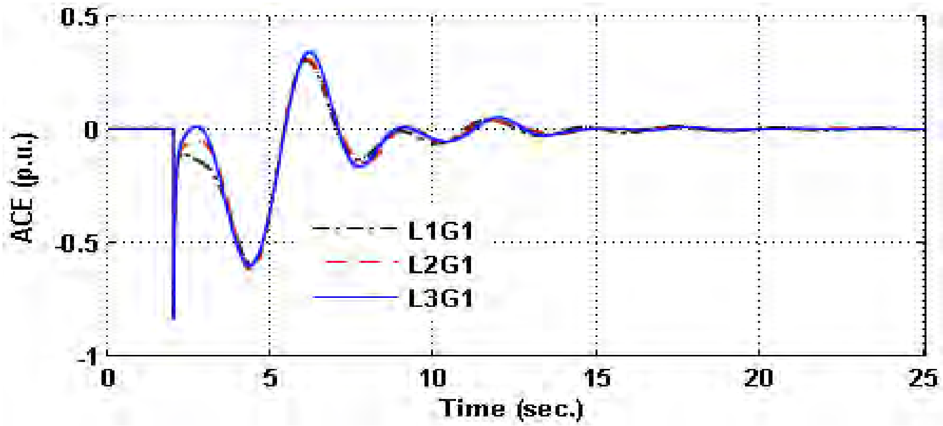

(a)

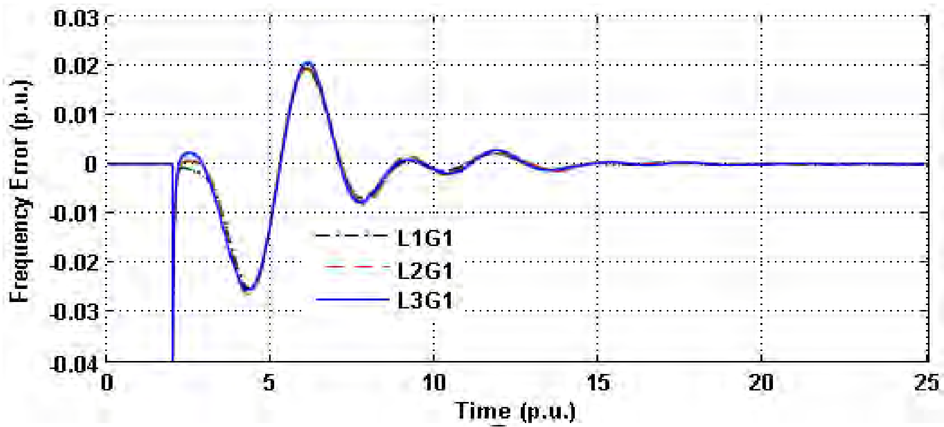

(b)

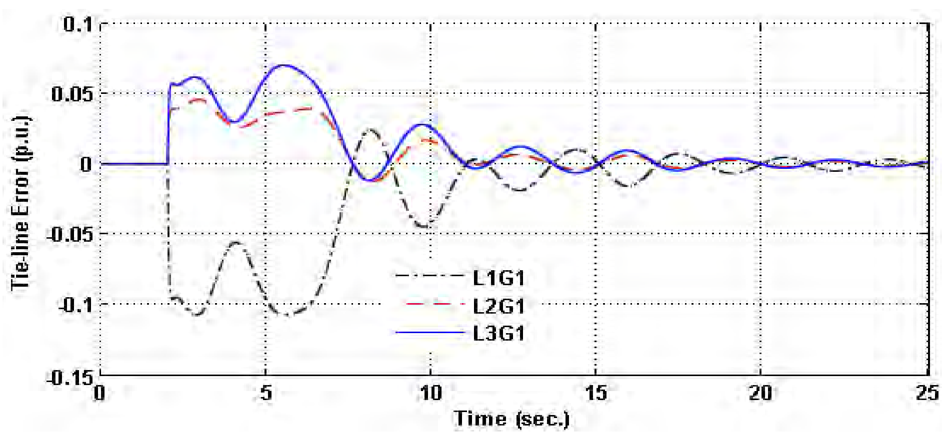

(c)

Fig. 5.2 Effect of electrical proximity to the point of impact on (a) ACE, (b) frequency error, and (c) tie-line error

If it has been desired that the disturbance nearer to the generator will response in almost all and rest of the generators will show smaller responses. It can be achieved by introducing a new gain block referred by Eq. (71) in the dynamic model of the interconnected power system and it has been shown in Fig. 5.4.

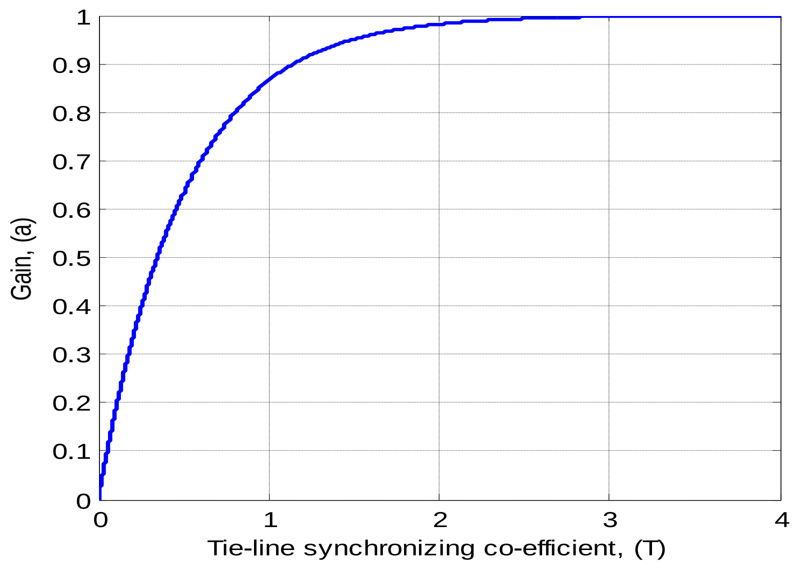

Fig.5.3 Relation between tie-line synchronizing coefficient (T) and new introduced gain (a)

$$a = 1 - e^{-2T} \tag{71}$$

In Eq. (71), T is the value of tie-line synchronizing coefficient and a determined the value of newly introduced gain. Tie-line power exchange of a power system is inversely proportional with the reactance of transmission line [55]. Besides, the reactance of the transmission lines is a function with the length of line. In Fig. 5.3, it has been seen that the value of gain has been varied with the variation of T and at a certain value of T; the value of gain has been fixed. That means generators situated at predetermine distance from the point of impact will show their response according to Eqs. (63) and (65). However, the generators nearer to the point of impact will pick up most of the disturbances.

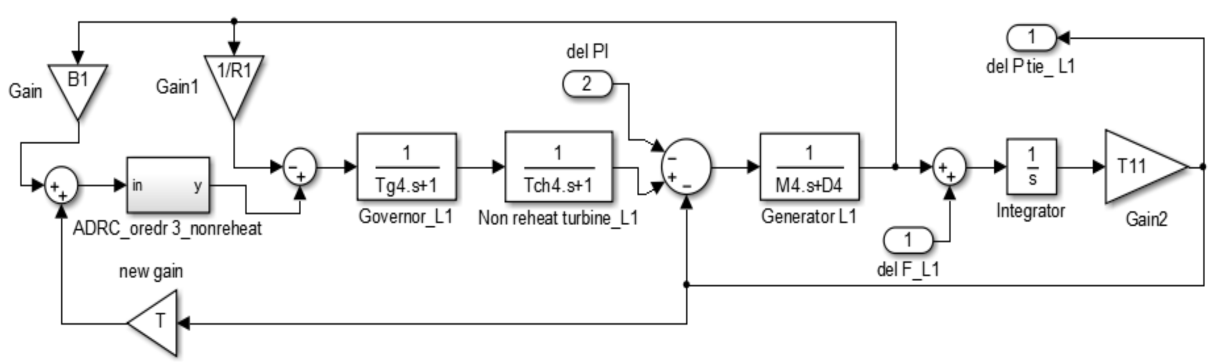

Fig. 5.4 Dynamic model of load change from L_1 to G_1 with new gain block

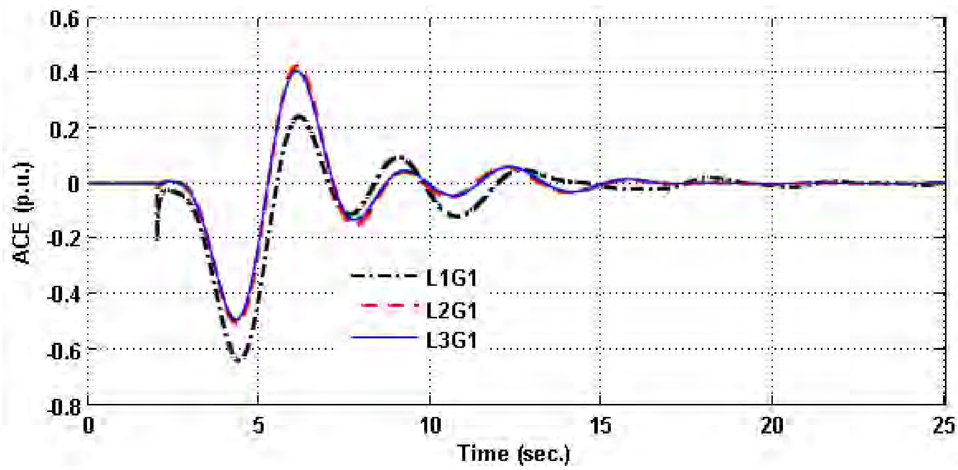

(a)

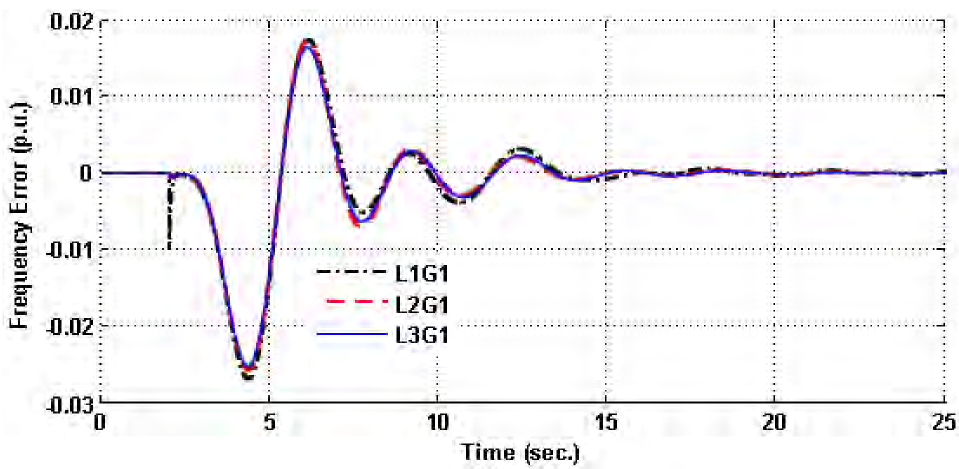

(b)

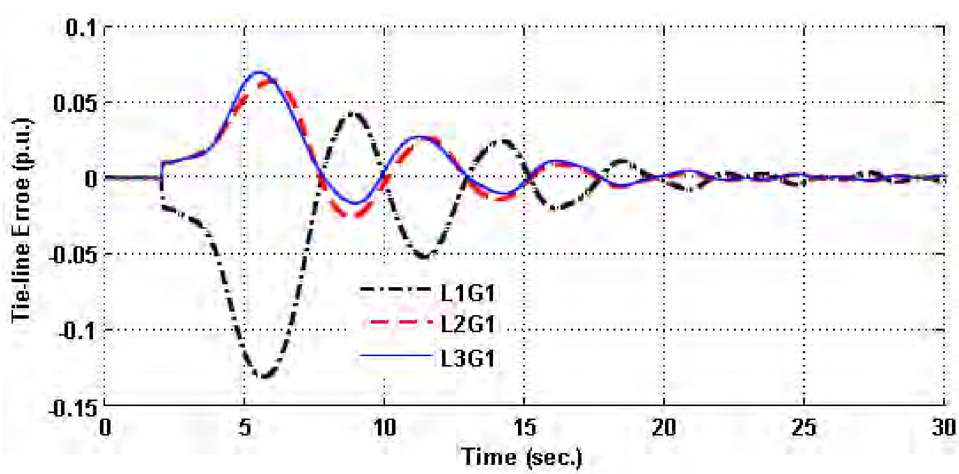

(c)

Fig. 5.5 Effect of electrical proximity to the point of impact on generator G_1 after introducing new gain on (a) ACE, (b) frequency error, and (c) tie-line error

The effects of generator electrical proximity to the point of impact after introducing new gain in an interconnected power system are revealed in Fig. 5.5 where the same amount of disturbance has been applied from the same distances of Fig. 5.2. A comparison study has been presented after and before introducing the new gain block in effect of generator electrical proximity to the point of impact in Table 5.1. Only the error magnitude ACE (p.u.) has been considered for comparison.

It can be seen from Table 5.1 that G_1 is sharing the strongest impact for the application of load change from the L_1. On the other hand, due to the load change from L_2 and L_3, a little influence of disturbance has been observed. The time required for settling down the tie-line power flow error has been observed longer after introducing new gain in Fig. 5.5(c). However, the magnitudes of ACE become lower after introducing the new gain block in Fig 5.5(a). It has been observed that ACE in L_1G_1 has been increased after introducing gain because L_1 is nearest to G_1. ACE increase of any generator means this generator is carrying more disturbances. So it can be said that the generators nearer to the disturbance of an interconnected power system will show the largest response and rest of the generators will show a smaller response.

Table 5.1 Comparison the performance on ACE of electrical proximity before and after introducing new gain with different feedback connection

Feedback Connection	**Tie-line Synchronizing Coefficient (T)**	**ACE (p.u.)**	
		Before Introducing Gain	**After Introducing Gain**
L_1G_1	80	0.59	0.65
L_2G_1	25	0.55	0.53
L_3G_1	50	0.56	0.53

Another study has been presented for the effects of generator electrical proximity to the point of impact in the interconnected power system in Fig. 5.6. The values of T have been listed in Table A-5 [Annexure A]. The disturbance of 0.4 p.u. has been applied from L_1 to G_1, G_2 and G_3 respectively. It has been seen that lowest ACE as 0.55 p.u. belong to G_2 and highest ACE as 0.59 p.u. belong to G_1 due to application of disturbance from L_1. It happens because G_1 is nearer to L_1 than G_2.

Again, if it is desired that the generator nearest to the disturbance will show the greatest response and rest of the generators will show smallest response, it can be achieved by introducing new gain block where same amount of disturbance has been applied on different generators. Fig. 5.7

shows that lowest ACE as 0.45 p.u. belong to G_3 and highest ACE as 0.65 p.u. belong to G_2 due to application of disturbance from L_1. The G_2 is the closest generator from the disturbance L_1.

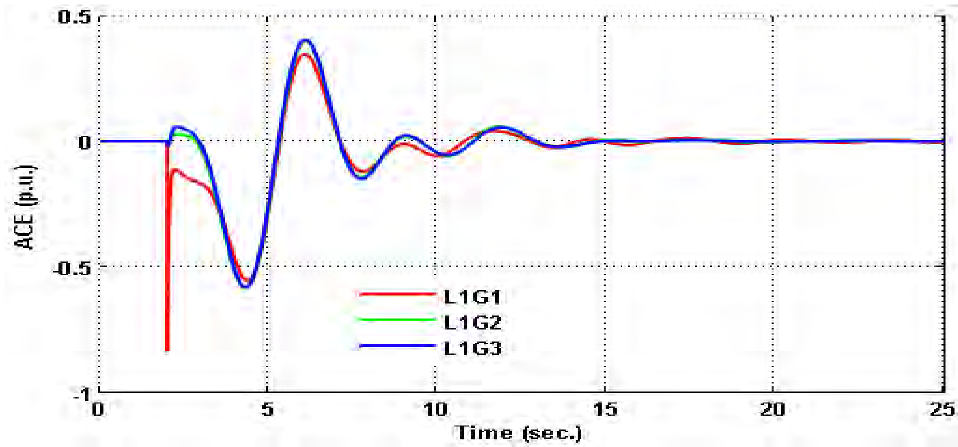

(a)

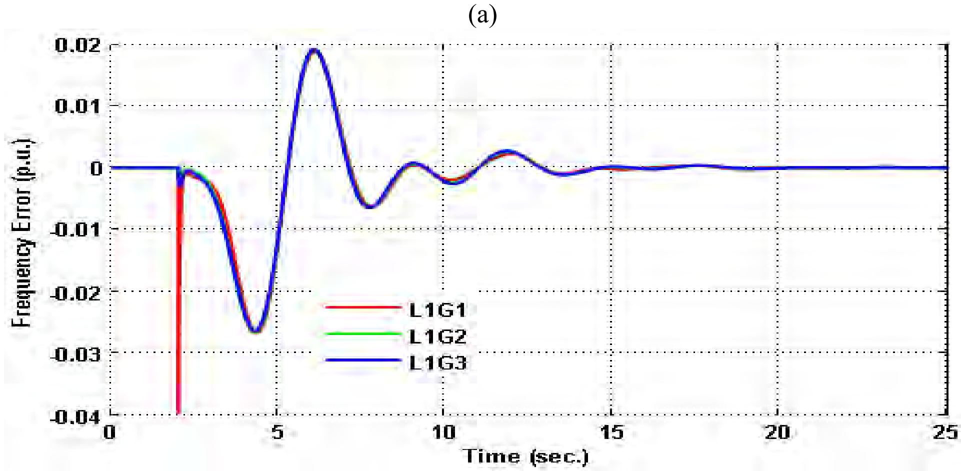

(b)

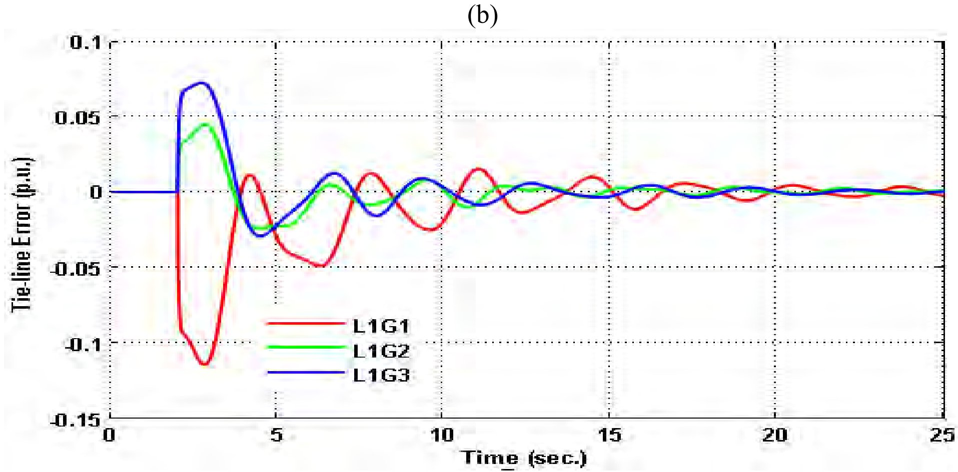

(c)

Fig. 5.6 Effect of electrical proximity to the point of impact for the same load change on different generator on (a) ACE, (b) frequency error, and (c) tie-line error

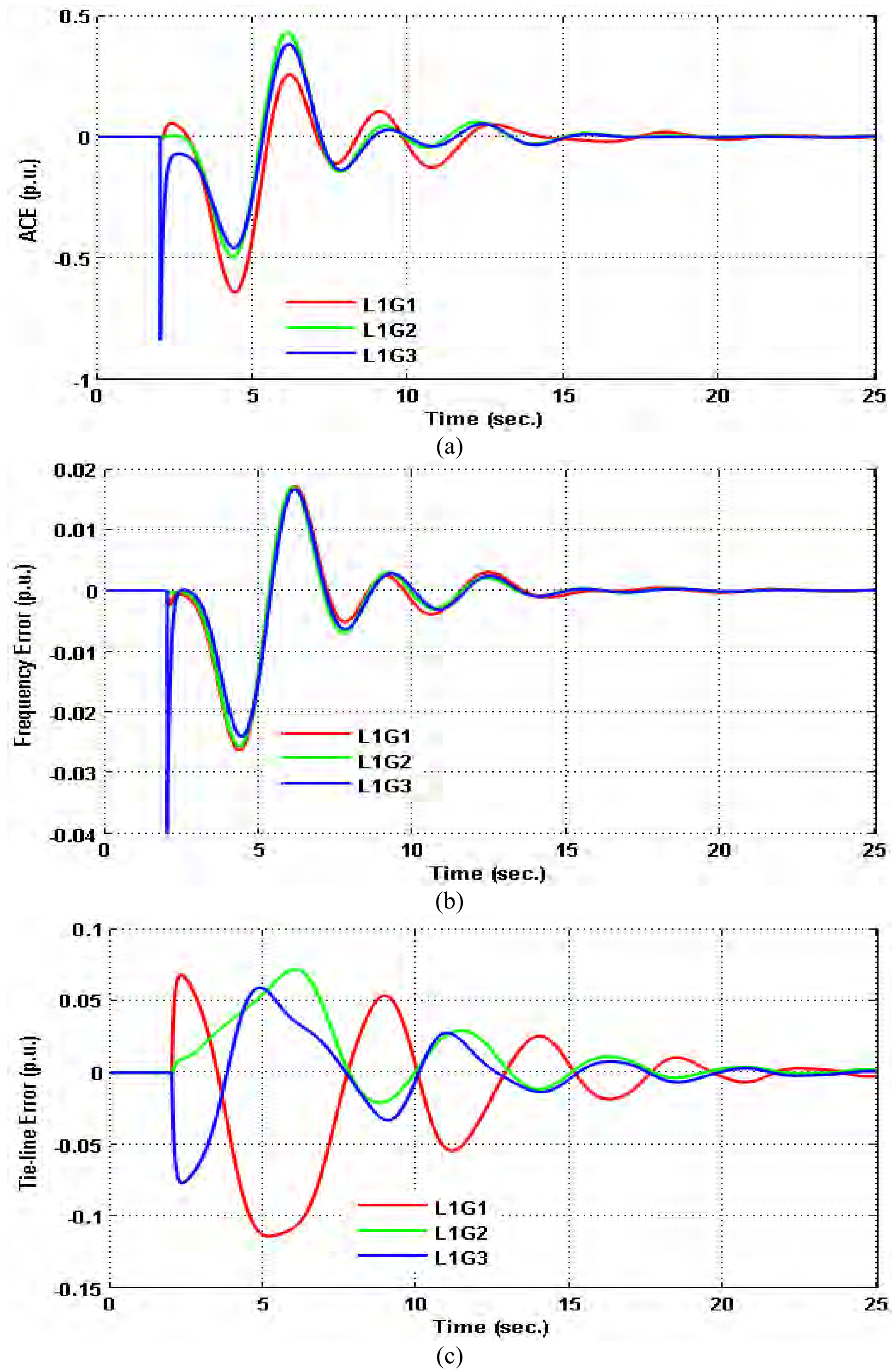

Fig. 5.7 Effect of electrical proximity to the point of impact for the same load change on different generator after introducing new gain on (a) ACE, (b) frequency error, and (c) tie-line error

The effect of generator electrical proximity to the point of impact has been studied by applying the same amount of disturbance from Li to G_1, G_2 and G_3 after introducing newly gain block in Fig.5.8. A comparison has been presented on ACE after and before introducing new gain block in Table 5.2. It has been observed that responses of L_1G_1 is highest (0.65 p.u.) than others.

Table 5.2 Comparison the performance on ACE of electrical proximity before and after introducing new gain with different feedback connection

Feedback Connection	**Tie-line Synchronizing Coefficient (*T*)**	**ACE (p.u.)**	
		Before Introducing Gain	**After Introducing Gain**
L_1G_1	25	0.55	0.50
L_1G_2	30	0.59	0.65
L_1G_3	28	0.58	0.45

5.3.2 Effect of *H*-Constant of Generator

The effect of H-constant of generator on LFC has been studied by applying a load change of 0.1 p.u. at t = 2 sec. by considering the different values of H constant. The output of LFC as ACE, frequency error and tie-line error has been presented in Fig. 5.8 after the application of disturbance.

It has been observed that minimum ACE belongs to the generator that has larger inertia constant (H = 7) and highest error magnitude belong to the generator which has lowest inertia constant (H = 3) in Fig. 5.8(a). The magnitude of frequency error for all cases has been examined almost same due to the same amount of load change applied. The oscillation of tie-line power flow error has been observed highest for the inertia constant (H = 3) and lowest for (H = 5) in Fig. 5.8(c) because the generator's having higher inertia constant is capable of continuing the stable operation during the disturbance.

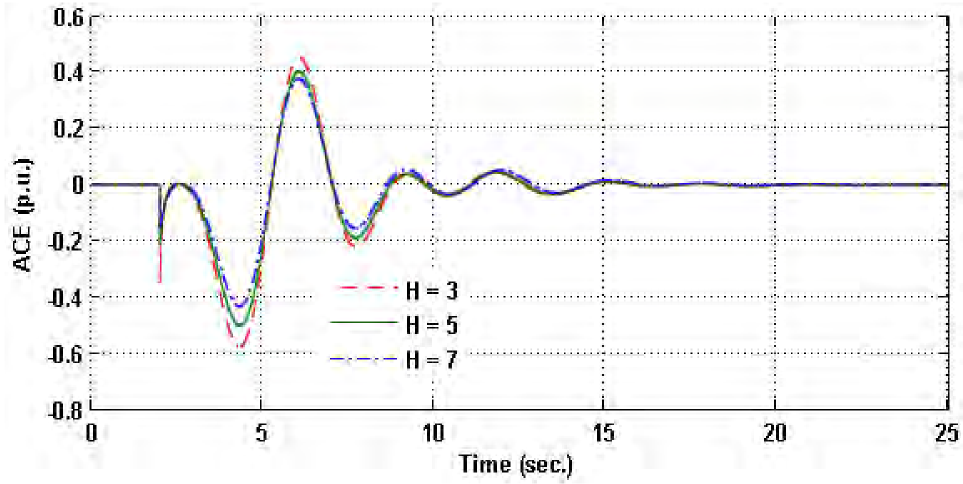

(a)

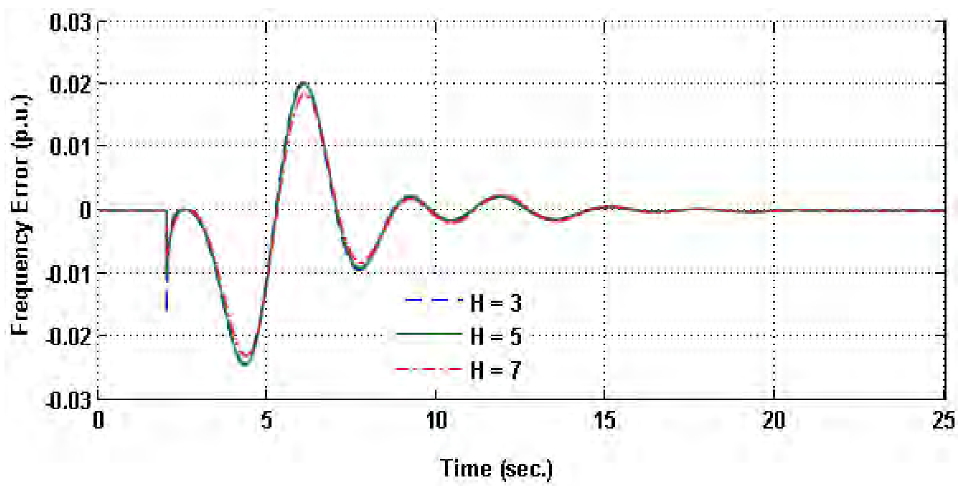

(b)

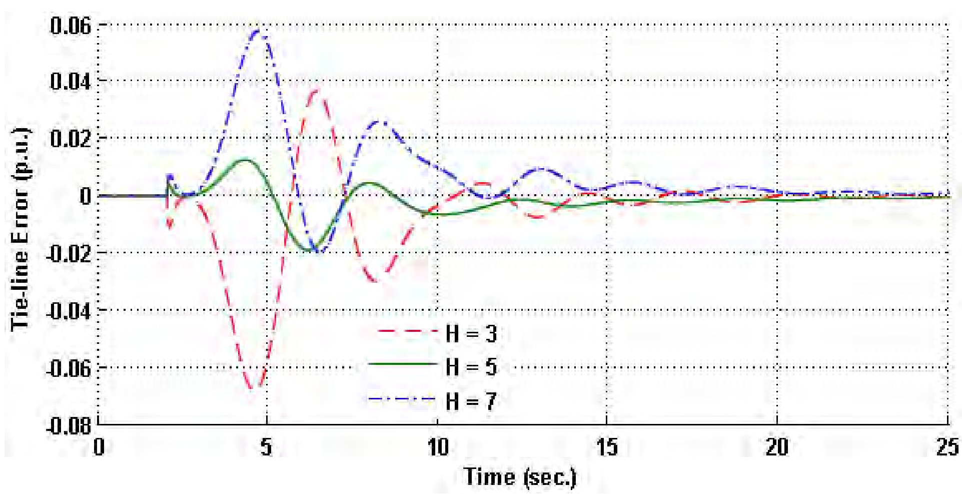

(c)

Fig. 5.8 Effect of *H*-parameter on (a) ACE, (b) frequency error, and (c) tie-line error

If it is desired that a generator with higher inertia constant should responds more during the disturbance. As a result, the interconnected power system will be able to carry more disturbances without any blackout. To achieve this, it is necessary to add an extra gain block to the dynamic model of the system. The value of extra gain block can be determined by normalizing the H-constant of existing generators. The average value of three generator's H-constant is 5, so normalized value has been considered as 5. The value of new gain block has been calculated by dividing the generator's *H* constant by 5. The system of normalizing the H-constant has been given in Table 5.3. The effect of H constants in LFC of an interconnected power system by introducing new gain has been represented in Fig. 5.10 by applying the same amount of disturbance as to in Fig. 5.8. The process of introducing new gain block has been shown in Fig. 5.9.

Table 5.3: Normalizing system of *H*-constant

Value of *H* Parameter	**Normalized Value**	**Value of New Gain**
3	5	3/5
5		1
7		7/5

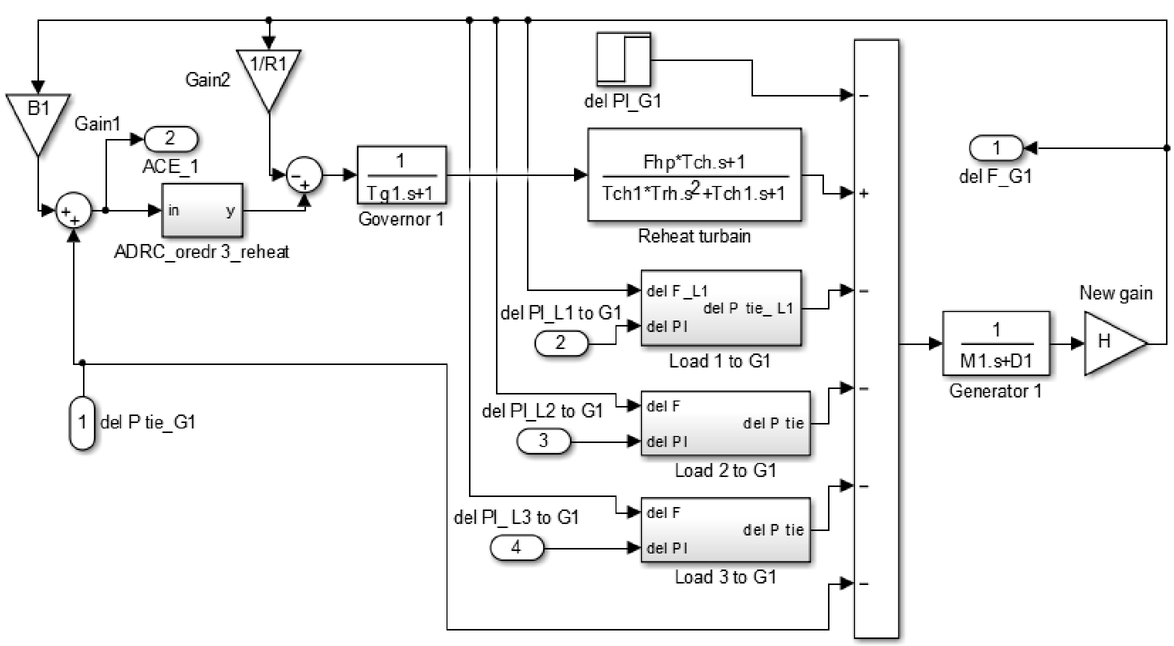

Fig. 5.9 Dynamic model of power plant 1 with new introduced gain

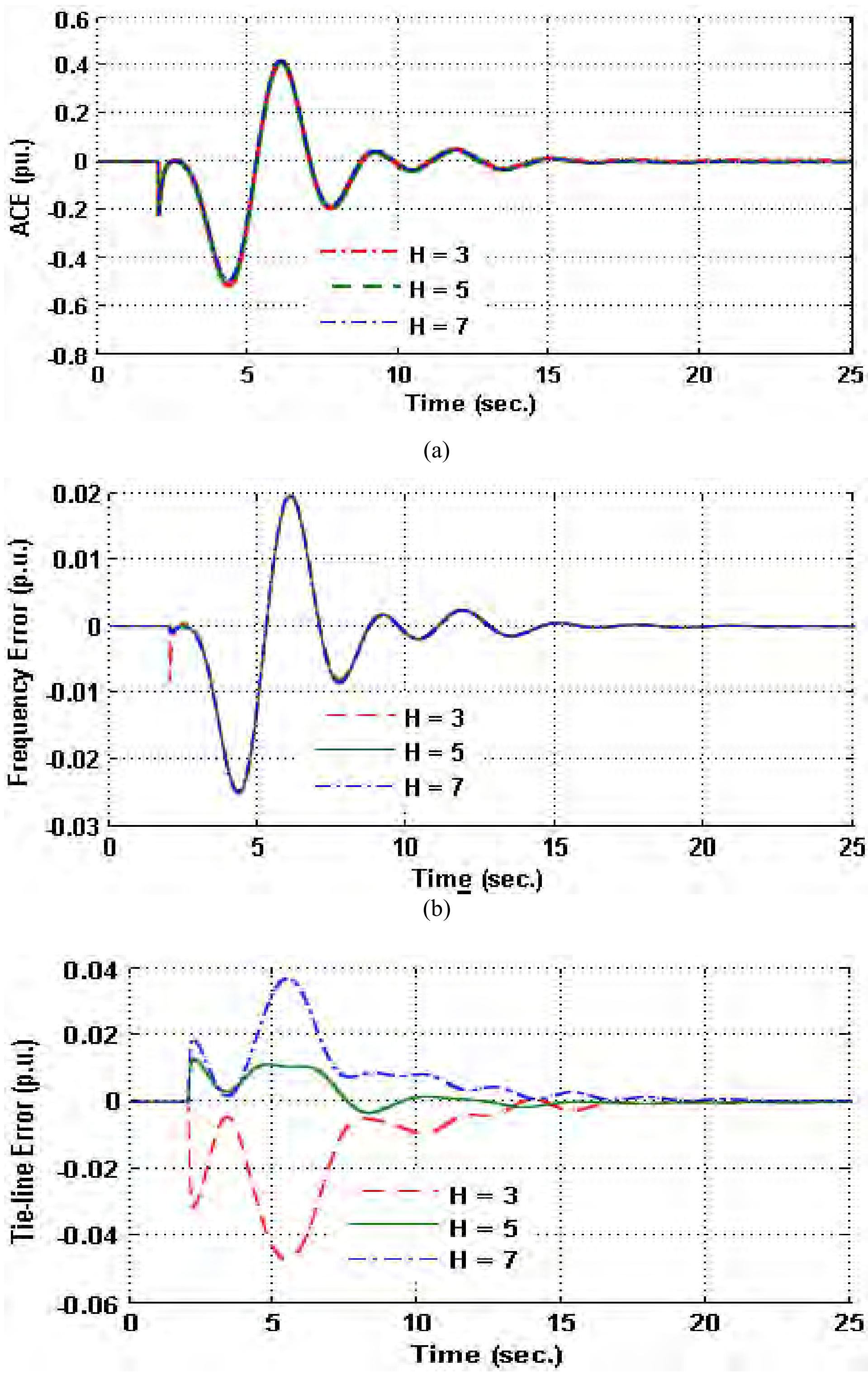

Fig. 5.10 Effect of *H* parameter on (a) ACE, (b) frequency error, and (c) tie-line error after introducing an extra gain block

It is seen from the Fig. 5.10, the responses of all generators are almost same and the magnitudes become lesser after applying the normalized gain parameters. So all the generators are showing same responses regardless of their *H*-parameter and time required to settle down the responses become lesser in Fig. 5.10.

5.3 Selection of Feedback Paths

In an interconnected complex power system, feedback connection is of great importance for its stability. Loads of all load centers may change either simultaneously or individually. Following study has been provided for selecting the feedback path. This works it is shown that consideration of individual load change is enough for selecting the right feedback paths rather than considering simultaneous load change of all load centers.

5.3.1 Effect of Simultaneous Load Changes

Possible feedback paths between load rich area and generation rich area has been shown in Fig. 11 by considering three generation rich areas and three load rich areas (3G3L). A certain feedback path L_1G_1 L_2G_2 L_3G_3 has been presented in Fig.12.

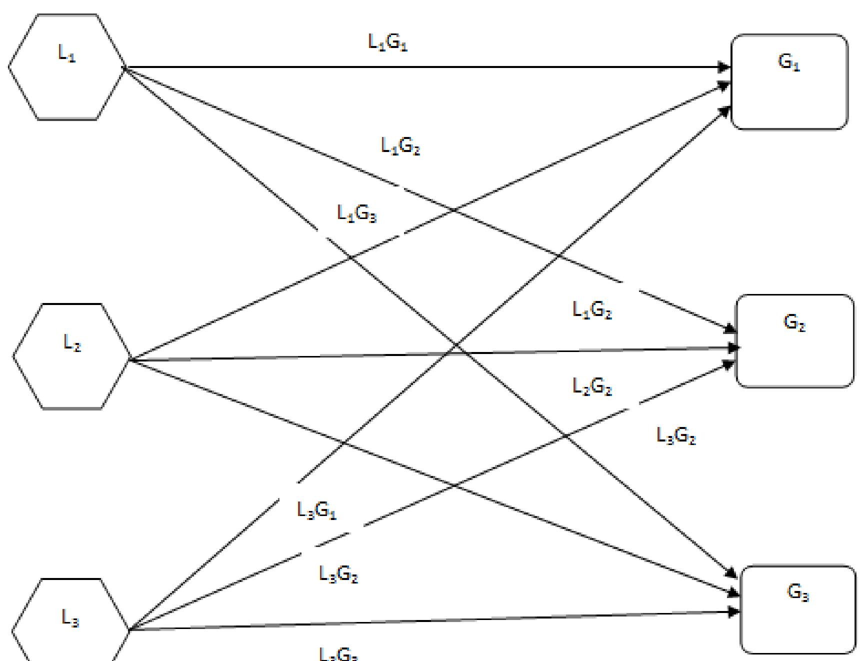

Fig. 5.11 Possible feedback paths between load rich areas and generation rich areas

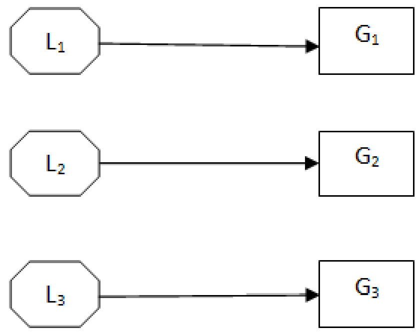

Fig. 5.12 Feedback paths: L_1G_1, L_2G_2 L_3G_3

The effects of simultaneous load changes on ACE, frequency error and tie-line error of the interconnected power system have been studied. A 0.1 p.u. load change has been applied simultaneously from L_1, L_2 and L_3. Considering all possible feedback paths Table 5.5 has been completed. For easily understanding Figs. 5.13 and 5.14 have been shown here and rest of the figures are given in Annexure A.

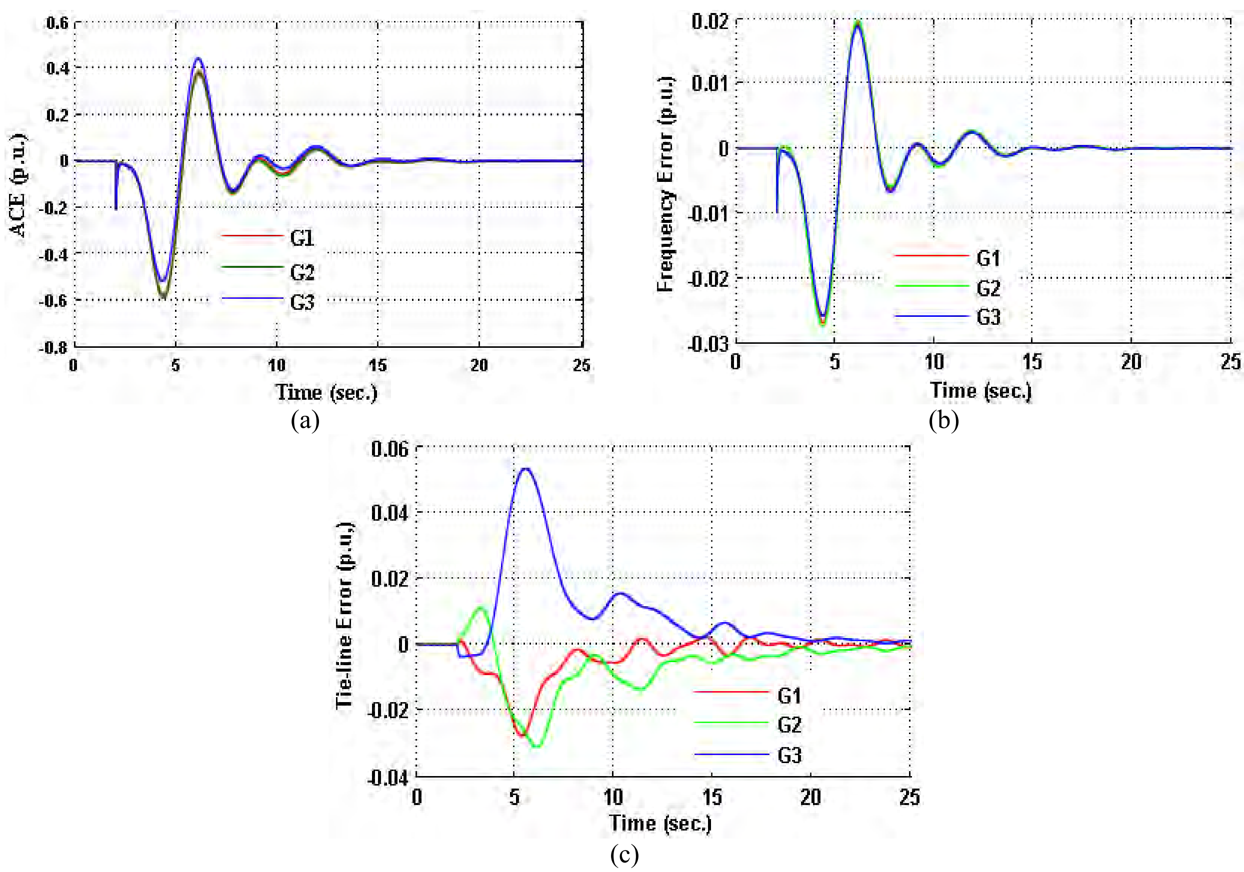

Fig 5.13 Effect of simultaneous load change on (a) ACE, (b) frequency error, and (c) tie-line error for feedback paths : L_1G_1 L_2G_2 L_3G_3

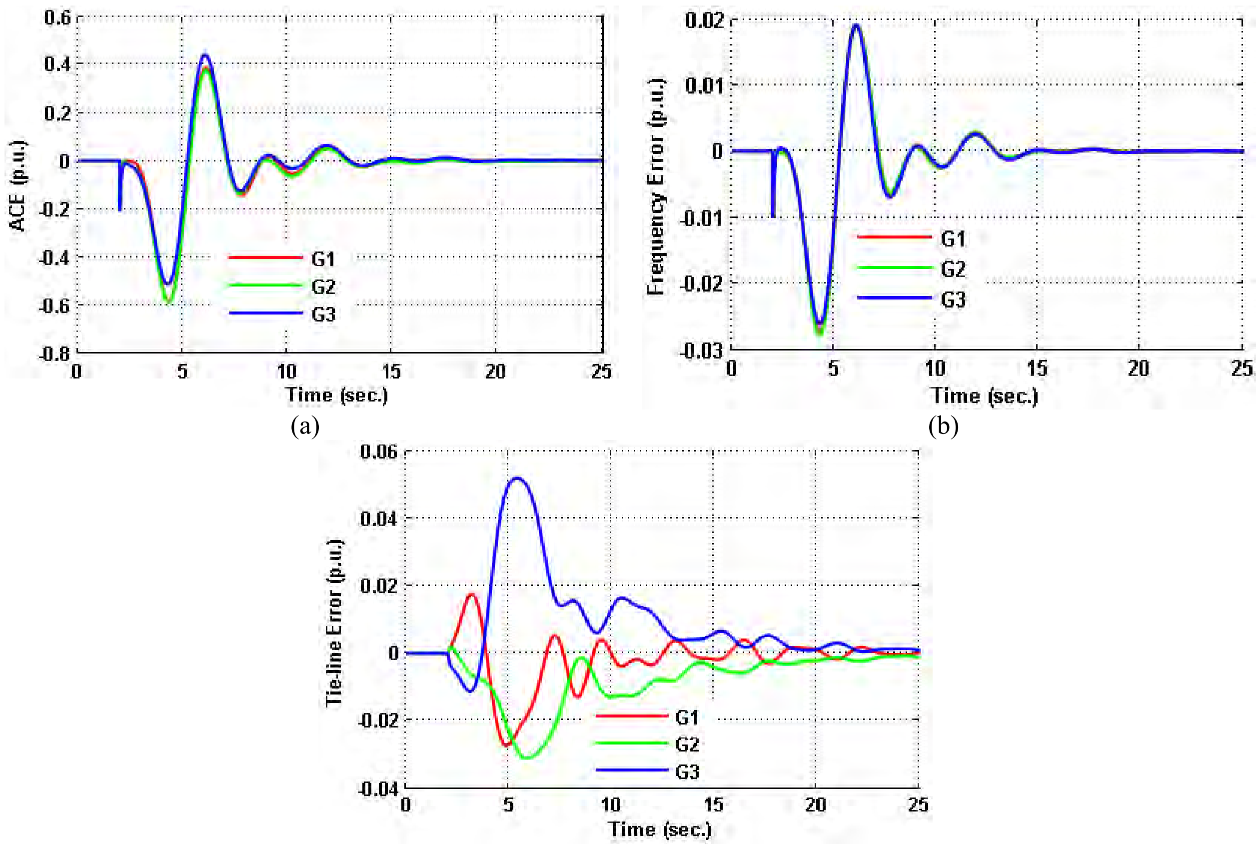

(c)

Fig 5.14 Effect of simultaneous load change on (a) ACE, (b) frequency error, and (c) tie-line error for feedback paths: L_2G_1 L_1G_2 L_1G_3

Table 5.4 Effect of simultaneous load change on ACE, frequency error and tie-line error for various feedback connections

Sl. No	Feedback Connection	ACE (p.u.)	Δf (p.u.)	ΔP_{12} (p.u.)
1	$L_1G_1L_1G_2L_1G_3$	0.5900	2.75 e-2	5.33 e-2
2	L_1G_1 L_1G_2 L_2G_3	0.5910	2.74 e-2	5.40 e-2
3	L_1G_1 L_1G_2 L_3G_3	0.5915	2.74 e-2	5.33e-2
4	$L_1G_1L_2G_2$ L_1G_3	0.5960	2.78 e-2	5.30 e-2
5	L_1G_1 L_2G_2 L_2G_3	0.5987	2.78 e-2	5.37 e-2
6	L_1G_1 L_2G_2 L_3G_3	0.6000	2.78 e-2	5.31 e-2
7	L_1G_1 L_3G_2 L_1G_3	0.5850	2.75 e-2	5.30 e-2
8	L_1G_1 L_3G_2 L_2G_3	0.5869	2.75 e-2	5.38 e-2
9	L_1G_1 L_3G_2 L_3G_3	0.5875	2.75 e-2	5.28 e-2
10	$L_2G_1L_1G_2L_1G_3$	0.5901	2.75 e-2	5.17 e-2
11	L_2G_1 L_1G_2 L_2G_3	0.5912	2.74 e-2	5.22 e-2
12	L_2G_1 L_1G_2 L_3G_3	0.5915	2.74 e-2	5.29 e-2
13	$L_2G_1L_2G_2$ L_1G_3	0.5960	2.78 e-2	5.52 e-2
14	L_2G_1 L_2G_2 L_2G_3	0.5990	2.78 e-2	5.19 e-2
15	L_2G_1 L_2G_2 L_3G_3	0.5950	2.78 e-2	5.27 e-2
16	L_2G_1 L_3G_2 L_1G_3	0.5860	2.74 e-2	5.51 e-2
17	L_2G_1 L_3G_2 L_2G_3	0.5876	2.73 e-2	5.21 e-2
18	L_2G_1 L_3G_2 L_3G_3	0.5876	2.73 e-2	5.24 e-2
19	$L_3G_1L_1G_2L_1G_3$	0.5901	2.75 e-2	5.17 e-2
20	L_3G_1 L_1G_2 L_2G_3	0.5925	2.75 e-2	5.67 e-2
21	L_3G_1 L_1G_2 L_3G_3	0.5895	2.75 e-2	5.59 e-2
22	$L_3G_1L_2G_2$ L_1G_3	0.5970	2.79 e-2	5.57 e-2
23	L_3G_1 L_2G_2 L_2G_3	0.5995	2.79 e-2	5.65 e-2
24	L_3G_1 L_2G_2 L_3G_3	0.600	2.79 e-2	5.59 e-2
25	L_3G_1 L_3G_2 L_1G_3	0.586	2.74 e-2	5.58 e-2
26	L_3G_1 L_3G_2 L_2G_3	0.5881	2.74 e-2	5.65 e-2
27	L_3G_1 L_3G_2 L_3G_3	0.5885	2.74 e-2	5.51 e-2

5.3.2 Effect of Individual Load Change

How load change may apply individually from a load rich area (L_1 to G_1) has been presented in Fig.5.15. To investigate the effect of individual load change on ACE, frequency error and tie-line error from load rich area to generation rich area, 0.1 p.u. load change at t = 2 second has been applied. The output of LFC for various feedback connections have been illustrated in Figs. 5.16 and 5.17 and the summary of this study has been presented in Table 5.6. For easily understanding Figs. 5.16 and 5.17 has been shown here and rest of the Figs. has been given in Annexure A.

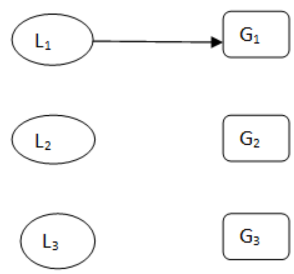

Fig. 5.15 Feedback path: L_1G_1

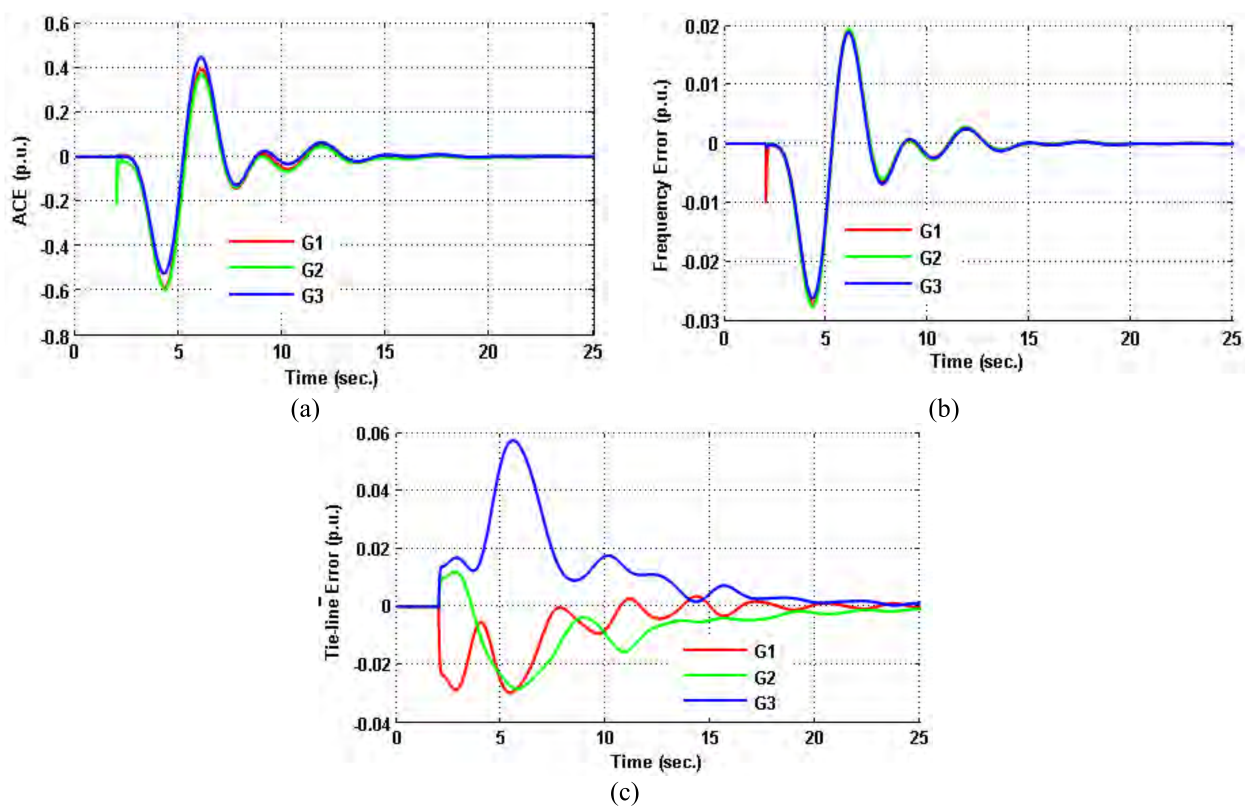

Fig. 5.16 Effect of individual load change on (a) ACE, (b) frequency error, and (c) tie-line error for feedback path L_1G_1

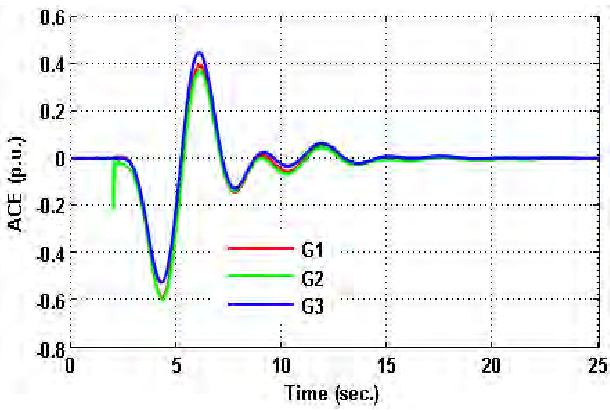

(a)

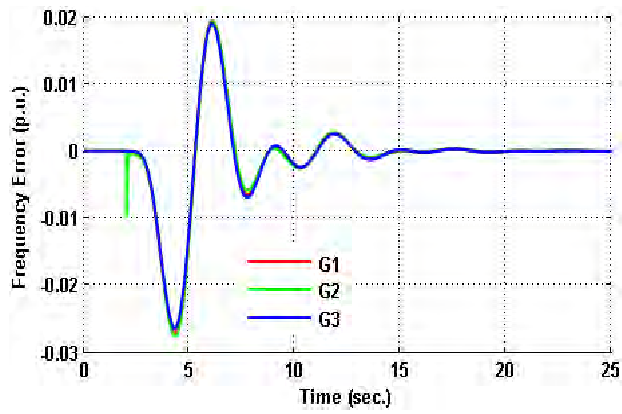

(b)

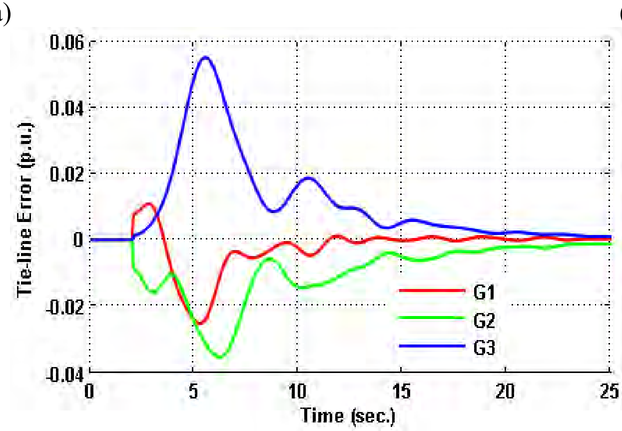

(c)

Fig. 5.17 Effect of individual load change on (a) ACE, (b) frequency error, and (c) tie-line error for feedback path: L_2G_1

Table 5.5 Effect of individual load change on ACE, frequency error and tie-line error for various feedback connections

Sl. No.	**Feedback Connection**	**ACE (p.u.)**	**Δf (p.u.)**	**ΔP_{12} (p.u.)**
1	L_1G_1	0.5950	0.0276	0.0572
2	L_2G_1	0.5958	0.0276	0.0555
3	L_3G_1	0.5960	0.0276	0.0600
4	L_1G_2	0.5915	0.0275	0.0550
5	L_2G_2	0.5990	0.0790	0.0546
6	L_3G_2	0.588	0.0274	0.0550
7	L_1G_3	0.5925	0.0277	0.0510
8	L_2G_3	0.5950	0.0276	0.0511
9	L_3G_3	0.5955	0.0277	0.0512

It is seen from Table 5.4 and 5.5; the lowest error magnitude has been obtained from the feedback path: L_1G_1 L_3G_2 L_1G_3 which is also same as the individual load change from L_1 to G_1, L_3 to G_2 and L_1 to G_3. Hence consideration of individual load change is enough for selecting the right feedback paths rather than considering simultaneous load change of all load centers.

5.4 Fast Acting ADRC based LFC

The comparison study among standard ADRC, ADRC with considering tie-line synchronizing co-efficient (T) and generator H-constant on ACE for LFC has been tabulated in Table 5.6. Load change of 0.1 p.u. has been applied from L_1, L_2 and L_3.

Table 5.6 Comparison among standard ADRC, ADRC with T and H-constant for ADRC based LFC

Sl. no.	**ADRC type**	**ACE (p.u.)**		
	Feedback Connection	**L_1G_1**	**L_1G_2**	**L_1G_3**
1	Standard ADRC	0.58	0.57	0.55
2	ADRC with T consideration	0.60	0.54	0.525
3	ADRC with T and new introduced gain consideration	0.83	0.50	0.45
4	ADRC with H-constant consideration	0.575	0.50	0.43
5	ADRC with H-constant and new introduced gain consideration	0.52	0.52	0.51

Magnitude of ACE represents the response of generator. The higher the magnitude of ACE of generator belongs to higher response due to load change. It can be seen from the second column of Table 5.6 that due to the same amount of disturbance, response of L_1G_1 becomes highest. Since, G_1 has been considered as nearest to the disturbance. In third row, due to new introduced gain with T consideration, error magnitude (ACE) of L_1G_1 has increased from 0.60 p.u. to 0.83 p.u. On the other hand, the error magnitudes have been decreased in L_1G_2 and L_1G_3. So nearest generator is carrying the highest impact of disturbance.

In fourth row, the H-constant of generator have been considered as 3, 5 and 7 for G_1, G_2 and G_3 respectively. So, due to the application of disturbance, the response of G_1 become highest where it is lowest of G_3. But, if all the generators of an interconnected power system response equally during the disturbance, then the generator's with higher *H*-constant will share the higher impact of load change.. It has been achieved by introducing new gain in fifth row.

So it can be said that it is a fast acting ADRC based LFC.

5.5 Summary of the Chapter

In this chapter, an ADRC based LFC of interconnected power system consisting of three generation rich areas and three load rich areas (3G3L) has been considered. A brief description of network elements of interconnected power system- tie-line synchronizing coefficient, generator inertia constant and generator electrical proximity to the point of impact has been given. In the last part of this chapter, the simulation result of effects of tie-line synchronizing coefficient, generator inertia constant and generator electrical proximity to the point of impact in ADRC based LFC of an interconnected power system has been presented.

Chapter VI
Conclusions

6.0 Introduction

This thesis proposed a faster acting ADRC based load frequency controller for interconnected power systems considering effect of generator electrical proximity to the point of impact, effect of inertia constant of generator. The main goal of LFC is to regulate the predetermined frequency but in this paper, the ACE has been considered in most of the cases. LFC regulates ACE to zero such that frequency and tie-line power errors are forced to zero. Also the proper feedback paths between load rich areas and generation rich areas of an interconnected power system have been presented.

6.1 Outcomes of this Thesis

Effectiveness of ADRC: ADRC shows superior advantages and effectiveness for LFC of power system over conventional control techniques such as PID control.

Parameterization of ADRC for LFC of power system: In ADRC based load frequency control, a controller bandwidth of 4 rad/sec for both power system (single- and multi- area) and selecting the observer bandwidth four times of controller bandwidth gives good result for single area power system. However, observer bandwidth should five times of controller bandwidth for multi-area power system to get the lower settling time and minimum ACE.

Effect of Generator Electrical Proximity to the Point of Impact: The machines electrically close to the point of impact always pick up the greater share of the load regardless of their size as the same in [51]. Moreover, in an interconnected power system, it is possible for the nearest generator to response at all for the occurrences of any disturbances and other generator will show a little bit response for the same disturbance by introducing a new gain determined by (71).

Effect of Inertia Constant of Generator: After a brief transient period the machines share in increase in load as a function only of their inertia constants as mention in [51]. In addition, in an interconnected power system, it is possible that all the generators connected with the system share the same amount of load change by introducing a new gain which can be determined by normalizing the entire generator’s inertia constant.

Selection of feedback paths between load rich area and generation rich area: Consideration of individual load change is enough for selecting the right feedback paths rather than considering simultaneous load change of all load centers. The farthest load rich area from the generation rich area should be feedback first.

6.2 Future work

In the future, the following research on both ADRC and the power system is expected to be conducted.

6.2.1 Improvement of ADRC

In the thesis, the designed ADRC can guarantee the fast response of the ACE with small overshoot. However, during the process of simulating ADRC in a power system, the magnitude of the control effort shows a big peak value at the initial stage of the simulation and the time required to settle down the response is long. There is a scope to reduce the peak amplitude of response and quickly settle down the response by improving the ADRC controller as well as ESO.

6.2.2 Improvements in Parameterization

In the future, the parameters for LFC of two- and three- area power system with re-heat turbines and hydro-electric turbine should be studied. It will help to enhance the range of applications of higher order ADRC to the power system.

6.2.3 Improvements in Power System Modeling

In this thesis, ADRC based LFC of interconnected power system has been considered with non-reheat and reheat turbine only but another commonly used turbine named hydraulic turbine has not been considered. For analyzing the LFC of interconnected power system, hydraulic turbine unit should be considered.

Reference:

[1] P. Kundur, Power System Stability and Control. New York: McGraw-Hill, 1994.

[2] U.S.-Canada Power System Outage Task Force, Interim Report: Causes of the August 14th Blackout in the United States and Canada, November 2003.

[3] Y.V. Makarov,V.I. Reshtov, V. A. Strove, et al., Blackout prevention in the United States, *Europe and Russia, Proc. IEEE*, 93 (11), pp. 1942- 1995, 2005.

[4] Q. Ahsan, A. H. Chowdhury, S. S. Ahmed, I. H. Bhuyan, A. Haque, and H. Rahman, “Frequency dependent auto load shedding scheme to prevent blackout in Bangladesh Power System,” in *Proc. 4th IASTED Asian Conf. Power and Energy Systems*, Phuket, Thailand, Nov. 24–26, 2010.

[5] Ibraheem; P. Kumar, and D.P. Kothari, “Recent philosophies of automatic generation control strategies in power systems,” *IEEE Transactions on Power Systems*, vol. 20(1), pp. 346-357, Feb 2005.

[6] Ibraheem, and P. Kumar, “Overview of power system operation and control philosophies,” *International Journal of Power and energy System*, vol. 26(1), pp. 203-214, 2006.

[7] D.R. Chaudhary, “*Modern control engineering,*” 3rd edition, PHI, Private Limited, 2005.

[8] D.M. Vinod Kumar, “Intelligent controllers for automatic generation control,” In Proc. 1998 IEEE region 10 International Conference on Global connectivity in Energy, Computer, Communication and Control, pp. 557-574, 1998.

[9] M.E. Mandour, E.S. Ali, M.E. Lotfy, “Modern Electric Power Systems (MEPS), *Proceedings of the International Symposium*, Wroclaw, pp. 1- 6, sep. 2010.

[10] C.S. Chang, W. Fu., and F. Wen, “Load frequency control using genetic algorithm based fuzzy gain scheduling of PI controllers,” *J. of Elect. Machines Power Syst.*, vol. 26(1), pp. 39–52, Jan 1998.

[11] J. Talaq, and F. Al-Basri, “Adaptive fuzzy gain scheduling for load frequency control,” *IEEE Trans. Power Syst*., vol. 14(1), pp. 145–150, Feb 1999.

[12] A. Morinec, and F. Villaseca, “Continuous-Mode Automatic Generation Control of a Three-Area Power System,” *The 33rd North American Control Symposium,* pp. 63–70, 2001.

[13] X. Yu, K. Tomsovic, “Application of Li near Matrix Inequalities for Load Frequency Control with Communication Delays”, *IEEE Transaction on Power Systems* , vol. 19, no. 3, pp.1508-1515, Aug. 2004.

[14] Y. L. Karnavas; and D.P. Papadopoulos, “AGC for autonomous power system using combined intelligent techniques,” *Elect. Power Syst. Res*., vol. 62(3), pp. 225-239, Jul 2002.

[15] A. Rubaai, and V. Udo, “Self-tuning LFC: Multilevel adaptive approach,” *Proc. Inst. Elect. Eng. Generation, Transmission, Distrib.,* vol. 141(4), pp. 285–290, Jul 1994.

[16] J. Han, “From PID to Active Disturbance Rejection Control,” IEEE Transactions on Industrial Electronics, vol. 56, no. 3, March 2009 pp 900 – 906.

[17] B. Anand; A. Ebenezer Jeyakumar, “Load frequency control with fuzzy logic controller considering non-linearities and boiler dynamics,” *ICGST-ACSE Journal,* vol. 8, pp. 15-20, Jan 2009.

[18] Q.P. Ha, “A fuzzy sliding mode controller for power system load frequency control,” In Proc. second international conference on knowledge based intelligent electronic systems, pp. 149-154, 1998.

[19] T. Hiyama, “Robustness of fuzzy logic power system stabilizers applied to multi machine power systems,” *IEEE Trans. on Energy Conversion*, vol. 9(3), pp. 451-459, Feb 1994.

[20] A. Ismail, “Robust load frequency control*,”* in Proc. IEEE Conf. Contr. App., 2, New York, Dayton, OH, 634–5, Sep.

[21] X. Meng, X. Gong, X. Feng, X. Zheng, and W. Zhang, “ PI fuzzy sliding mode load frequency control of multiarea interconnected power systems,” *Proceedings of the 2003 IEEE International Symp*. On Intelligent Control, Houston, Texas, pp. 5-8, Oct 2003.

[22] D. XIUXIA, L. PINGKANG, “Fuzzy logic control optimal realization using GA for multi-area AGC systems,” *Int. J. Inf. Technol.,* vol. 12(7), pp. 63–72, 2006.

[23] Chaturvedi D.K, “*Soft Computing: Applications to Electrical Engineering Problem,”* 1st ed., Springer Verlag, 2007.

[24] R. Umrao, and D.K. Chaturvedi, “Load Frequency Control using Polar Fuzzy Controller,” IEEE conference, Tencon, Fukuoka, Japan, pp. 557- 562, 21-24 November 2010.

[25] D.K. Chaturvedi, O.P. Malik, and U.K. Choudhury, “Polar fuzzy adaptive power system stabilizer,” *The Institution of Engineers(India),* vol. 90, pp. 35-45, 2009.

[26] A. Demiroren, Sengor N.S., and H.L. Zeynelgil, “Automatic generation control by using ANN technique,” Elect. Power Compon. Syst., vol. 29(10), pp. 883–896, Oct 2001

[27] ADITYA, “Design of Load Frequency Controllers Using Genetic Algorithm for Two Area Interconnected Hydro Power System,” *Electric Power Components and Systems*, vol. 31(1),

pp. 81-94, Jun 2010.

[28] S. Bhongade, B. Tyagi, H.O. Gupta, “Genetic algorithm based PID controller design for a multi-area AGC scheme in a restructured power system,” *International Journal of Engineering, Science and Technology*, Vol. 3(1), pp. 220-236, 2011.

[29] B.S.A. Omari, and A.S.A. Hinai, “Design of PID-Swarm Load Frequency Controller of Interconnected Power System,” International Conference on Communication, Computer & Power (ICCCP’07) Muscat, pp. 1-5, Feb. 2007.

[30] S.M.S. Boroujeni, B.K. Boroujeni, M. Abdollahi, and A. Delafkar, “Multi-area Load Frequency Control using IP Controller Tuned by Particle Swarm Optimization*,” Research Journal of Applied Sciences, E&T*, vol. 3(12), pp.1396-1401, 2011.

[31] .F. Juang, “A hybrid of genetic algorithm and particle swarm optimization for recurrent network design*,” IEEE Trans. Syst*., vol. 34(2), pp. 997–1006, Nov 2004.

[32] S.K. Aditya, and D. Das, “Design of load frequency controllers using genetic algorithm for two area interconnected hydro power system*,”Elect. Power Compon. Syst*., vol. 31(1), pp. 81–94, Jan 2003.

[33] M. Kothari, N. Sinha and M. Rafi, “Automatic Generation Control of an Interconnected Power System under Deregulated Environment,” Power Quality,vol. 18, pp. 95–102, Jun. 1998.

[34] A. Morinec, and F. Villaseca, “Continuous-Mode Automatic Generation Control of a Three-Area Power System,” *The 33rd North American Control Symposium,* pp. 63–70, 2001.

[35] Z. Gao, Y. Huang, and J. Han, “An Alternative Paradigm for Control System Design,” *Proceedings of IEEE Conference on Decision and Control,* vol. 5, no. 4–7, pp. 4578– 4585, Dec. 2001.

[36] Z. Gao, “Active Disturbance Rejection Control: A Paradigm Shift in Feedback Control System Design,” Proceedings of American Control Conference, pp. 2399–2405, Jun. 2006.

[37] Z. Gao, “Scaling and Parameterization Based Controller Tuning,” *Proceedings of American Control Conference,* vol. 6, no. 4–6, pp. 4989–4996, June 2003.

[38] R. Miklosovic, and Z. Gao, “A Robust Two-Degree-of-Freedom Control Design Technique and Its Practical Application,” The 39th IAS Annual Meeting, Industry Applications Conference, vol. 3, pp. 1495–1502, Oct. 2004.

[39] G. Tian, and Z. Gao, “Frequency Response Analysis of Active Disturbance Rejection Based

Control System," *Proceedings of IEEE International Conference on Control Applications,* pp. 1595–1599, Oct. 2007.

[40] B. Sun, and Z. Gao, "A DSP-Based Active Disturbance Rejection Control Design for a 1-kW H-bridge DC-DC Power Converter," *IEEE Transactions on Industrial Electronics,* vol. 52, no.5, pp. 1271–1277, Oct. 2005.

[41] Z. Chen, Q. Zheng, and Z. Gao, "Active Disturbance Rejection Control of Chemical Processes," *Proceedings of IEEE International Conference on Control Applications,* pp. 855–861, Oct. 2007.

[42] W. Zhou, and Z. Gao, "An Active Disturbance Rejection Approach to Tension and Velocity Regulations in Web Processing Lines," *IEEE International Conference on Control Applications,* pp. 842–848, Oct. 2007.

[43] L. Dong, Q. Zheng, and Z. Gao, "A Novel Oscillation Controller for Vibrational MEMS Gyroscopes," *Proceedings of American Control Conference,* pp. 3204–3209, Jul. 2007.

[44] L. Dong, and D. Avanesian, "Drive-mode Control for Vibrational MEMS Gyroscopes," *IEEE Transactions on Industrial Electronics*, vol. 56, no. 4, pp. 956–963, 2009.

[45] L. Dong, Q. Zheng, and Z. Gao, "On Control System Design for the Conventional Mode of Operation of Vibrational Gyroscopes," *IEEE Sensors Journal*, vol. 8, no. 11, pp. 1871–1878, Nov. 2008.

[46] L. Dong, and J Edwards, "Robust Controller Design for an Electrostatic micromechanical Actuator," IJCSE, 3(1); 8-21, 2013.

[47] Q. Zhang, L. Guo, and L. Huo, " Research of Automatic disturbance Rejection Controller for Fiber optic Gyro Servo Stabilized System," 3rd EEIC, 2013.

[48] Y. Ma, J. Zhobo, and X. Zhou, "The Research of ADRC on Shunt Hybrid Active Power Filter," IWIEE, 2012.

[49] L. Dong, P. Kandula, D. Wang and Z. Gao, **"**On a robust control system design for an electric power assist steering system," American Control Conference (ACC), pp. 5356 – 5361, June 30-July 2, 2010.

[50] Dan Wu, K. Chen, and X. Wang," Tracking control and active disturbance rejection with application to nonlinear machining," International Journal of Machine Tools and Manufacture, vol. 47, pp. 2207-2217, 2007.

[51] Y. Zhang, L. Dong, "On design of a robust load frequency controller for interconnected

power system," American control conference, July, 2010.

[52] Y. Zhang, L. Dong and Z. Gao, "A robust decentralized load frequency controller for interconnected power system," ISA Transactions vol. 51, pp. 410-419, 2012.

[53] S. Shi, J. Lu and S Zhao, "On design analysis of linear active disturbance rejection control for uncertain system, "International Journal of Control and Automation, vol.7. No.3, pp. 225-236, 2014.

[54] A. H. M. Sayem, Zhenwei and Zhihong Man "Performance Enhancement of ADRC using RC for Load Frequency Control of Power System," IEEE 8th Conference on Industrial Electronics and Applications (ICIEA) , 2013.

[55] V. S. Dundaram, T., Jatabarathi,"A novel approach of load frequency control in multi area power system," International Journal of Engineering Science and Technology (IJEST), ISSN : 0975-5462 Vol. 3 No. 3 Mar 2011.

[56] P.M. Anderson, and A. A., Fouad, "Power System Control and Stability," Second edition, IEEE Press, 2002.

[57] M. Parniani, and A. Nasri, "SCADA based under frequency load-shedding integrated with rate of frequency decline," IEEE Power Engineering Society General Meeting, 2006.

[58] A. H. M. Sayem, "Active disturbance rejection control for load frequency control of Bangladesh power system," M. Sc. Eng. thesis, Bangladesh University of Engineering and Technology, Bangladesh, Nov. 2012.

[59] Yao Zhang, "Load frequency control of multi-area power system," M. Sc in Electrical engineering thesis in Cleveland State University, USA, August, 2009.

Annexure A

Table A-1: System Parameters for Fig. 4.1

Parameters	Definition	Value
T_{ch} (sec.)	Turbine time constant	0.3
R (Hz/p.u.)*	Speed regulation coefficient	0.05
F_{hp} (p.u.)	High pressure stage rating	0.3
M (p.u.sec.)	Area inertia constant	10
D(p.u./Hz)	Area load damping constant	1.0
T_g (sec.)	Governor time constant	0.2

*: p.u. represents per unit.

Table A-2: ADRC and PID Parameters for Fig.4.1

ADRC		PID	
Order of ESO	3	P	0
ω_c	4	I	-0.293980028198636
ω_0	16	D	0
B	70.0		

Table A-3: System parameters for Fig.4.9

Non-reheat		Reheat	
T_{ch1} (sec.)	0.3	T_{ch2} (sec.)	0.3
R_1 (Hz/p.u.)	0.05	R_2 (Hz/p.u.)	0.05
M_1(p.u.sec.)	10.0	M_2 (p.u.sec.)	10.0
D_1(p.u./Hz)	1.0	D_2(p.u./Hz)	1.0
T_{g1} (sec.)	0.1	T_{g2} (sec.)	0.2
		F_{hp} (p.u.)	0.3
		T_{rh} (sec.)	7.0

Table A-4: Value of Tie-line synchronizing coefficient for Table 5.2

Tie-line synchronizing coefficient	Value	Tie-line Synchronizing coefficient	Value
T_{11}*	25	T_{32}	25
T_{21}	30	T_{13}	20
T_{31}	40	T_{23}	35
T_{12}	30	T_{33}	30
T_{22}	24		

*: $T_{\text{Load rich area, Generation rich area}}$

Table A-5: Value of Tie-line synchronizing coefficient for Fig. 5.9 to Fig. 5.32

Tie-line synchronizing coefficient	Value	Tie-line Synchronizing coefficient	Value
T_{11}	25	T_{32}	120
T_{21}	80	T_{13}	20
T_{31}	50	T_{23}	40
T_{12}	30	T_{33}	80
T_{22}	60		

Figure showing effects of simultaneous load changes

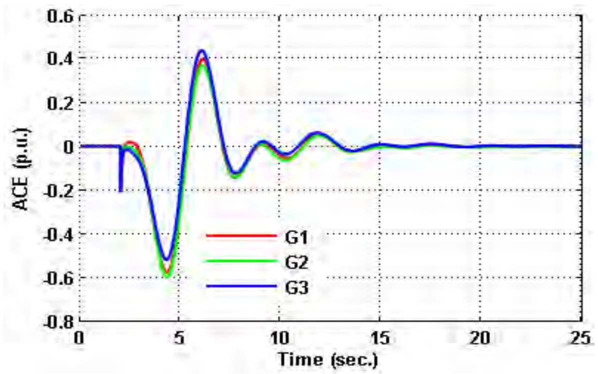

(a)

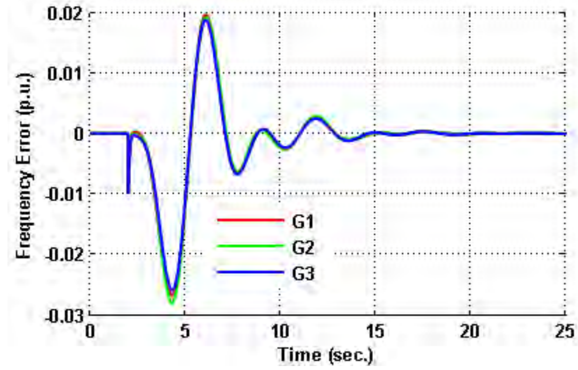

(b)

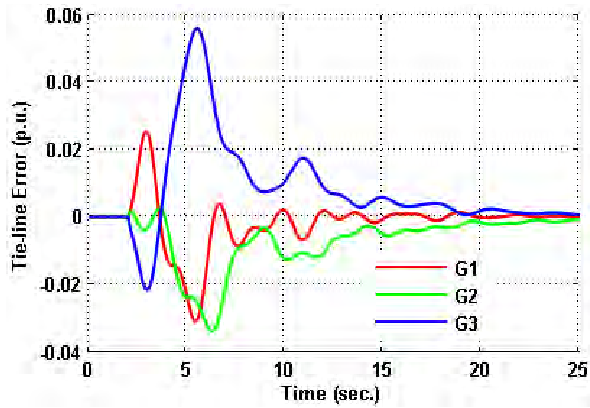

(c)

Fig. A-1 Effect of simultaneous load change on ACE, (a), frequency error, (b) and tie-line error, (c) for feedback paths: L_1G_1 L_2G_2 L_1G_3

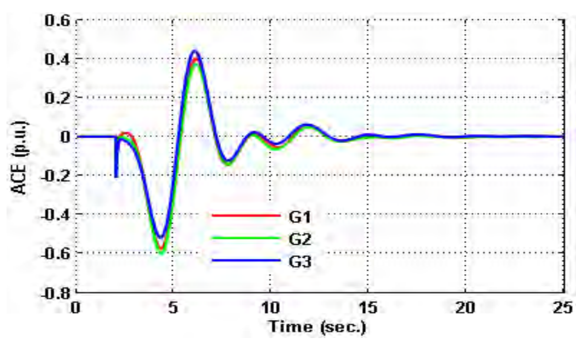

(a)

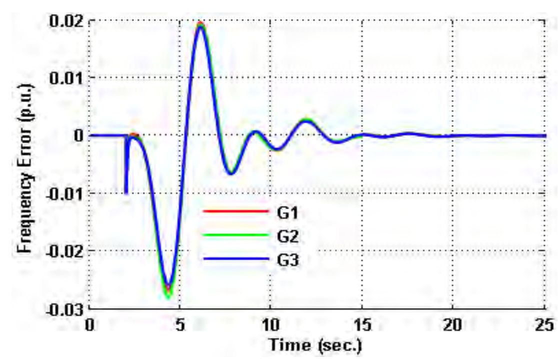

(b)

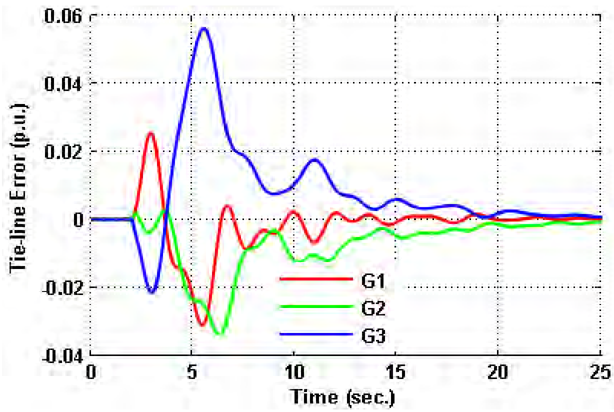

(c)

Fig. A-2 Effect of simultaneous load change on ACE, (a), frequency error, (b) and tie-line error, (c) for feedback paths: L_1G_1 L_3G_2 L_1G_3

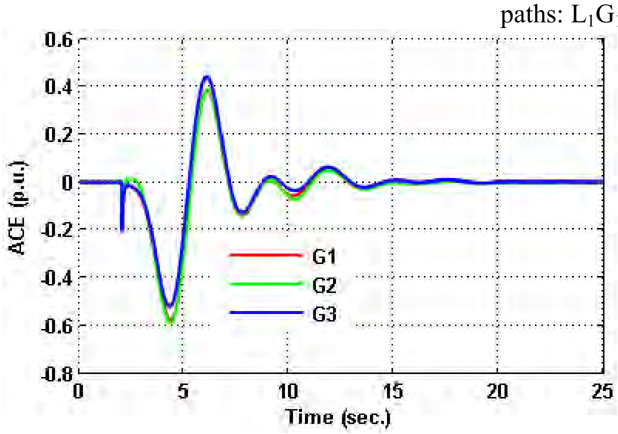

(a)

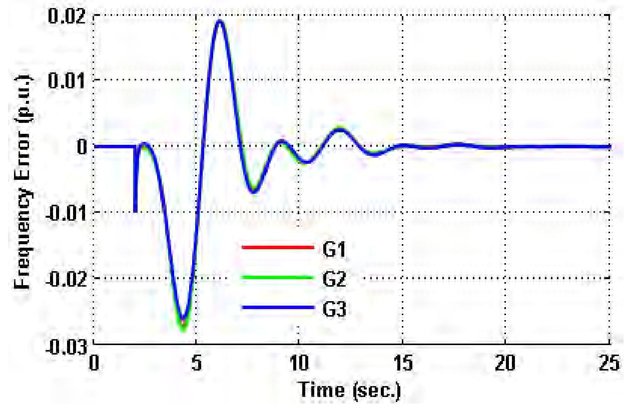

(b)

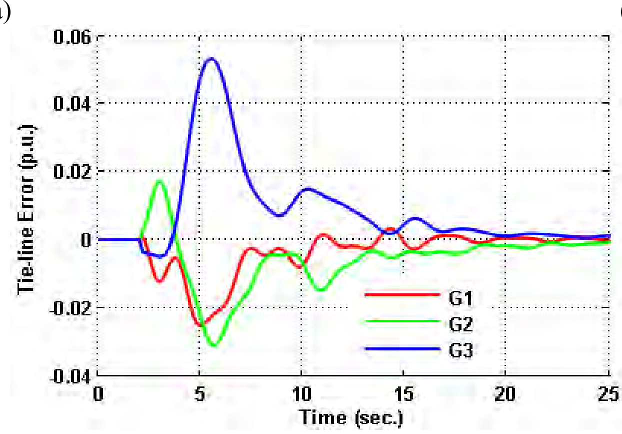

(c)

Fig. A-3 Effect of simultaneous load change on ACE, (a), frequency error, (b) and tie-line error, (c) for feedback paths: L_1G_1 L_3G_2 L_1G_3

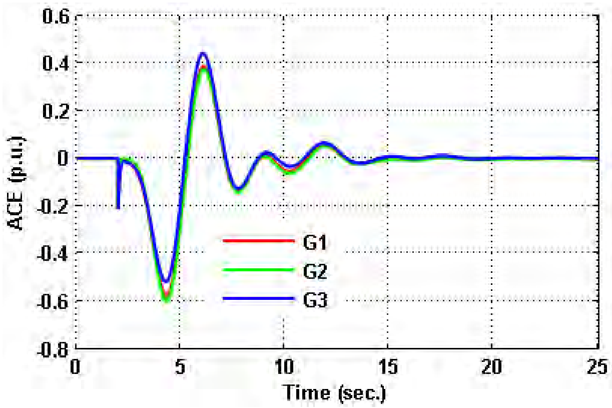

(a)

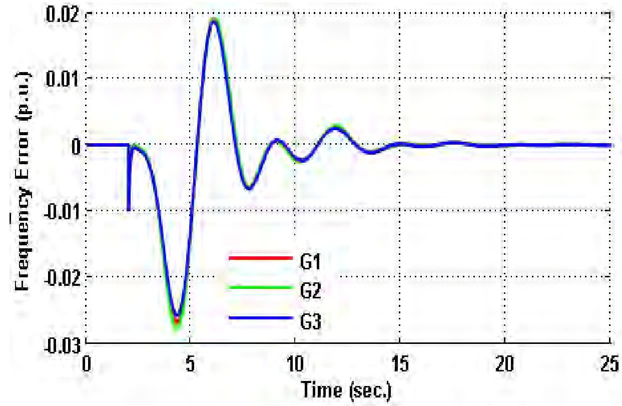

(b)

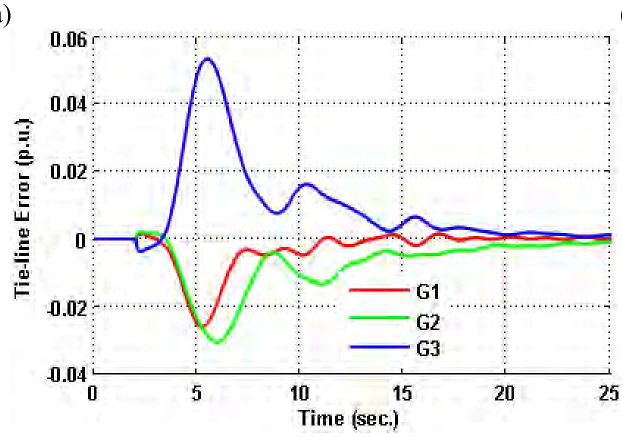

(c)

Fig. A-4 Effect of simultaneous load change on ACE, (a), frequency error, (b) and tie-line error, (c) for feedback paths: L_1G_1 L_1G_2 L_3G_3

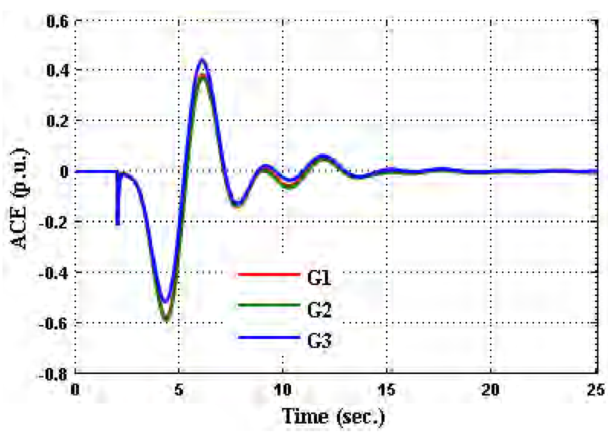

(a)

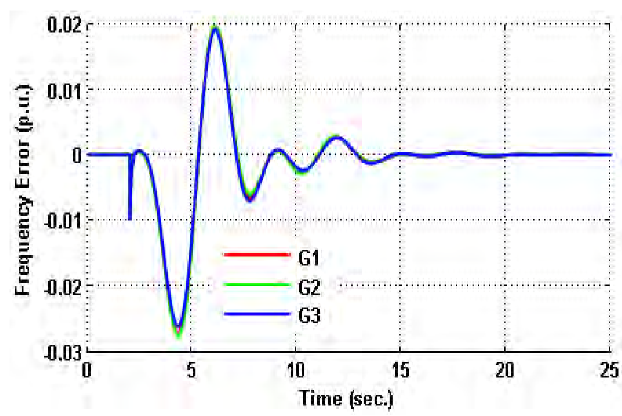

(b)

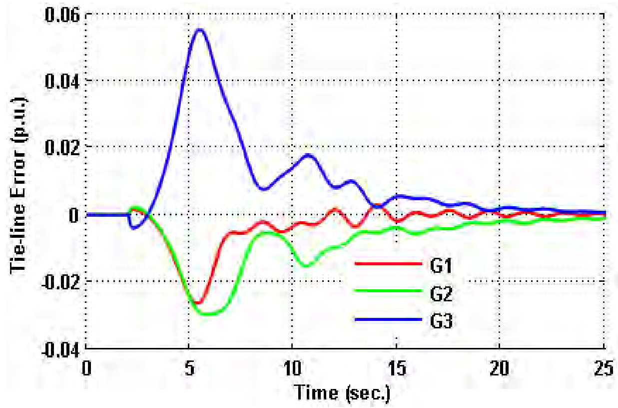

(c)

Fig. A-5 Effect of simultaneous load change on ACE, (a), frequency error, (b) and tie-line error, (c) for feedback paths: L_2G_1 L_2G_2 L_1G_3

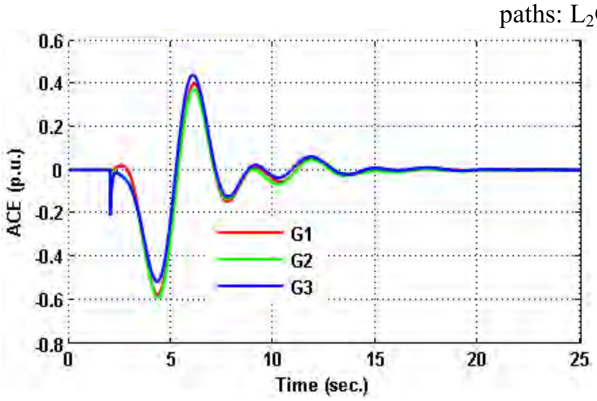

(a)

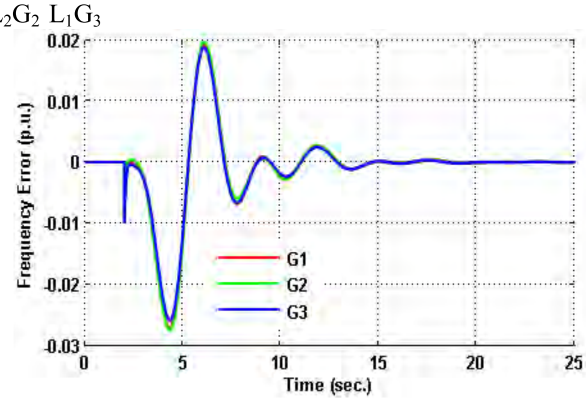

(b)

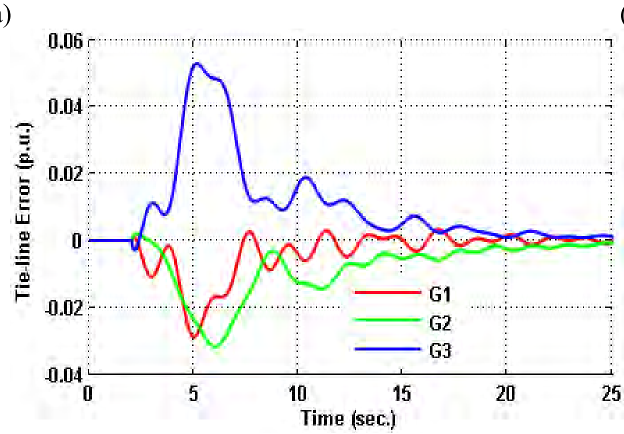

(c)

Fig. A-6 Effect of simultaneous load change on ACE, (a), frequency error, (b) and tie-line error, (c) for feedback paths: L_2G_1 L_3G_2 L_1G_3

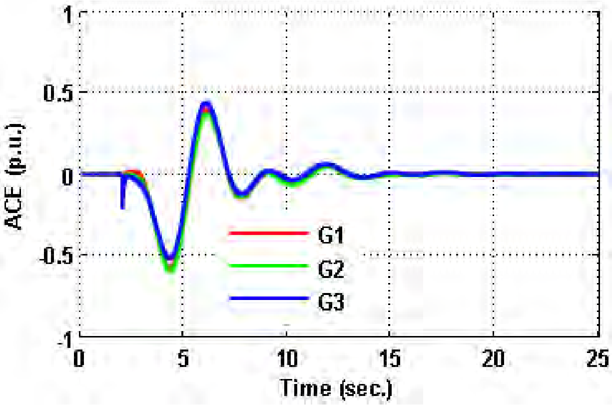

(a)

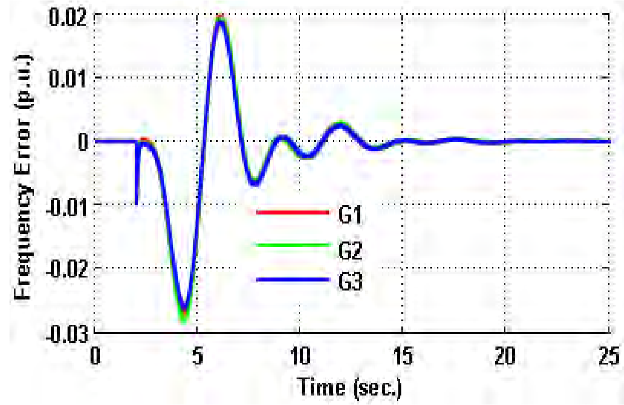

(b)

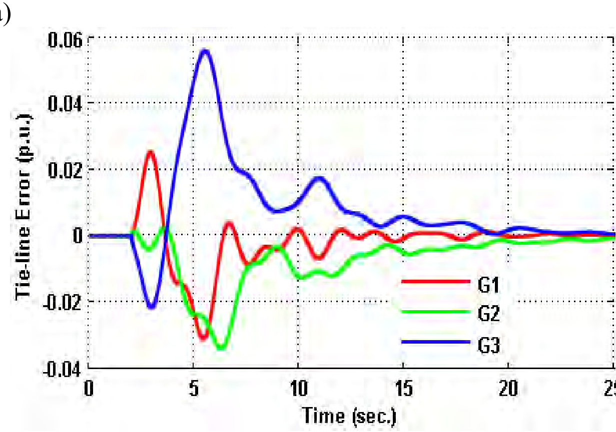

(c)

Fig. A-7 Effect of simultaneous load change on ACE, (a), frequency error, (b) and tie-line error, (c) for feedback paths: L_3G_1 L_2G_2 L_2G_3

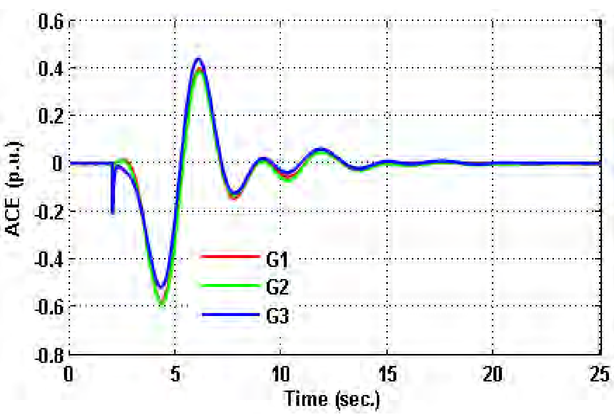

(a)

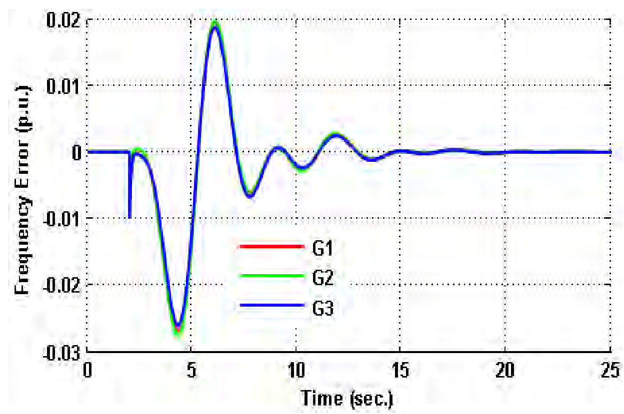

(b)

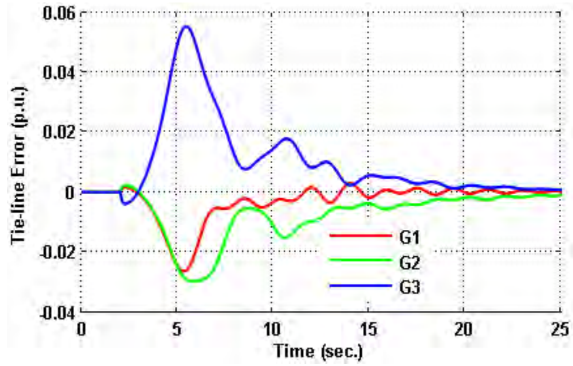

(c)

Fig. A-8 Effect of simultaneous load change on ACE, (a), frequency error, (b) and tie-line error, (c) for feedback paths: L_3G_1 L_3G_2 L_1G_3

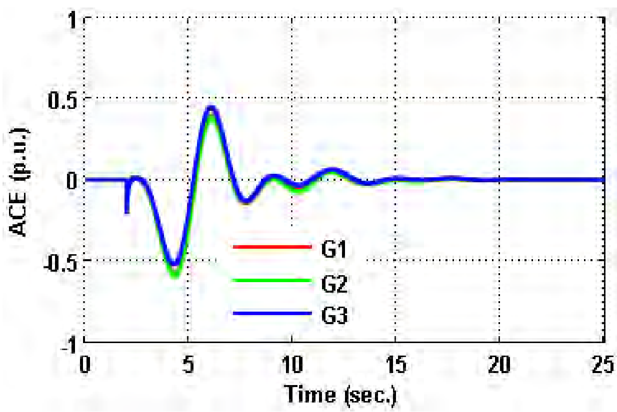

(a)

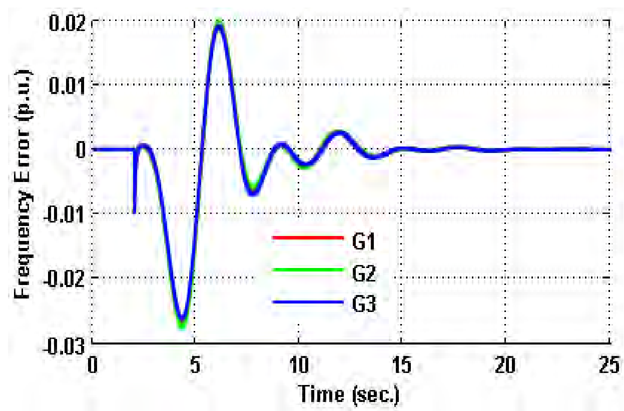

(b)

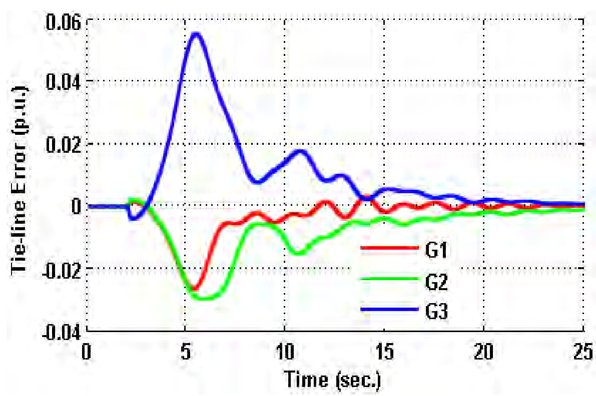

(c)

Fig. A-9 Effect of simultaneous load change on ACE, (a), frequency error, (b) and tie-line error, (c) for feedback paths: L_2G_1 L_2G_2 L_3G_3

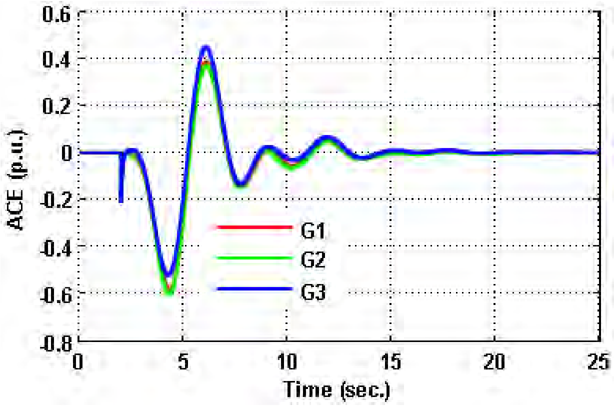

(a)

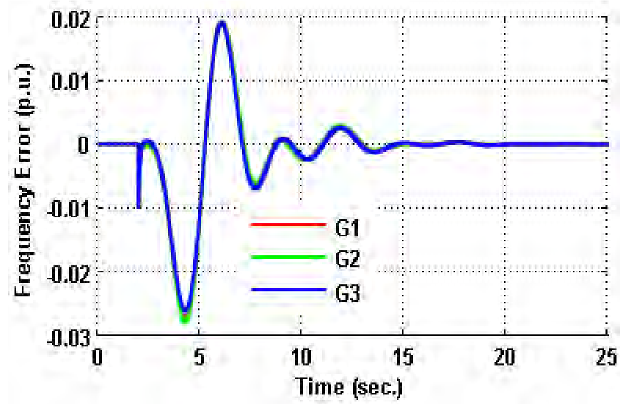

(b)

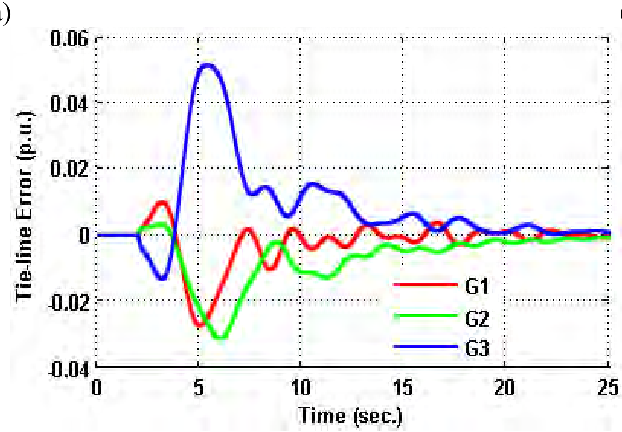

(c)

Fig. A-10 Effect of simultaneous load change on ACE, (a), frequency error, (b) and tie-line error, (c) for feedback paths: L_2G_1 L_2G_2 L_1G_3

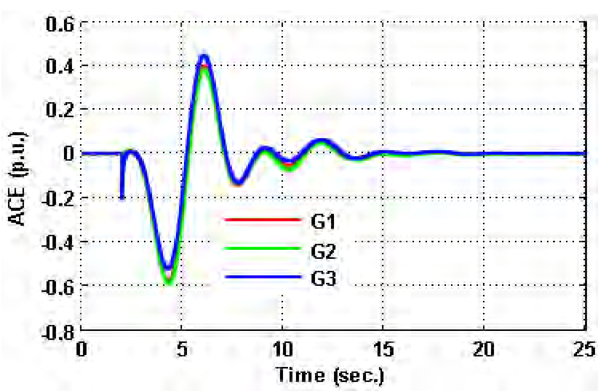

(a)

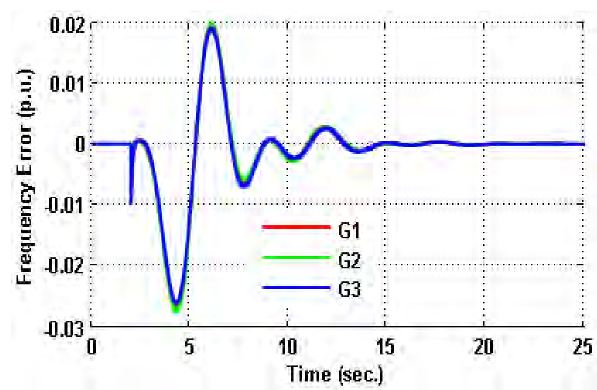

(b)

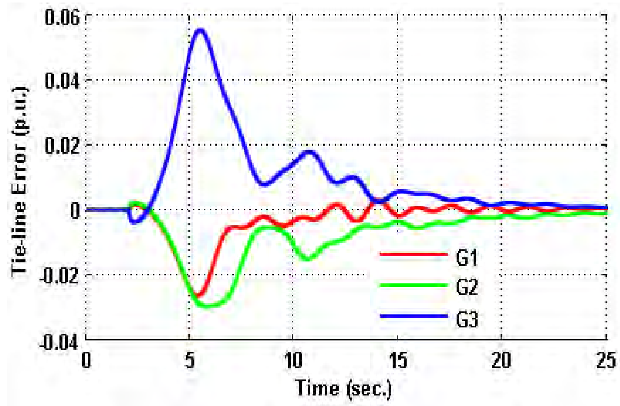

(c)

Fig. A-11 Effect of simultaneous load change on ACE, (a), frequency error, (b) and tie-line error, (c) for feedback paths: L_1G_1 L_2G_2 L_3G_3

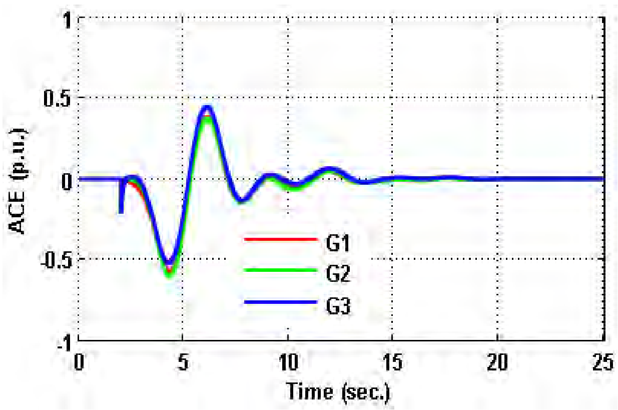

(a)

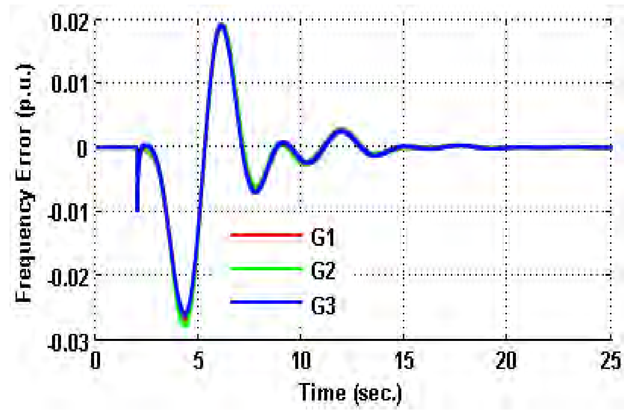

(b)

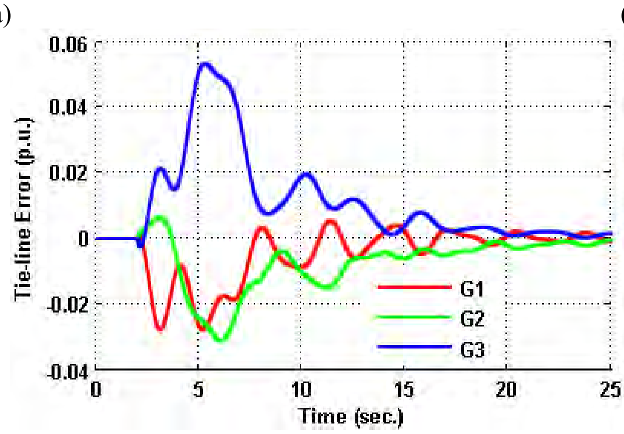

(c)

Fig. A-12 Effect of simultaneous load change on ACE, (a), frequency error, (b) and tie-line error, (c) for feedback paths: L_3G_1 L_2G_2 L_1G_3

Figure showing effect of individual load change

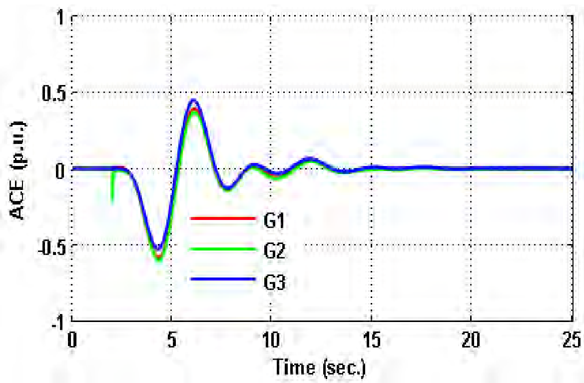

(a)

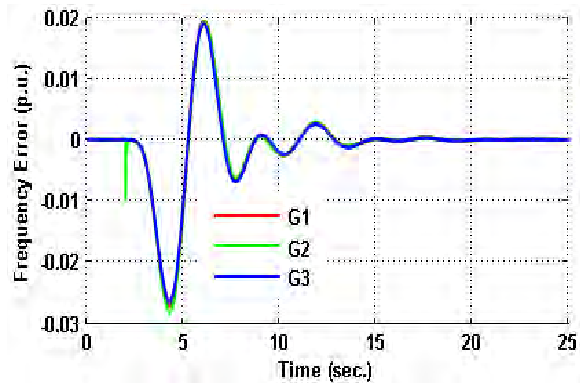

(b)

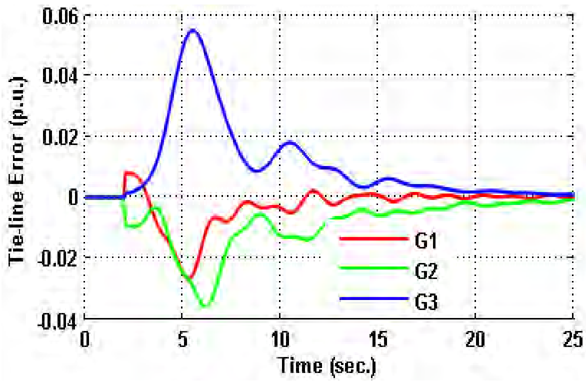

(c)

Fig. A-13 Effect of simultaneous load change on ACE, (a), frequency error, (b) and tie-line error, (c) for feedback path: L_2G_3

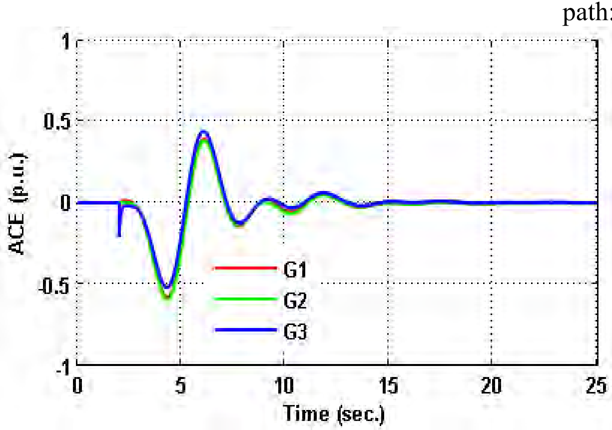

(a)

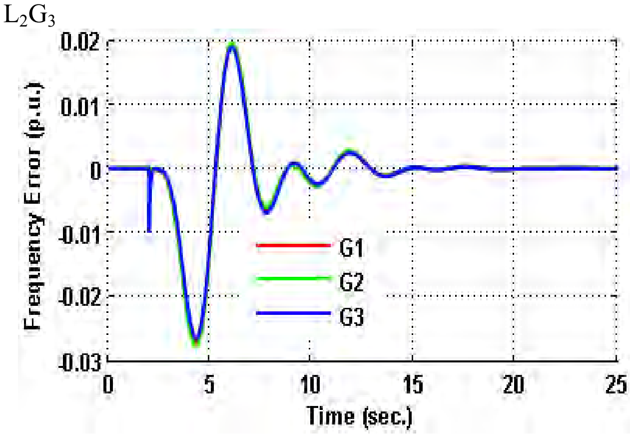

(b)

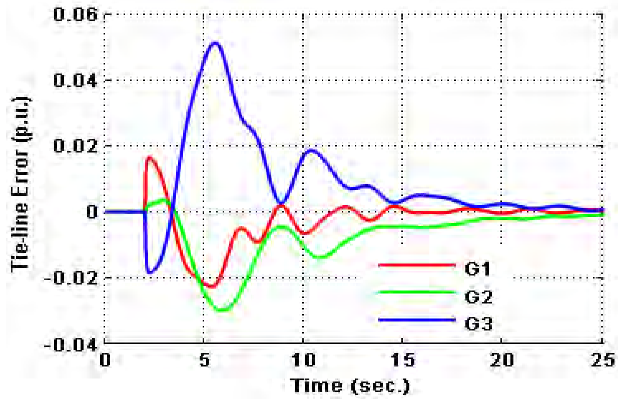

(c)

Fig. A-14 Effect of simultaneous load change on ACE, (a), frequency error, (b) and tie-line error, (c) for feedback path: L_3G_2

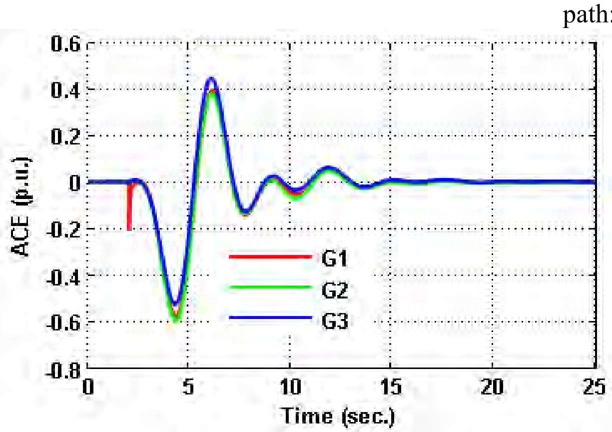

(a)

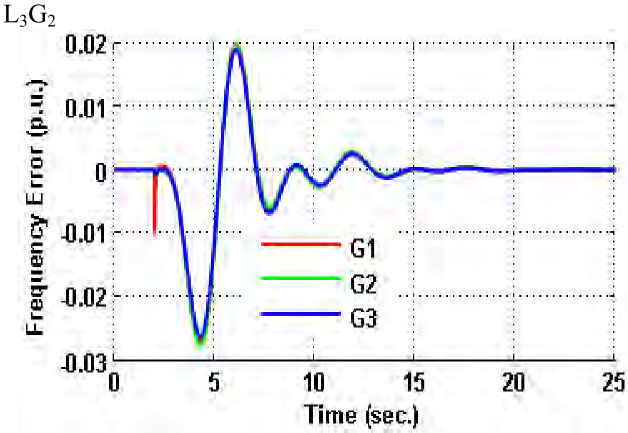

(b)

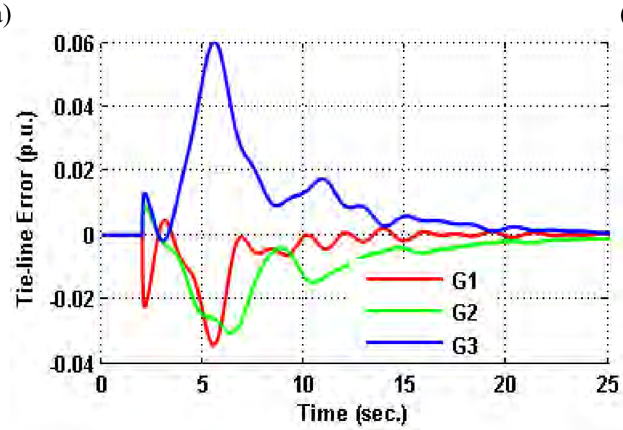

(c)

Fig. A-15 Effect of simultaneous load change on ACE, (a), frequency error, (b) and tie-line error, (c) for feedback path: L_1G_3

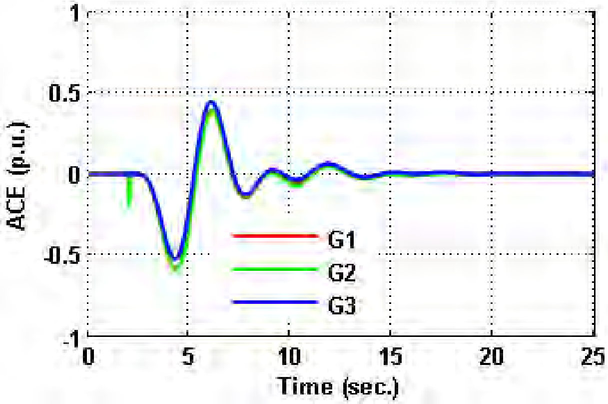

(a)

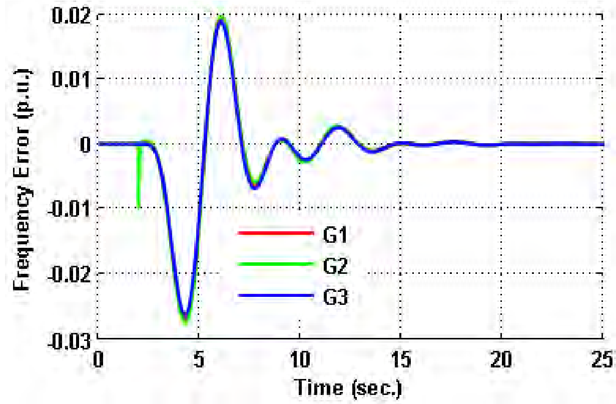

(b)

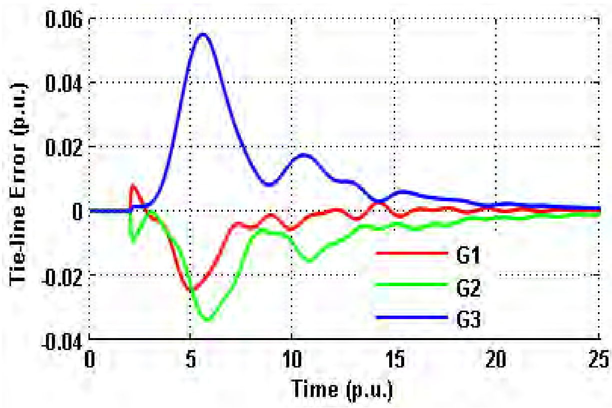

(c)

Fig. A-16 Effect of simultaneous load change on ACE, (a), frequency error, (b) and tie-line error, (c) for feedback path: L_2G_3

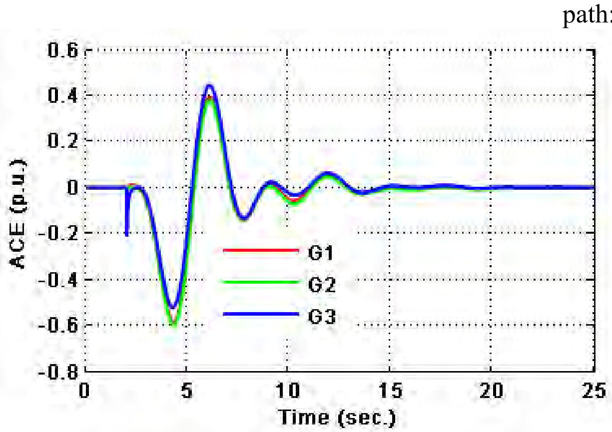

(a)

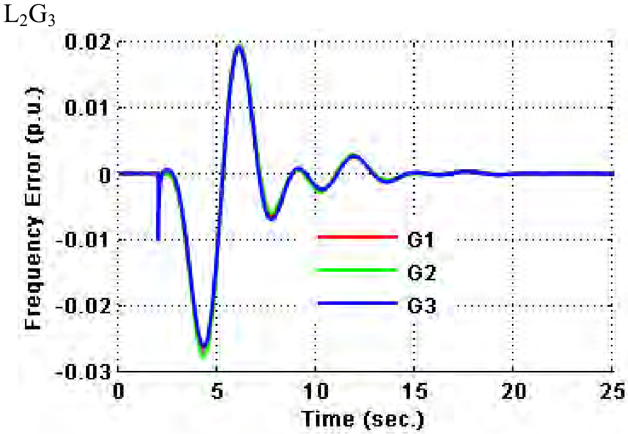

(b)

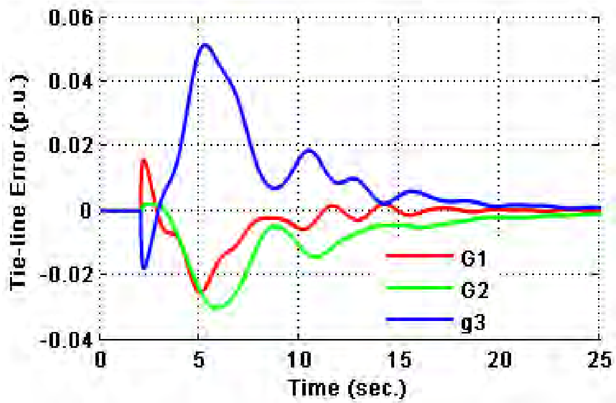

(c)

Fig. A-17 Effect of simultaneous load change on ACE, (a), frequency error, (b) and tie-line error, (c) for feedback path: L_3G_3